Article

Cell Chemical Biology

Inhibition of Glucose Transporters and Glutaminase Synergistically Impairs Tumor Cell Growth

Graphical Abstract

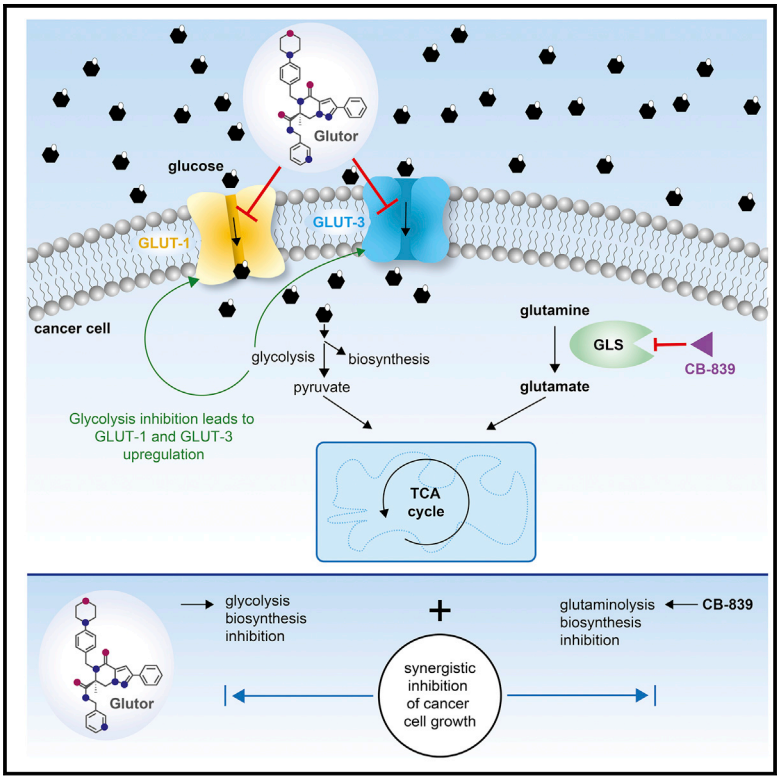

Highlights

- Development of the GLUT-1-3-selective inhibitor Glutor to suppress glucose uptake
- Glutor potently induces cell death in 2D and 3D cancer cell culture
- Glutor-induced hypoglycemia upregulates GLUT-1/-3
- Glutor and GLS inhibitor CB-839 synergistically inhibit cell growth

Authors

Elena S. Reckzeh, George Karageorgis, Melanie Schwalfenberg, ..., Carsten Strohmann, Slava Ziegler, Herbert Waldmann

Correspondence

herbert.waldmann@mpi-dortmund.mpg.de

In Brief

Cell-based screening identified the piperazin-2-one Glutor as a nanomolar inhibitor of glucose uptake that targets the glucose transporters GLUT-1/-3. Glutor inhibits glycolysis and effectively incudes cell death of monolayer- and spheroid-cultured cancer cells. Glutor-mediated glucose starvation upregulates GLUT-1/-3 expression. Glutor and glutaminase inhibitor CB-839 synergistically inhibit cancer cell growth.

Reckzeh et al., 2019, Cell Chemical Biology *26*, 1–15
September 19, 2019
https://doi.org/10.1016/j.chembiol.2019.06.005

CellPress

Please cite this article in press as: Reckzeh et al., Inhibition of Glucose Transporters and Glutaminase Synergistically Impairs Tumor Cell Growth, Cell Chemical Biology (2019), https://doi.org/10.1016/j.chembiol.2019.06.005

Cell Chemical Biology
Article

Inhibition of Glucose Transporters and Glutaminase Synergistically Impairs Tumor Cell Growth

Elena S. Reckzeh,[1,2] George Karageorgis,[1,4] Melanie Schwalfenberg,[1] Javier Ceballos,[1,5] Jessica Nowacki,[1,6] Marcus C.M. Stroet,[1,7] Aylin Binici,[1] Lena Knauer,[2] Silke Brand,[1] Axel Choidas,[3] Carsten Strohmann,[2] Slava Ziegler,[1] and Herbert Waldmann[1,2,8,*]

[1]Max Planck Institute of Molecular Physiology, Department of Chemical Biology, Otto-Hahn-Strasse 11, 44227 Dortmund, Germany
[2]Technical University Dortmund, Faculty of Chemistry and Chemical Biology, Otto-Hahn-Strasse 6, 44227 Dortmund, Germany
[3]Lead Discovery Center GmbH, Otto-Hahn-Strasse 15, 44227 Dortmund, Germany
[4]Present address: School of Chemistry, University of Leeds, LS2 9JT Leeds, UK
[5]Present address: Laboratory of Catalysis and Organic Synthesis, EPFL SB ISIC LCSO, BCH 4221, CH-1015 Lausanne, Switzerland
[6]Present address: Chemical Genomics Center, Otto-Hahn-Strasse 15, 44227 Dortmund, Germany
[7]Present address: Optical Molecular Imaging/SPECTRIM/Radiochemistry, Radiology Department, Erasmus Medical Center, Dr. Molewaterplein 40, 3015 GD Rotterdam, The Netherlands
[8]Lead Contact
*Correspondence: herbert.waldmann@mpi-dortmund.mpg.de
https://doi.org/10.1016/j.chembiol.2019.06.005

SUMMARY

Cancer cells sustain growth by altering their metabolism to accelerated aerobic glycolysis accompanied by increased glucose demand and employ glutamine as additional nutrient source. This metabolic adaptation induces upregulation of glucose transporters GLUT-1 and -3, and simultaneous targeting of both transporters and of glutamine metabolism may offer a promising approach to inhibit cancer cell growth. We describe the discovery of the very potent glucose uptake inhibitor Glutor, which targets glucose transporters GLUT-1, -2, and -3, attenuates glycolytic flux and potently and selectively suppresses growth of a variety of cancer cell lines. Co-treatment of colon cancer cells with Glutor and glutaminase inhibitor CB-839 very potently and synergistically inhibits cancer cell growth. Such a dual inhibition promises to be particularly effective because it targets the metabolic plasticity as well as metabolic rescue mechanisms in cancer cells.

INTRODUCTION

Proliferating cells, such as cancer cells, activated T cells, and endothelial cells ensure rapid growth and proliferation by upregulating glycolysis, even under aerobic conditions (this phenomenon is termed the Warburg effect) (Koppenol et al., 2011; Vander Heiden et al., 2009). Aerobic glycolysis is characteristic for several diseases, including cancer and inflammatory diseases such as psoriasis (Hanahan and Weinberg, 2011; Zhang et al., 2018). In particular, various cancers upregulate facilitative glucose transporters (GLUTs) to increase nutrient uptake, for example, thyroid carcinomas (Jóźwiak et al., 2012), endometrial and breast cancer (Krzeslak et al., 2012), colon- and pancreatic cancer (Yamamoto et al., 1990), head and neck tumors (Ayala et al., 2010; Mellanen et al., 1994), and non-small-cell lung cancer (Younes et al., 1997). Glucose transporters are involved in central cellular processes, such as insulin secretion in the pancreas (GLUT-2) and insulin-regulated glucose transport (GLUT-4), and are expressed tissue specifically, i.e., GLUT-1 is ubiquitously expressed in normal tissue, whereas GLUT-3 is primarily expressed in neurons (Zhao and Keating, 2007). These findings have led to the notion that selective inhibition of the major facilitative transporter GLUT-1 may open up a promising approach for the treatment of cancer (Shi et al., 2018), and recently the first GLUT-1-selective inhibitor has been reported (Siebeneicher et al., 2016a, 2016b). However, in the cancers mentioned above, both GLUT-1 and GLUT-3 are upregulated, and in esophageal adenocarcinoma GLUT-3 expression was increased in patients undergoing radiotherapy or surgery, which indicates clonal selection (Fonteyne et al., 2009). Thus, dual-specific GLUT-1/-3 inhibitors may be required for cancer targeting, and we recently identified such a compound, albeit with moderate potency (Karageorgis et al., 2018).

In addition, rapidly dividing (e.g., cancer) cells rely on glutamine as C- and N-source, and interference with glutamine metabolism is considered a promising approach for cancer drug discovery (Martinez-Outschoorn et al., 2017). Reduction of GLUT-1 expression sensitizes lung cancer cells to inhibition of glutamine utilization and causes apoptosis and growth reduction and effective combinatory inhibition of glutaminolysis and glycolysis was described for ovarian cancer (Lee et al., 2016; Sun et al., 2017). Hence, combination of a GLUT-1/-3 inhibitor with an inhibitor of glutamine metabolism might synergistically inhibit cancer cell growth and, therefore, target the metabolic plasticity and overcome cellular rescue mechanisms of cancer cells.

Here we describe the identification of the GLUT inhibitor Glutor (glucose uptake inhibitor), which defines an unprecedented glucose uptake inhibitor chemotype. Glutor selectively targets GLUT-1, -2, and -3 with low nanomolar potency, induces

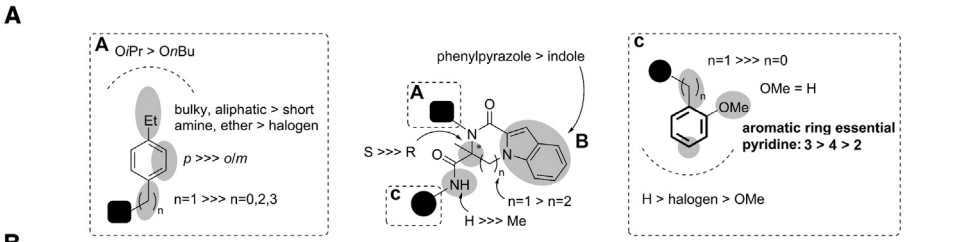

B

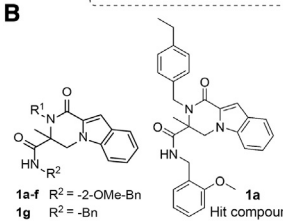

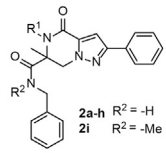

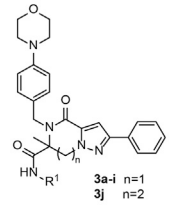

entry	cmpd	R^1	IC_{50}(±s.d.)[n]/ µM
1	**1a**	— 4-Et-Bn	3.29(±2.04)[12]
2	**1b**	— 4-OMe-Bn	3.67(±1.40)[15]
3	**1c**	— 3-OMe-Bn	25.63(±4.37)[6]
4	**1d**	— 2-OMe-Bn	n.a.[3]
5	**1e**	— 4-F-Bn	n.a.[3]
6	**1f**	— 4-Et-Ph	n.a.[3]
7	**1g**	— 4-Et-Bn	3.64(±1.73)[18]

entry	cmpd	R^1	IC_{50}(±s.d.)[n]/ µM
8	**2a**	— 4-SMe-Bn	1.65(±1.10)[21]
9	**(*S*)-2a**	— 4-SMe-Bn	0.88(±0.23)[12]
10	**(*R*)-2a**	— 4-SMe-Bn	n.a.[6]
11	**2b**	— 4-NEt_2- Bn	0.33(±0.09)[3]
12	**2c**	— 4-NMe_2-Bn	0.42(±0.27)[12]
13	**2d**	— 4-OEt-Bn	0.46(±0.27)[15]
14	**2e**	— 4-O*i*Pr-Bn	0.19(±0.06)[12]
15	**2f**	— 4-O*n*Bu-Bn	1.94(±1.60)[15]
16	**2g**	— CH_2-(4-OEt-Bn)	>30[3]
17	**2h**	— 4-Et-Bn	0.23(±0.11)[6]
18	**2i**	— 4-SMe-Bn	n.a.[3]

entry	cmpd	R^1	IC_{50}(±s.d.)[n]/ µM
19	**3a**	— CH_2-(3-pyridyl)	0.03(±0.01)[12]
20	**(*S*)-3a**	— CH_2-(3-pyridyl)	0.019(±0.002)[12]
21	**(*R*)-3a**	— CH_2-(3-pyridyl)	n.a.[9]
22	**3b**	— CH_2-(5-Me-3-pyridyl)	0.48(±0.09)[6]
23	**3c**	— CH_2-(4-pyridyl)	0.12(±0.01)[6]
24	**3d**	— CH_2-(2-pyridyl)	21.82(±2.14)[3]
25	**3e**	— *t*Bu	n.a.[3]
26	**3f**	— Bn	0.16(±0.09)[9]
27	**3g**	— 4-F-Bn	2.98(±0.09)[6]
28	**3h**	— 4-F-Ph	n.a.[9]
29	**3i**	— 4-OMe-Bn	19.22(±9.53)[9]
30	**3j**	— CH_2-(3-pyridyl)	1.33(±0.5)[6]

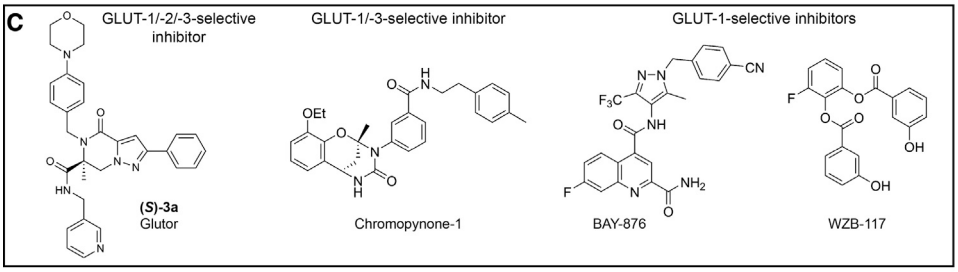

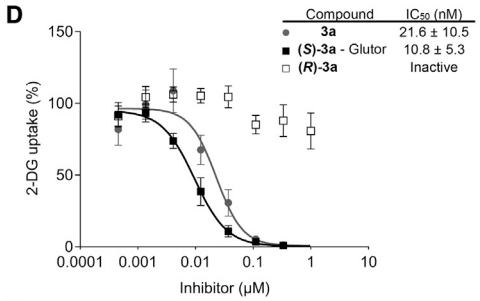

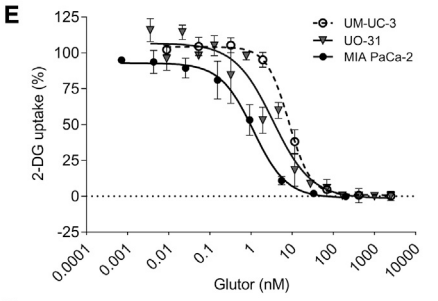

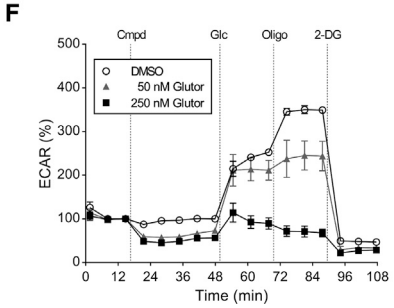

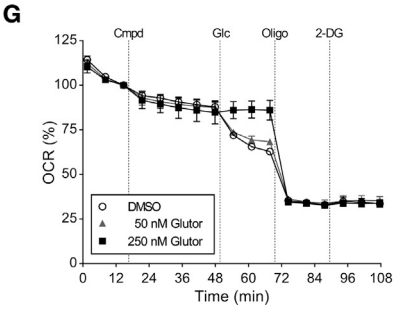

(legend on next page)

upregulation of GLUT-1 and -3 in cancer cells, inhibits glycolysis and efficiently suppresses the growth of various cancer cell lines. Co-treatment with Glutor and the glutaminase inhibitor CB-839 (Gross et al., 2014) synergistically inhibits cancer cell growth.

RESULTS

Identification of Glucose Uptake Inhibitors

Glucose uptake inhibitors were identified by means of a semi-automated HCT116 colon cancer cell-based screen that monitors the uptake of 2-deoxy-D-glucose (2-DG) (Yamamoto et al., 2006) (for details see Figure S1A). The screen employed a library of over 150,000 compounds from different commercial and academic sources that were selected according to chemical diversity and drug likeness. In addition, the collection included natural products and sp^3-rich compounds from Edelris. The screen identified piperazin-2-one-based hit compound **1a** as 2-DG uptake inhibitor with an half maximal inhibitory concentration (IC_{50}) value of 3.29 ± 2.04 μM in the semi-automated screen and 588.0 ± 143.3 nM in a separate manually performed assay (Figures S1B and S1C).

For delineation of a structure-activity relationship (SAR) a total of 95 analogs was synthesized by means of a modified Ugi four-component reaction as described by Ivachtchenko and colleagues (Ilyn et al., 2005) (for details see the STAR Methods) or obtained from commercial sources (ChemDiv, UK). Investigation of the compounds in the semi-automated 2-DG uptake assay revealed a coherent SAR. General trends are illustrated in Figure 1A. Thus, replacement of the 4-ethyl substituent in the *N*-benzyl amide (**A**) of the hit compound **1a** (IC_{50} = 3.29 ± 2.04 μM) by a 4-methoxy group (**1b**) did not alter the activity of the compound (Figure 1B, left panel, compare entries 1 and 2). However, introduction of a methoxy group in the 3-position (**1c**) reduced the activity ca. 7-fold (Figure 1B, left panel, compare entries 1 and 3). If the methoxy group was placed in the 2-position (**1d**) inhibiting activity was lost (Figure 1B, left panel, compare entry 2 with entries 3 and 4). Replacement of the *p*-ethyl substituent in the benzyl amide **A** by a fluorine (Figure 1B, left panel, compare entries 1 and 5) or other halogens (Table S1, entry 17) led to loss of activity. Replacement of the 2-methoxy benzyl amide **C** by a benzyl group (**1g**) did not alter the potency (Figure 1B, left panel, compare entries 1 and 7). However, if in **1g** (IC_{50} = 3.64 ± 1.73 μM) the indole heterocycle (**B**) was replaced by a 3-phenylpyrazole scaffold (**2h**), the IC_{50} value was lowered by one order of magnitude to 0.23 ± 0.11 μM (Figure 1B, left and central panel, compare entries 7 and 17). Therefore, further compound optimization was performed with the 3-phenylpyrazole scaffold as core structure. Replacement of the 4-ethyl group in the *N*-benzyl amide (**A**) of 3-phenylpyrazole **2h** by disubstituted amines (**2b**, **2c**) or an ethyl ether (**2d**) did not alter the activity substantially (Figure 1B, central panel; compare entries 11–13 with entry 17). However, bulky substituents in the 4-position of *N*-benzylamide **A** led to an increase in potency (Figure 1B, central and right panel; compare entries 14 and 26 with entry 17) to 0.19 ± 0.06 μM (**2e**) and 0.16 ± 0.09 μM (**3f**). The highest potency was recorded for compound **3f** which embodies a morpholino group as 4-substituent of *N*-benzyl amide **A**. Activity was also lower when larger unbranched substituents were introduced in the 4-position (see, e.g., **2a** and **2f**, entries 8 and 15). Thus, for further optimization the 4-morpholino group was kept.

Methylation of the exocyclic secondary amide of **2a** to yield **2i** (R^2 = Me) rendered the compound inactive (Figure 1B, central panel, compare entries 8 and 18). To improve the solubility of **3f**, a nitrogen was introduced in the phenyl ring of benzyl amide **C** (**3a**). Notably, the 3-pyridine group (**3f**) enhanced the inhibitory potency by nearly one order of magnitude (Figure 1B, right panel; compare entries 19 and 26) to yield the most potent glucose import inhibitor **3a**. If the 3-pyridyl (**3a**) group was replaced by a 2-pyridyl (**3d**) the biological activity was lowered by 30-fold and replacement by a 4-pyridyl group (**3c**) reduced the activity by 4-fold to 0.12 ± 0.01 μM (Figure 1B, right panel, compare entry 19 with entries 23 and 24). Introduction of additional substituents such as fluorine or a methoxy group reduced activity as well (Figure 1B; right panel). Separation of the enantiomers of the most active compound **3a** revealed that the (+)-enantiomer inhibits glucose uptake with IC_{50} = 19 ± 2 nM, whereas the (−)-enantiomer was inactive at 30 μM (Figure 1B, compare entries 20 and 21). Crystal structure analysis (Figure S1D, CCDC: 1883523) unambiguously proved that the inactive enantiomer was *R*-configured. By analogy the (*S*)-configuration was assigned to the active (+)-enantiomer of **3a**, which we termed Glutor (**(*S*)-3a**, Figure 1C). Irrespective of the originating tissue, Glutor reduced the uptake of 2-DG with similar potency in different cancer cell lines such as HCT116 (IC_{50} = 10.8 ± 5.3 nM), UM-UC-3 (IC_{50} = 8.3 ± 2.0 nM, urinary bladder), UO-31 (IC_{50} = 3.6 ± 1.5 nM, kidney), and MIA PaCa-2 (IC_{50} = 1.1 ± 0.3 nM, pancreas) (Figures 1D and 1E). Furthermore, Glutor does not interfere with cellular hexokinase activity (Figure S1E) and potently reduces glycolytic flux in HCT116 cells (Figure 1F), which prevents a decrease in oxidative phosphorylation (OXPHOS) rate upon glucose addition (Figure 1G). The compound does not induce mitochondrial toxicity (Marroquin et al., 2007) in HCT116 cells (Figures S1F and S1G).

Glutor is an unprecedented GLUT inhibitor substance class (Figure 1C) with distant structural similarity (*N*-heterocycle

Figure 1. Glutor Inhibits 2-DG Uptake and Thereby Reduces Glycolytic Flux in HCT116 Cells

(A) Structure-activity relationship for the piperazin-2-one class (see also Tables S1 and S2).

(B) IC_{50} values for 2-DG uptake inhibition by selected Glutor derivatives (see also Tables S1 and S2). Data are mean values ± SD of n = 3–21. cmpd, compound; n.a., not active at 30 μM.

(C) Structural comparison of selected GLUT inhibitors.

(D and E) Dose-response curve for 2-DG uptake inhibition by Glutor (see also Figure S1A). The graphs show mean values ± SD. n = 3, N = 3 for HCT116 (D), MIA PaCa-2 (E), and UM-UC-3 (E); n = 4, N = 3 for UO-31 (E).

(F and G) Glycolytic stress test of Glutor-treated HCT116 cells. The extracellular acidification rate (ECAR) (F) and the oxygen consumption rate (OCR) (G) were measured for 2 h. Data are mean values ± SD (n = 3, N = 3). Cmpd, Glutor/DMSO; Glc, 10 mM glucose; Oligo, 2.5 μM oligomycin; 2-DG, 50 mM 2-DG. See also Figures S1F and S1G for mitochondrial toxicity.

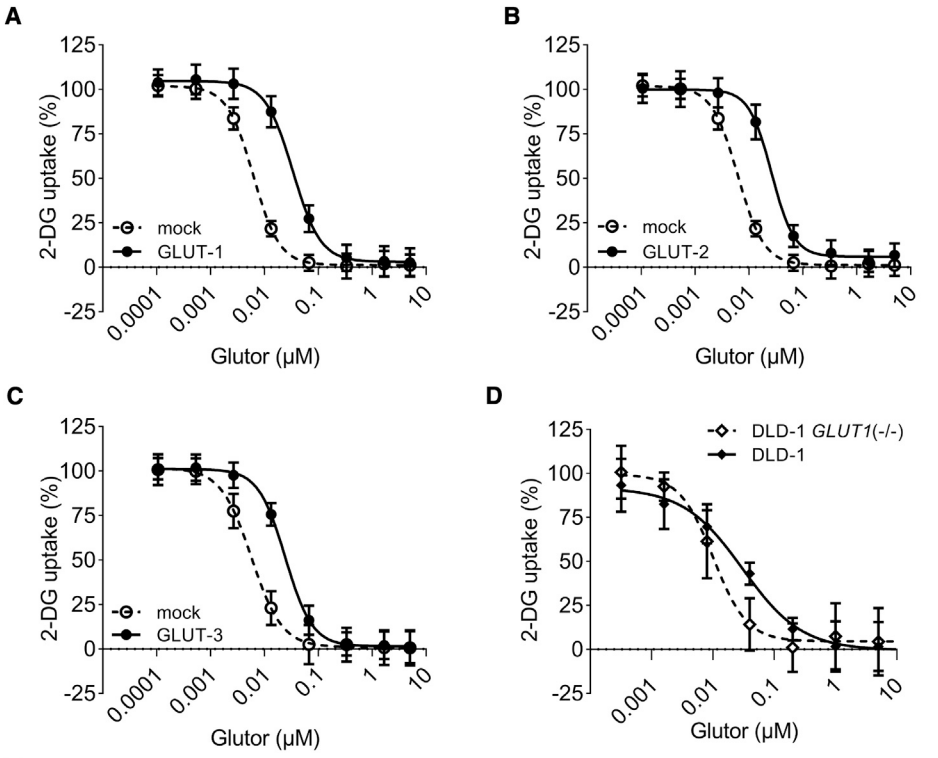

E

CHO	IC_{50}(GLUT-1)	IC_{50}(GLUT-2)	IC_{50}(GLUT-3)	IC_{50}(GLUT-4)	DLD-1	IC_{50}
Mock	6.2 ± 1.2 nM	6.2 ± 1.2 nM	5.9 ± 1.6 nM	6.2 ± 1.2 nM	wt	35.5 ± 4.8 nM
Overexpression	34 ± 3.5 nM	26 ± 2.9 nM	24 ± 2.6 nM	6.4 ± 1.7 nM	*GLUT1*(-/-)	9.8 ± 1.4 nM
Fold increase	**6.5 x**	**4.2 x**	**4.1 x**	**1.0 x**	Fold decrease	**3.6 x**

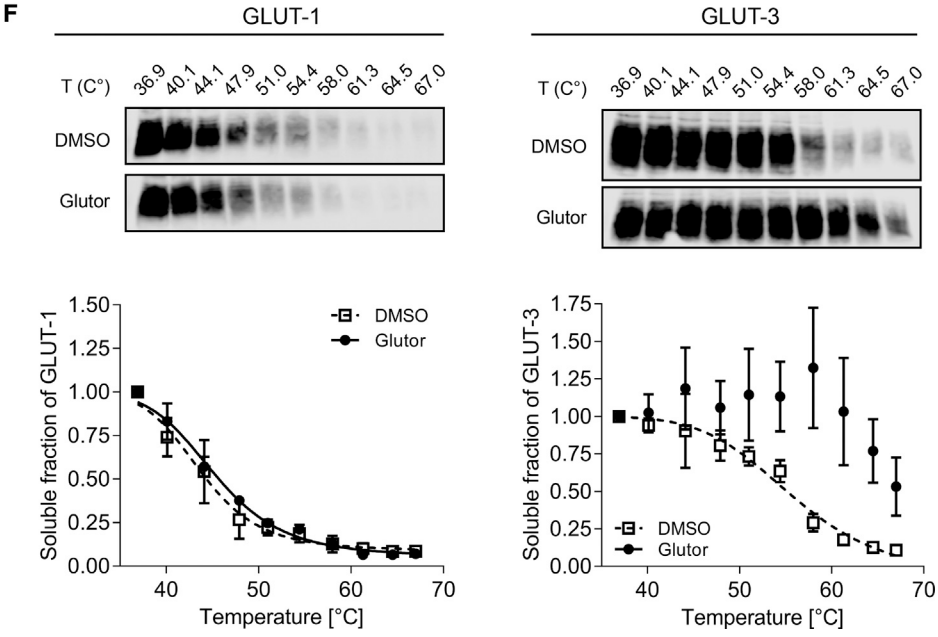

Figure 2. GLUT Isoform Selectivity of Glutor

(A–C) CHO cells were transfected with a plasmid coding for the different isoforms (see also Figures S2A–S2D) GLUT-1 (A), GLUT-2 (B), GLUT-3 (C), or GLUT-4 before performing the 2-DG uptake assay (see also Figure S2E). Mock transfected CHO cells served as control. Data are mean values ± SD (n = 3, N = 3).

(legend continued on next page)

containing medium-sized small molecules) to the GLUT-1/-3 selective Chromopynone-1 (Karageorgis et al., 2018) and the GLUT-1 selective inhibitor BAY-876 (Siebeneicher et al., 2016b) (Figure 1C). The GLUT-1 selective inhibitor WZB117 (Liu et al., 2012) is structurally distinct from the aforementioned small molecules (Figure 1C).

Glutor Targets GLUT-1, -2, and -3

To determine the isoform-selectivity of Glutor by means of a rescue experiment, the different GLUT isoforms were overexpressed (9- to 15-fold) in CHO cells (Figures S2A–S2D) (Karageorgis et al., 2018). Determination of 2-DG uptake revealed that overexpression of GLUT-1, GLUT-2, and GLUT-3 led to a shift to higher IC_{50} values for treatment with Glutor and, therefore, a partial rescue (Figures 2A–2C, 2E, and S2E). GLUT-1 overexpression increased the IC_{50} from 6.2 ± 1.2 to 34 ± 3.5 nM (6.5-fold) (Figures 2A and 2E) and GLUT-2 overexpression to 26 ± 2.9 nM (4.2-fold) (Figures 2B and 2E). GLUT-3 overexpression shifted the IC_{50} value from 5.9 ± 1.6 to 24 ± 2.6 nM (4.1-fold) (Figures 2C and 2E). In contrast, overexpression of GLUT-4 did not rescue the 2-DG uptake inhibition by Glutor (IC_{50} = 6.4 ± 1.7 nM compared with 6.2 ± 1.2 nM in mock transfected CHO cells; Figures 2E and S2E). These data suggest that Glutor inhibits 2-DG uptake by GLUT isoforms 1, 2, and 3, but most likely not by GLUT-4. Targeting of GLUT-1 and GLUT-3 was further confirmed by comparing inhibition of 2-DG uptake in DLD-1 cells, which mainly express GLUT-1, and the isogenic DLD-1 *GLUT1* (−/−) cell line which mainly expresses GLUT-3 (Figures S2F and S2G) (Karageorgis et al., 2018). In DLD-1 cells, 2-DG uptake was potently inhibited with an IC_{50} value of 35.5 ± 4.8 nM, and in DLD-1 *GLUT1* (−/−) cells uptake was inhibited with IC_{50} of 9.8 ± 1.4 nM (Figures 2D and 2E). In addition, Glutor increased the thermal stability of GLUT-3 in SW480 whole-cell lysates, which exhibit high GLUT-1 and GLUT-3 content (Schmidt et al., 2018) in a cellular thermal shift assay with a shift in melting temperature $\Delta T_m > 10^{\circ}C$ (Figure 2F), which further proves that the compound targets GLUT-3. The thermal shift of GLUT-1 in the presence of Glutor was smaller (Figure 2F). Overall, these results demonstrate engagement of GLUT-1 and GLUT-3, and suggest a more potent inhibition of GLUT-3 than GLUT-1 by Glutor.

Glutor Selectively Impairs Cancer Cell Growth and Inhibits Glycolytic Flux

Since inhibition of glucose uptake is expected to impair cell viability and proliferation, we investigated growth of 94, mostly malignant cell lines of different origin by means of sulforhodamine B assay after 72 h treatment with Glutor (Figure 3A; Table S3). The observed IC_{50} values ranged from low nanomolar (nM) to micromolar (μM) activity, and cell lines with IC_{50} > 30 μM were regarded as resistant to Glutor treatment. Gratifyingly, the growth of the non-malignant peripheral blood mononuclear cells (PBMCs) and IMR-90 embryonic lung cells was not impaired. The growth of 44 cancer cell lines of diverse tissue origin was suppressed with IC_{50} < 100 nM (Figure 3A, white bars). Among the nine most sensitive cell lines (upper 10%, $IC_{50} \leq 11$ nM, Figure 3A), three cell lines originate from urinary bladder carcinoma and are known to be glucose addicted, i.e., UM-UC-3 (Lea et al., 2015; Massari et al., 2016) (IC_{50} = 4 nM), 5637 (Lea et al., 2015) (IC_{50} = 6 nM), and T-24 (Lea et al., 2015) (IC_{50} = 11 nM). Aerobic glycolysis is the prevalent metabolic pathway in most urinary bladder cancers which renders this cancer highly glucose dependent (Lea et al., 2015). Other cell lines within the most sensitive 10% of the cell panel are MIA PaCa-2 (Daemen et al., 2015) (IC_{50} = 4 nM, pancreas), SK-N-AS (Huang et al., 2015) (IC_{50} = 6 nM, brain), and SU-DHL-6 (Liu et al., 2018) (IC_{50} = 11 nM, hematologic) cells, which are also known to exhibit high glucose dependence or sensitivity toward glycolytic inhibitors. To the best of our knowledge, for the remaining three cell lines within the upper 10% of the panel (TE671, WSU-NHL, and A431) no records about their metabolic phenotypes are available. Pancreatic cancer cell lines exhibited a similar sensitivity toward glucose starvation by means of Glutor treatment as urinary bladder cancer, except for the BxPC-3 (IC_{50} > 30 μM) cell line that was resistant (Figure 3A). In agreement with these results, BxPC-3 cells exhibit a lipogenic and non-glycolytic phenotype (Daemen et al., 2015). Growth of the model cell line HCT116 employed in the 2-DG import assay was impeded with an IC_{50} value of 40 nM (Figure 3A). The observed sensitivity tendencies in UM-UC-3, MIA PaCa-2, and HCT116 cells could be confirmed by means of kinetic live-cell analysis (Figures S3A–S3C). Growth rate determination revealed 50% of maximal growth inhibition (GI_{50}) values of 10.2 ± 1.1 nM for UM-UC-3, 58.4 ± 30.5 nM for MIA PaCa-2, and 428.1 ± 157.3 nM for HCT116 cells (Figures S3D and S3E). The sensitivities apparent from the cell line panel may provide guidance for possible applications of glucose import inhibition in particular cancers, such as urinary bladder carcinomas or pancreatic cancers, which are strongly dependent on glucose for proliferation.

Investigation of small-molecule activity in 2D culture systems is considered to be of limited significance (Moffat et al., 2017), and 3D cell culture systems are regarded as more physiologically relevant. Therefore, we generated spheroids of HCT116 cells of ca. 800 and 380 μm diameter as suggested by Kunz-Schughart and colleagues (Friedrich et al., 2009). Spheroid size determines gradients of, for example, O_2 and nutrients and formation of a necrotic core and may influence compound activity (Friedrich et al., 2009). Under conditions of glucose reduction (0 and 5 mM glucose), cytotoxic events (monitored by propidium iodide [PI] staining) were observed in 800-μm spheroids after 24 h and resulted in the enlargement of the necrotic spheroid core area and, finally, in spheroid bursting under glucose-free conditions (Figures S4A and S4B). Treatment with Glutor mirrored the effect of glucose starvation in a concentration-dependent manner (Figures S4C and S4D). Glucose starvation or treatment of HCT116 spheroids with a diameter of approximately 380 μm with increasing concentrations of Glutor revealed a similar behavior without bursting of the spheroid (Figure 3B). In cells cultured in monolayer with equal seeding density, onset of cytotoxicity

(D) 2-DG uptake assay was performed with DLD-1 and DLD-1 *GLUT1* (−/−) cells (see also Figures S2F and S2G). Data are mean values ± SD (n = 3, N = 3).
(E) Summary of IC_{50} values and fold change in IC_{50} values (A–D) (see also Figure S2E).
(F) Cellular thermal shift assay in SW480 whole-cell lysates by means of immunoblot-based detection of GLUT-1 and GLUT-3 (representative immunoblots) after compound or DMSO treatment. Data are mean values ± SD (n = 3).

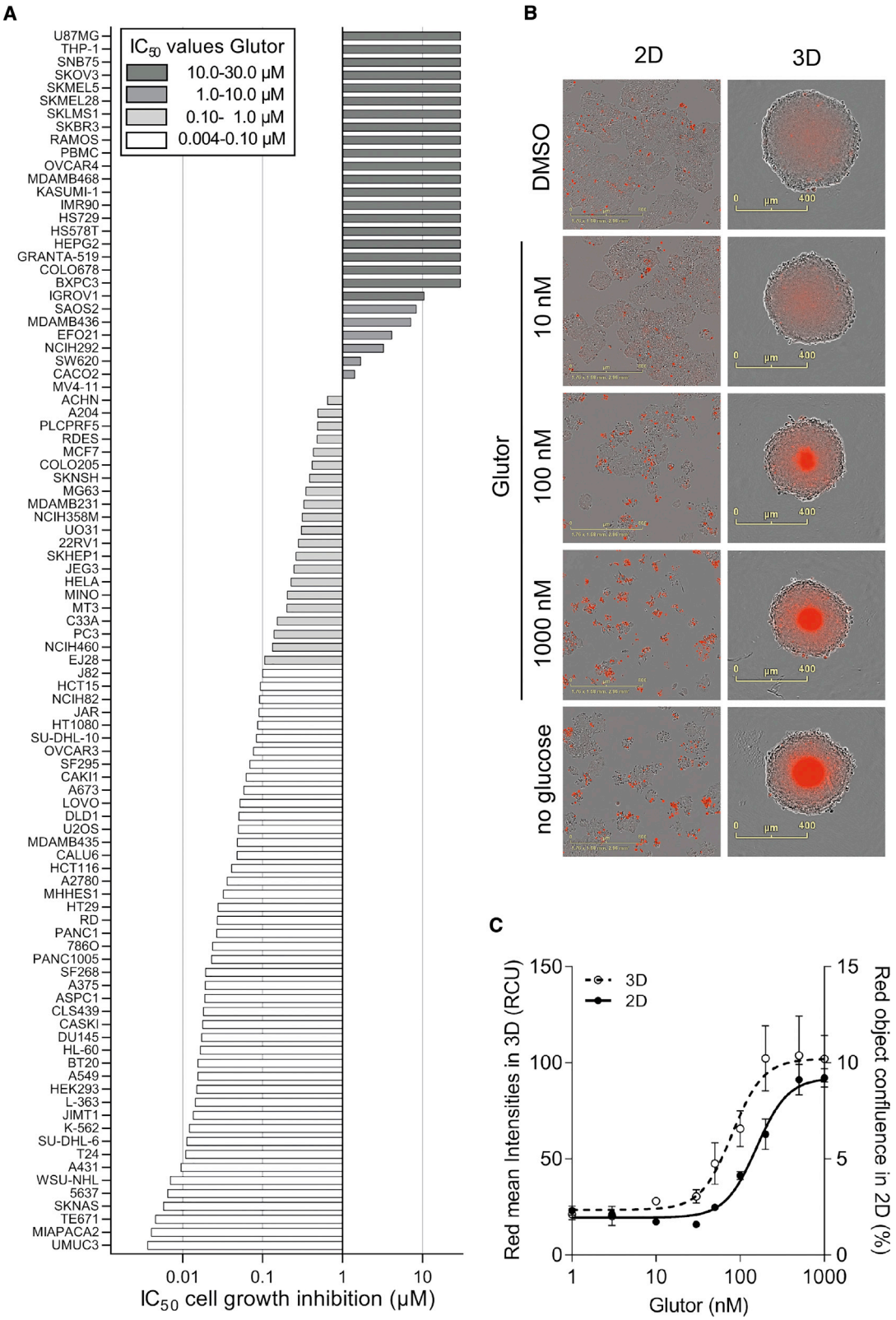

Figure 3. Glutor Impairs Cancer Growth and Enhances Formation of Necrotic Center in Spheroids

(A) Growth inhibition (IC_{50}) of 94 different cell lines by means of Glutor treatment was assessed using a sulforhodamine B assay (Vichai and Kirtikara, 2006) after 72 h (see also Figure S3).

(legend continued on next page)

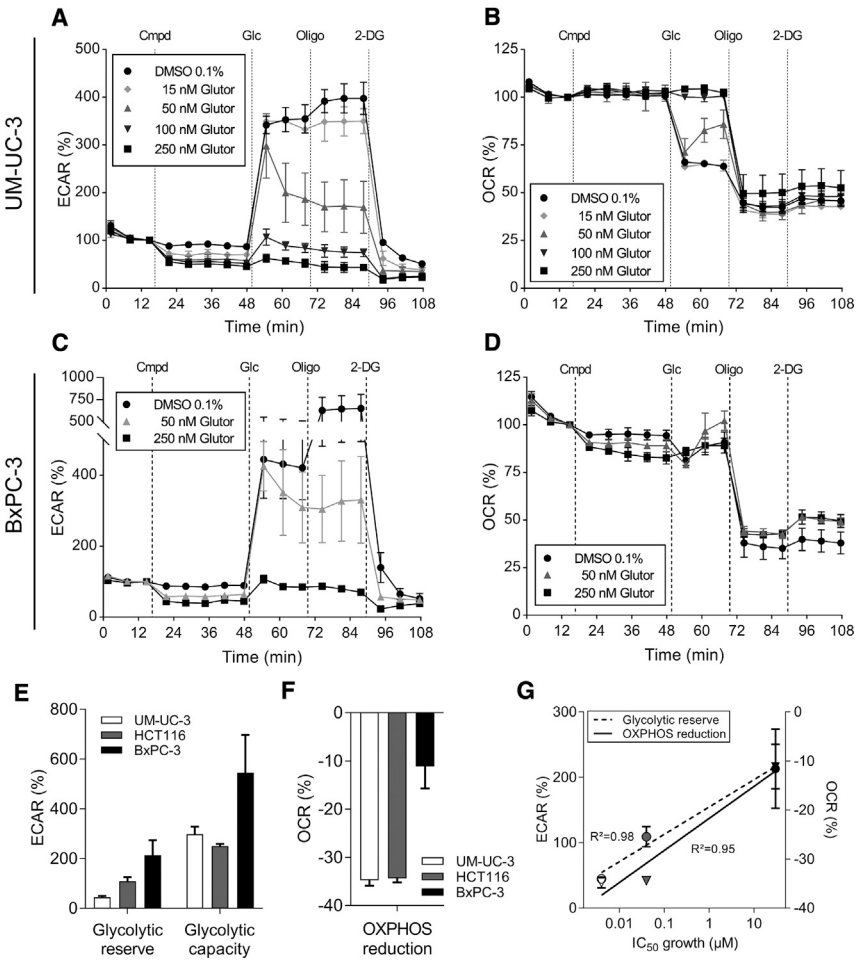

Figure 4. Glutor Inhibits Glycolytic Flux

(A–D) The impact of Glutor on glycolysis (extracellular acidification rate [ECAR]) and oxidative phosphorylation (oxygen consumption rate [OCR]) was assessed for UM-UC-3 cells (A and B) and BxPC-3 cells (C and D) using a glycolysis stress test. Data are mean values ± SD (n = 3, N = 3). Cmpd, compound; Glc, 10 mM glucose; Oligo, 2.5 μM oligomycin; 2-DG, 50 mM 2-deoxy-D-glucose.

(E and F) Glycolytic capacity, glycolytic reserve (E), and reduction of OCR after glucose addition (OXPHOS reduction) (F) of UM-UC-3, HCT116, and BxPC-3 cells were determined during the glycolysis stress test depicted in Figures 1E and 1F (HCT116) and (A–D) (UM-UC-3, BxPC-3).

(G) Linear regression and correlation coefficient R^2 of the glycolytic reserve and OXPHOS reduction as shown in (E and F) with IC_{50} values from the sulforhodamine B assay were determined (Figure 3A; Table S3).

was observed after 6 h of treatment. Quantification of PI staining after 72 h revealed that Glutor was 2-fold more effective in inducing cytotoxic events in spheroids (half maximal effective concentration [EC_{50}] = 81.7 ± 13.1 nM) than in cells cultured in monolayer (EC_{50} = 192.9 ± 34.4 nM) (Figure 3C). Of note, irrespective of the spheroid size, the cells at the outer border of the spheroid stayed viable during the experiment. These results prove that the potent growth inhibitory effect of GLUT inhibition observed in 2D cell culture can be recapitulated under 3D cell culture conditions.

To gain further insight into the different cell line responses to Glutor treatment, the metabolic profiles of the most sensitive cell line UM-UC-3 (Figures 4A and 4B), the Glutor-sensitive HCT116 cell line (Figures 1F and 1G), and the resistant BxPC-3 cell line (Figures 4C and 4D) were analyzed in a glycolytic stress test after 1.5 h glucose deprivation. Addition of 250 nM Glutor blocked glycolytic flux (ECAR) in all investigated cell lines (Figures 1F, 4A, and 4C). However, glycolytic stress responses in untreated cell lines revealed differences (Figures 4E–4G). The Glutor-sensitive cell lines HCT116 (Figures 1F and 1G) and UM-UC-3 (Figures 4A and 4B) switched from OXPHOS to glycolysis upon glucose addition, which reduced the oxygen consumption rate by 34% (Figures 4F and 4G). In contrast, the Glutor-resistant BxPC-3 cell line (Figures 4C and 4D) increased glycolysis upon glucose addition (Glc), but respiration remained at a constant high level (OXPHOS reduction 11%, Figures 4F and 4G). Impairment of mitochondrial ATP production by oligomycin (Figure 4D) induced a strong shift from OXPHOS to glycolysis in BxPC-3 cells such that these cells displayed the highest glycolytic capacity (545% ECAR, Figure 4E) and reserve (213% ECAR, Figures 4E and 4G). As mentioned before, BxPC-3 cells possess a lipogenic and non-glycolytic phenotype, which matches with our observations (Daemen et al., 2015). The Glutor-sensitive cell lines HCT116 and UM-UC-3 accelerated the rate of glycolysis after OXPHOS blockage by 109% and 45%, respectively (glycolytic reserve, Figure 4E). The cellular growth behavior of HCT116 and UM-UC-3 cells is known to depend on glucose (Ma et al., 2014; Massari et al., 2016). Notably, the switch from respiration to glycolysis upon glucose addition, as well as the glycolytic reserve of the investigated cell lines, correlated with the IC_{50} for growth inhibition (Table S3; Figure 3A) and, therefore, the cellular sensitivity toward compound treatment (Figure 4G). Similar observation was described by Liu et al. (2018), whereby glucose-dependent B cell lymphoma possessed a lower glycolytic reserve than lymphoma cell lines that are dependent on other nutrients (in this case glutamine).

(B) HCT116 cells were seeded in monolayer (2D) or as spheroids (3D, 380 μm diameter) and treated with varying Glutor or glucose concentrations and propidium iodide (PI) to detect dead cells. Cell growth and toxic events were monitored by means of live-cell imaging. Representative images are shown for 72 h of compound treatment (see also Figures S4A and S4C).

(C) Toxicity was analyzed by means of PI intensity (3D) or red confluence (2D) (see also Figures S4B and S4D). Data are representative values ± SD (n = 3, N = 8).

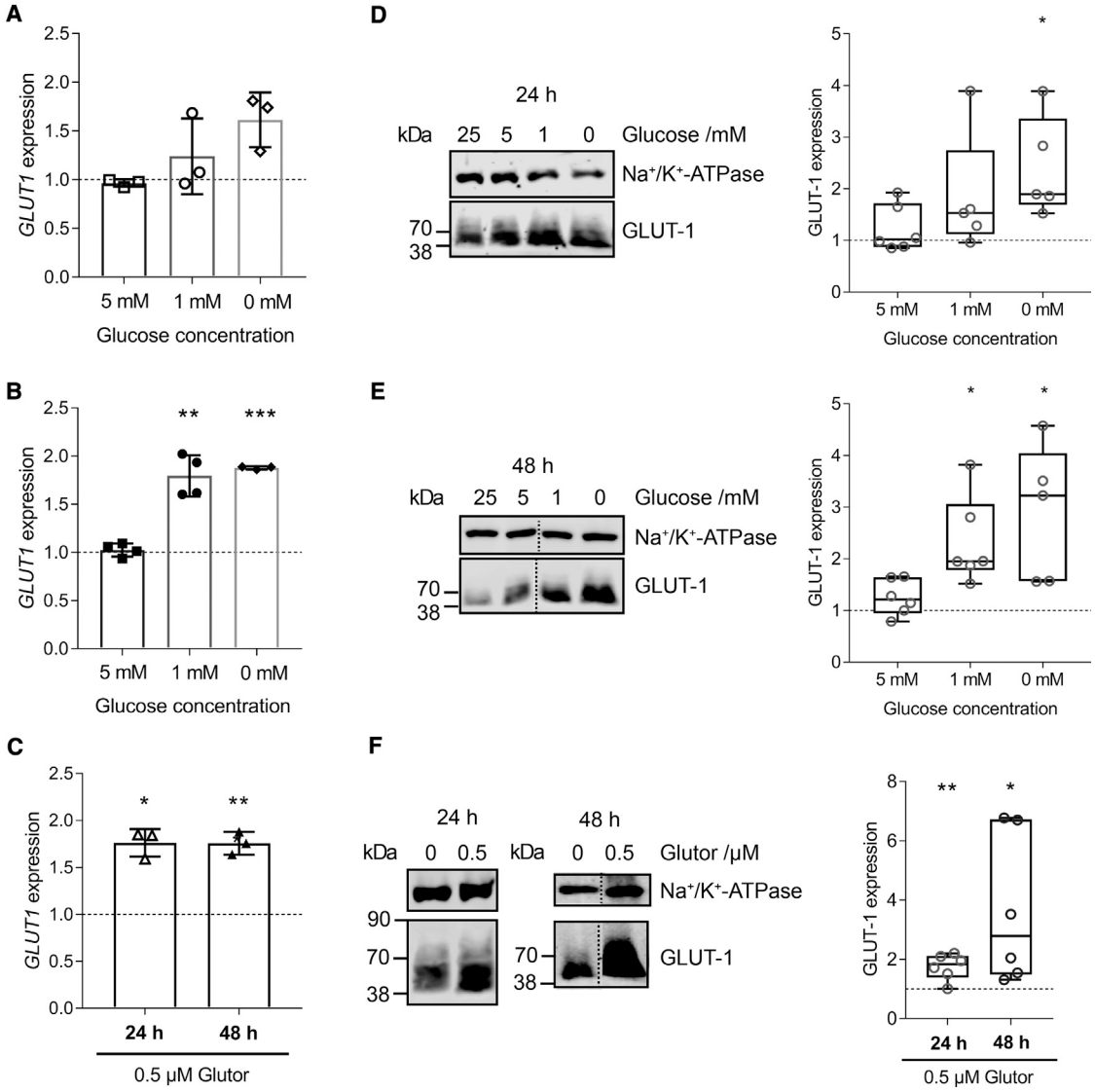

Figure 5. Glutor and Glucose Starvation Lead to GLUT-1 Upregulation

(A–C) DLD-1 cells were treated with the indicated glucose concentrations for 24 h (A and D) or 48 h (B and E) or with 0.5 μM Glutor at 25 mM glucose for 24 or 48 h (C and F). (A–C) qRT-PCR was performed using specific primers for *GLUT1* or *ATP1A1*, *TUBB*, and *ACTB* as reference genes. All values were normalized to values of cells treated with 25 mM glucose (A and B) (dotted line) or DMSO (C) (dotted line), respectively. Data shown are mean values ± SD of n = 3 (A and C) or n = 4 (B) (see also Figures S4E and S4F). (D–F) Cells were lysed and GLUT-1 and Na^+-K^+-ATPase were detected using immunoblotting. Representative immunoblots of six biological replicates are depicted. A dashed line indicates cropped immunoblot images from the same blot. The band intensities for GLUT-1 were normalized to the values for Na^+-K^+-ATPase and the respective control (D and E) (25 mM glucose, dotted line); (F) (DMSO, dotted line). Data are median values of n = 6 with the interquartile range. Statistical analysis was performed using unpaired two-tailed t test with Welch's correction. *p < 0.05, **p < 0.01, ***p < 0.001. See also Figure S4G for qRT-PCR data on HCT116 cells.

Inhibition of Glucose Uptake by Glutor Induces Upregulation of GLUT-1 and GLUT-3 Expression

In cancer cells (Marín-Hernández et al., 2014) and in neuronal rat cells (Nagamatsu et al., 1994) GLUT-1 and GLUT-3 expression is upregulated under glucose deprivation to increase nutrient uptake. To investigate whether this rescue mechanism is also operative upon inhibition of glucose import, we investigated *GLUT1-4* (also known as *SLC2A1-4*) expression after treatment with Glutor in comparison with glucose depletion. To this end, the colorectal carcinoma-derived DLD-1 cells, which mainly express GLUT-1, were treated with 0.5 μM Glutor in the presence of high glucose concentration (25 mM) for 24 and 48 h, and mRNA (*GLUT1-4*) and protein (only GLUT-1 and -3) levels were quantified by means of qRT-PCR and immunoblotting, respectively. By analogy, the cells were cultured in the absence of the inhibitor, employing 25 mM glucose, physiological glucose concentration (5 mM) (Güemes et al., 2016), or under glucose deprivation (1 mM glucose or no glucose) for 24 and 48 h (Figures 5 and 6).

Under hypoglycemic conditions (1 mM glucose or no glucose) after 24 and 48 h *GLUT1* and *GLUT3* mRNA levels had increased

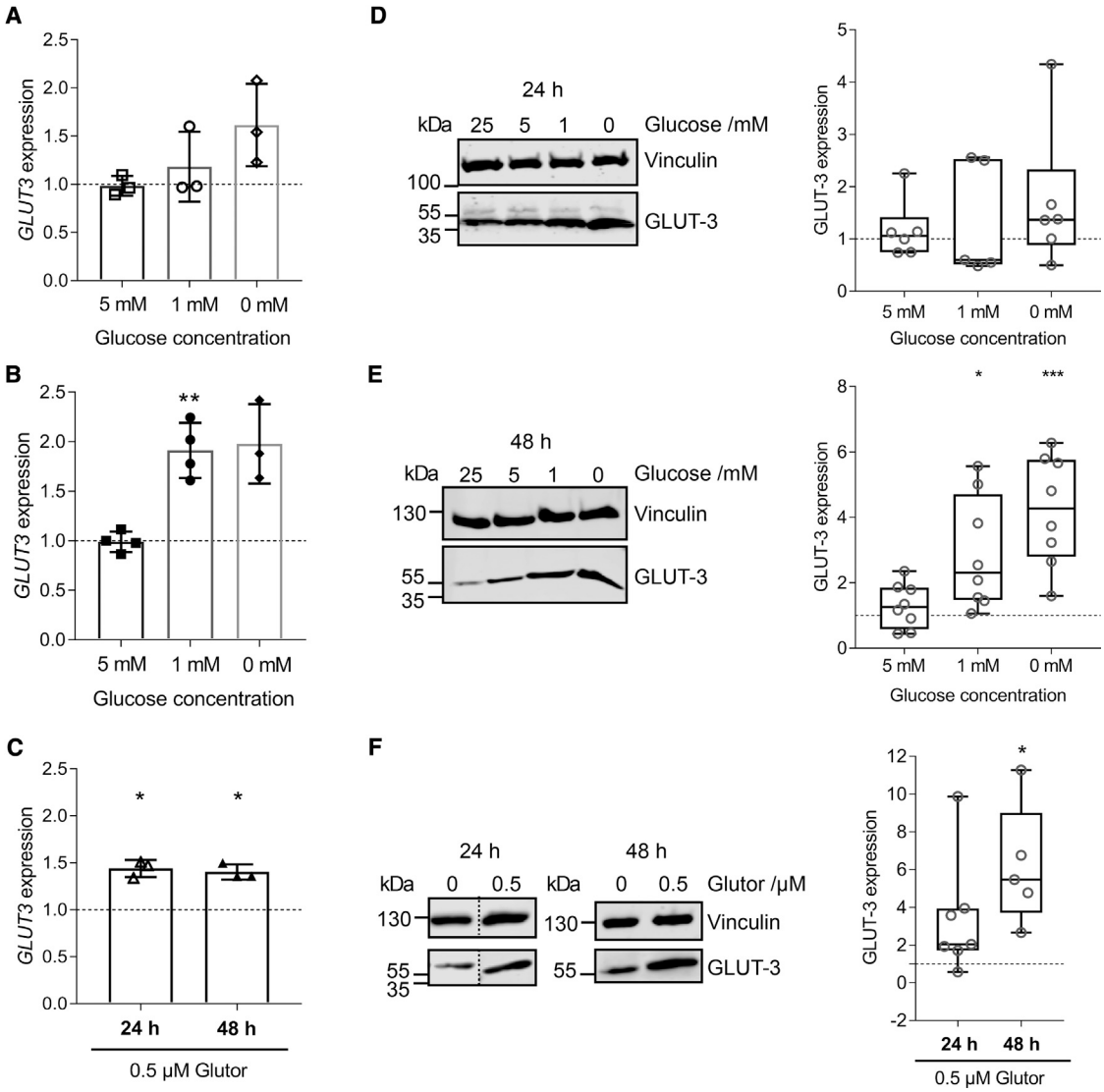

Figure 6. Glutor and Hypoglycemia Lead to GLUT-3 Upregulation

(A–C) DLD-1 cells were treated with the indicated glucose concentrations for 24 h (A and D) or 48 h (B and E) or were treated with 0.5 μM Glutor at 25 mM glucose for 24 or 48 h (C and F). (A–C) qRT-PCR was performed using specific primers for *GLUT3* or *ATP1A1*, *TUBB* and *ACTB* as reference genes All values were normalized to values of cells treated with 25 mM glucose (A and B) (dotted line) or DMSO (C) (dotted line), respectively. Data shown are mean values ± SD of n = 3 (A and C) or n = 4 (B) (see also Figures S4E and S4F). (D–F) Cells were lysed and GLUT-3 and Vinculin were detected using immunoblotting. Representative immunoblots of n = 6 (D), n = 8 (E), or n = 7 (F) are depicted. A dashed line indicates cropped immunoblot images from the same blot. The band intensities for GLUT-3 were normalized to the values for Vinculin and the respective control (D and E) (25 mM glucose, dotted line); (F) (DMSO, dotted line). Data are median values of n = 6 (D), n = 8 (E), or n = 7 (F) with the interquartile range. Statistical analysis was performed using unpaired two-tailed t test with Welch's correction. *p < 0.05, **p < 0.01, ***p < 0.001. See also Figure S4G for qRT-PCR data on HCT116 cells.

ca. 1.6-fold (Figures 5A, 5B, 6A, and 6B). After treatment with Glutor the level of *GLUT1* (Figure 5C) and *GLUT3* (Figure 6C) mRNA already increased significantly after 24 h by 1.8- and 1.4-fold, respectively. Under hypoglycemic conditions (no glucose or in the presence of 0.5 μM Glutor) the level of the GLUT-1 protein already increased by ca. 2-fold after 24 h (Figures 5D and 5F), and, after 48 h, a ca. 3-fold increase was detected (Figures 5E and 5F). Under hypoglycemic conditions and in the presence of Glutor, a significant increase in GLUT-3 protein level was observed after 48 h (4.3- and 5.5-fold, respectively, Figures 6E and 6F). Notably, GLUT-3 protein expression increased more than GLUT-1 expression (4.3- versus 3.2-fold in the absence of glucose; 5.5- versus 2.8-fold in the presence of 0.5 μM Glutor; compare Figures 5E, 5F, 6E, and 6F). Expression of *GLUT4* was not increased under glucose starvation conditions upon treatment with Glutor after 24 and 48 h (see Figures S4E and S4F). *GLUT2* mRNA could not be detected for all tested conditions.

A significant upregulation of *GLUT3* mRNA by 1.5-fold could be also observed for HCT116 cells after 48 h of treatment with 0.5 μM Glutor or under glucose reduction (0 or 1 mM) (Figure S4G). However, the *GLUT1* mRNA level was unaltered under

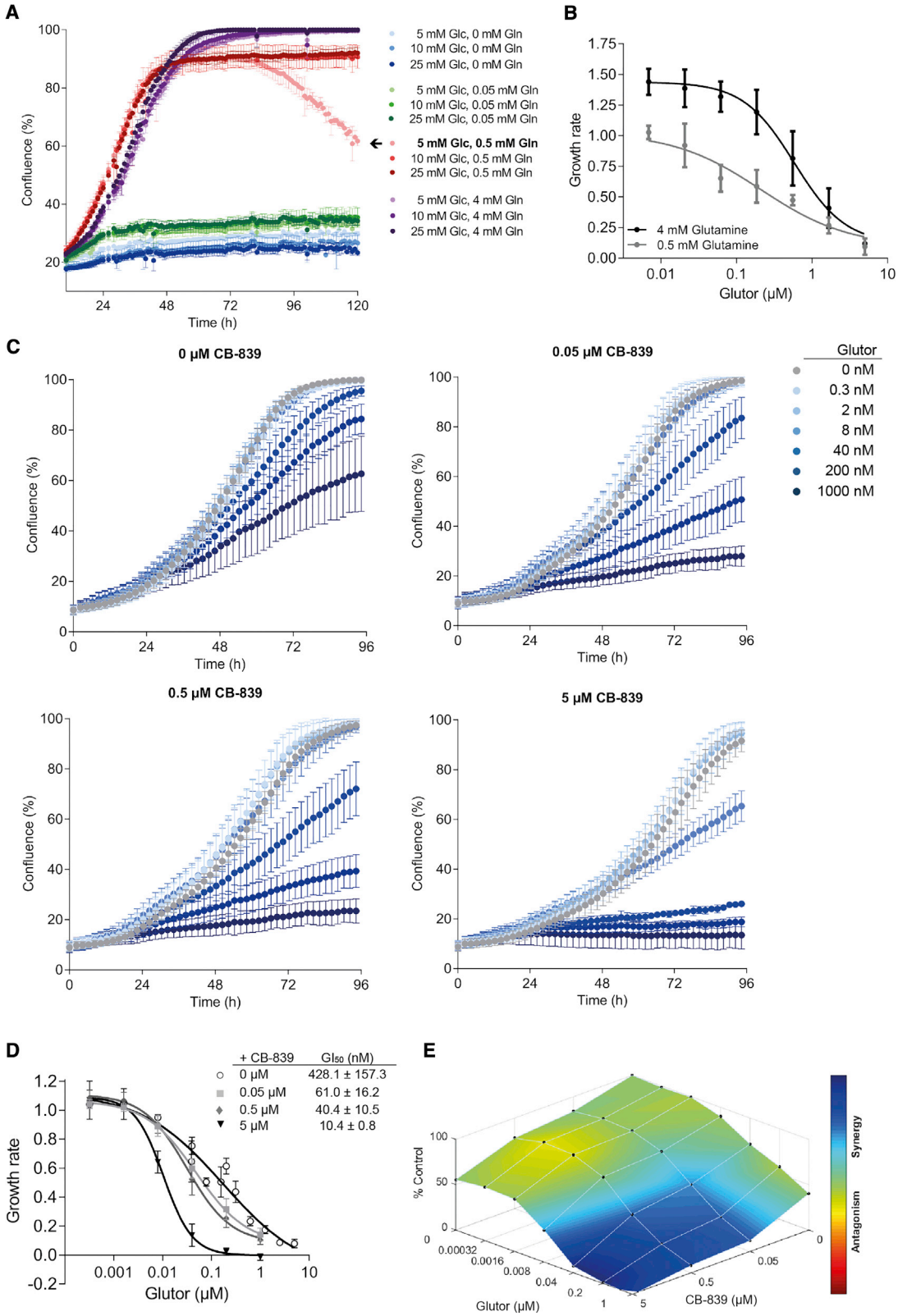

Figure 7. Disruption of Glutamine Metabolism Sensitizes HCT116 Cells to Glucose Deprivation

(A) HCT116 cells were cultured over 120 h under different nutrient concentrations (see also Figure S4H). Cell growth was monitored via live-cell imaging over a period of 5 days. Cellular confluence was analyzed as a measure of growth. Data show representative values ± SD (n = 3, N = 3).

(legend continued on next page)

hypoglycemic conditions (Figure S4G). These findings confirm the observations that a hypoglycemic environment induces overexpression of GLUT-1, and especially GLUT-3 (Marín-Hernández et al., 2014) and proves that the same effect is achieved by inhibition of glucose import through Glutor. As observed in adipose tissue (Khayat et al., 1998), cancer cells only increase GLUT-1 and GLUT-3 mRNA and protein level, but not *GLUT4* (and *GLUT2*) mRNA, under glucose deprivation. Thereby cancer cells employ a rescue mechanism to increase glucose uptake in times of glucose shortage. Thus, inhibition of GLUT-1 alone may not be sufficient to efficiently inhibit cancer cell growth, and the GLUT-2 inhibiting activity of Glutor is at least less important for reduction of cancer cell growth in the presence of the inhibitor.

Glucose Uptake Inhibition by Glutor and Glutaminase GLS Inhibition Synergistically Inhibits Cell Growth

Nutrient uptake, utilization, and dependence of cancer cells may differ and vary depending on cancer cell type and growth conditions; for example, nutrient availability and microenvironment (Davidson et al., 2016; Stock et al., 2016). In particular, cancer cells use glutamine for amino acid synthesis and redox balance maintenance to enable cell growth, and some cancers are glutamine addicted (Eagle, 1955). Thus, combination of glucose uptake inhibition with inhibition of glutamine metabolism may synergistically suppress cell growth.

Investigation of HCT116 revealed that, under glutamine depletion (0 mM glutamine and 25 mM glucose), cell growth is more reduced than under glucose withdrawal (0 mM glucose and 4 mM glutamine) (Figure S4H), suggesting that reduction of glutamine concentration might sensitize the cells toward glucose starvation. Thus, we examined the growth of HCT116 cells in the presence of different glucose and glutamine concentrations (Figure 7A). At low glutamine concentration (0.05 and 0 mM) cell growth was impeded, regardless of the prevalent glucose concentration (25, 10, or 5 mM) (Figure 7A). At physiological glutamine concentration (0.5 mM) (Scriver and Rosenberg, 1973), reduced glucose (5 mM) led to strong growth reduction that could only be circumvented in the presence of higher glucose levels (10 or 25 mM). On the contrary, at physiological glucose concentration (5 mM) (Güemes et al., 2016), the growth of HCT116 cells was dependent on the presence of sufficient amounts of glutamine (Figure 7A). This finding suggests that impairment of HCT116 cell growth by means of glucose import inhibition should be more efficient at reduced glutamine concentrations. Indeed, in the presence of 4 mM glutamine, Glutor inhibited HCT116 growth with a GI_{50} value of 604.1 ± 21.0 nM, whereas in the presence of 0.5 mM glutamine the GI_{50} value was lowered to 210.3 ± 43.7 nM (Figure 7B).

In light of this finding, we investigated co-treatment with Glutor and the glutaminase (GLS) inhibitor CB-839 (Gross et al., 2014), which inhibits growth of triple-negative breast cancer with low nanomolar activity. We treated HCT116 cells, which are less sensitive toward CB-839 treatment (GI_{50} = 16.2 μM) (National Cancer Institute, 2019; NCI-60 panel, CAS(CB-839) 1439399-58-2), with CB-839 at different concentrations together with varying concentrations of Glutor in the presence of 4 mM glutamine and 25 mM glucose (Figures 7C–7E and S5). The co-treatment led to a maximal 40-fold improvement of the GI_{50} from 428.1 ± 157.3 nM (0 μM CB-839) to 10.4 ± 0.8 nM in the presence of 5 μM CB-839 (Figure 7D). The GI_{50} of CB-839 then decreased from 11.8 μM (0 μM Glutor), which is in line with the reported GI_{50} value from the NCI-60 panel, to GI_{50} < 50 nM (1 μM Glutor) (Figures S5A and S5B). Analysis of the data employing three independent classical synergy models, namely Loewe (1953) (Figures 7E and S5D), highest single agent (Tan et al., 2012) (Figures S5E and S5F), and Bliss (1939) (Figures S5G and S5H), confirmed the synergistic effect with regard to growth inhibition in a concentration range for Glutor between 8 nM to 1 μM and 50 nM to 5 μM CB-839 (Figures 7E and S5, see Supplemental Information for model definitions). The analysis clearly indicates that dual targeting of glutamine metabolism and glucose uptake may offer a promising approach for synergistic inhibition of tumor cell growth. Moreover, Glutor acts not only synergistically with CB-839 but may sensitize cell lines to GLS inhibition.

DISCUSSION

Cancer, immune and stem cells adapt their metabolism to meet the requirements of sustained proliferation by increasing aerobic glycolysis (Warburg effect) and glucose uptake (Cliff and Dalton, 2017; Jones and Bianchi, 2015). To meet this demand, cancer cells upregulate facilitative GLUTs, in particular GLUT-1, and small-molecule inhibition of glucose uptake has been proposed as a promising approach to cancer drug discovery. Because the relevant glucose transporter isoforms GLUT-1-4 are expressed in a tissue-specific manner and are involved in various central processes, selective inhibition of GLUT-1 was deemed necessary for a wide therapeutic window. However, both GLUT-1 and GLUT-3 are upregulated in various cancers, suggesting that dual inhibition of both transporters may be required for successful glucose deprivation. A potent and selective GLUT-1 inhibitor has been developed, but data on its application have not been reported (Siebeneicher et al., 2016a, 2016b). We recently described a dual-selective GLUT-1/-3 inhibitor, which, however, suffers from low potency (Karageorgis et al., 2018).

We discovered the piperazin-one Glutor (**(S)-3a**) as a potent glucose uptake inhibitor. Glutor targets glucose transporters GLUT-1, -2, and -3. Inhibition of glucose uptake by Glutor attenuates glycolytic flux and increases the expression of GLUT-1 and GLUT-3. Glutor potently suppresses growth of a

(B) HCT116 cells were cultured over 96 h under high (4 mM) or physiological (0.5 mM) glutamine concentration and in presence of 25 mM glucose. The growth behavior was assessed by means of live-cell imaging. Cellular confluence was analyzed as a measure of cell growth. The slopes of the exponential growth phase were used for GI_{50} determination. Data show mean values ± SD (n = 3, N = 3).

(C–E) HCT116 cells were cultured under 25 mM glucose and 4 mM glutamine and treated with different concentrations of CB-839 and Glutor. Cell growth was monitored via live-cell imaging over 5 days. Cellular confluence was analyzed as a measure of growth (C). GI_{50} values for Glutor in the presence of different CB-839 concentrations were determined using the growth rates between 24 and 72 h (D). For better visualization all values were normalized to the 0 μM CB-839 control. Synergism and antagonism scores were determined with the software combenefit (Di Veroli et al., 2016) (see also Figure S5) employing the Loewe model and the score distribution is depicted in the dose-response surface within the concentration space. Data represent mean values ± SD (n = 3, N = 3).

variety of cancer cell lines of different origin in 2D (monolayer) and 3D (spheroids) culture systems, but not of non-malignant IMR-90 and PBMCs, which were employed to assess unspecific cytotoxicity. Nearly half of the examined cancer cell lines (44) were inhibited with an IC_{50} below 100 nM, thus demonstrating the broad applicability for treatment against diverse cancer types. Furthermore, urinary bladder and pancreatic cancer cell lines were among the most sensitive cell lines within the conducted cell panel. Glucose dependence is a metabolic phenotype observed in both tissue-derived cancer types, and interference of the glycolytic flux alone or in combination with other cancer targeting agents were proposed as therapeutic approaches (Daemen et al., 2015; Lea et al., 2015; Massari et al., 2016).

Our results indicate that dual inhibition of GLUT-1 and -3 should be particularly effective for inhibition of tumor cell growth. We demonstrate that tumor cells upregulate mainly *GLUT3* and *GLUT1* in a cell-dependent manner (but not *GLUT2*) upon glucose starvation or treatment with Glutor. Hence, a dual-specific inhibitor will be more efficacious than a mono-selective compound, and may overcome this cellular rescue mechanism (Marín-Hernández et al., 2014; Nagamatsu et al., 1994). In fact, targeting of upregulated GLUT-3 may be particularly relevant, because GLUT-3 has a lower K_m value for glucose (K_m for 2-DG = 1.4 mM) than GLUT-1 (K_m for 2-DG = 5 mM) (Zhao and Keating, 2007), thereby assuring efficient glucose uptake also at low glucose concentrations. By analogy, GLUT-3 may have a protecting function from inhibitor influence for neurons, which express mainly GLUT-3 and rely on glucose. The low K_m and high capacity of GLUT-3 should give neurons a competitive advantage with respect to glucose at environmental glucose concentrations (1–2 mM) (Simpson et al., 2008).

Apart from glucose, cells metabolize glutamine, which is the most abundant amino acid in plasma (Daye and Wellen, 2012). An intricate interplay between glucose and glutamine metabolism exists in cells that coordinate ATP supply and availability of biosynthetic precursors, which are required for proliferation, as well as redox balance maintenance. While in normal cells glucose is converted to citrate, which fuels fatty acid synthesis, glutamine is used as an anaplerotic precursor for the tricarboxylic acid cycle and supports mitochondrial respiration, ATP production, and synthesis of nucleotides and some amino acids. Cells can synthesize glutamine, and glutamine is non-essential in normal, non-dividing tissue. However, under conditions of stress or proliferation (e.g., T cell activation) (Ardawi, 1988; Carr et al., 2010), the glutamine consumption outpaces the glutamine supply, and glutamine becomes an essential amino acid (Still and Yuneva, 2017). Thus, small-molecule inhibitors of glutamine metabolism are actively being developed as anti-cancer drugs (Akins et al., 2018). Various genetic alterations are known to drive glutamine metabolism, for example, in MYC, KRAS, HIF1, HER2, p53, JAK/STAT, mTOR, and NRF2 activation, PKCζ loss, PTEN loss, and RB1 loss (Altman et al., 2016), and can confer glutamine/glutaminolysis dependence. Thus, cancer cells rely on both glucose and glutamine, and despite fulfilling separate roles in cellular metabolism both metabolic pathways may compensate for one another (Daye and Wellen, 2012). Due to this metabolic plasticity, cancer cells may adapt to glucose- or glutamine-deprived conditions, for example, upregulating glutamine metabolism during glycolysis suppression (Lukey et al., 2018). In this context, reduction of GLUT-1 expression sensitizes lung cancer cells to inhibition of glutamine utilization (Lee et al., 2016). Naturally, the concomitant targeting of glutamine (unspecific transaminase inhibitor aminooxyacetate) and glucose metabolism (with 2-DG) has a cumulative effect on ovarian cancer cell growth suppression (Sun et al., 2017).

We demonstrated that co-treatment of HCT116 cells with Glutor and glutaminase inhibitor CB-839 very potently and synergistically inhibited cancer cell growth at high glucose and glutamine levels. Thus, simultaneous inhibition of the two major nutrient supply mechanisms employed by cancer cells can synergistically reduce cancer cell growth. Such a dual inhibition may enable particularly effective suppression of cancer cell growth to avoid therapy resistance through metabolic plasticity. Overall, our findings suggest that both cellular rescue mechanisms (i.e., upregulation of glucose import) and the metabolic plasticity of cancer to increase alternative use of glutamine as nutrient may be synergistically overcome by simultaneous inhibition of glucose transporters GLUT-1 and -3 and glutamine metabolism, for example, by inhibition of glutaminase GLS.

Finally, we note that, beyond the potential application in the discovery of anti-cancer agents, inhibition of glucose uptake via GLUTs may offer promising opportunities for the treatment of diseases related to inflammation, immunity, and infection, such as graft-versus-host disease (Macintyre et al., 2014), colitis (Macintyre et al., 2014), systemic lupus erythematosus (Yin et al., 2015), psoriasis (Zhang et al., 2018), rhinoviral (Gualdoni et al., 2018) and bacterial infections (Escoll and Buchrieser, 2018), and HIV persistence (Palmer et al., 2016), because all these diseases are connected to an increased glucose utilization.

SIGNIFICANCE

Cancer cell growth is sustained by increased glucose demand, which frequently induces upregulation of glucose transporters GLUT-1 and -3. Therefore, interference with tumor metabolism by means of GLUT inhibition is considered a relevant strategy to impair cancer growth. However, currently available inhibitors of the glucose transporters (GLUTs) suffer from low potency or mainly target GLUT-1. We discovered a GLUT-1/-2/-3-selective inhibitor that potently inhibits glucose entry, glycolysis, and cancer cell growth in monolayer and spheroids. The use of GLUT-1/-3 targeting—rather than isoform-specific inhibitors—enables efficient suppression of glucose uptake because cells upregulate both GLUT-1 and GLUT-3 upon glucose starvation caused by small-molecule-mediated inhibition of glucose uptake. Cancer cell growth and survival may also be supported by glutamine as an additional nutrient source, which confers metabolic flexibility. We demonstrate that simultaneous targeting of glucose uptake by means of GLUT-1/-3 inhibition and glutaminolysis synergistically inhibits cancer cell growth. This dual strategy may open up unprecedented opportunities to overcome rescue mechanisms and metabolic plasticity in cancer, and may inspire chemical biology

and medicinal chemistry programs aimed at the discovery of alternative strategies and compound classes for the treatment of cancer.

STAR★METHODS

Detailed methods are provided in the online version of this paper and include the following:

- KEY RESOURCES TABLE
- CONTACT FOR REAGENT AND RESOURCE SHARING
- EXPERIMENTAL MODEL AND SUBJECT DETAILS
  - Cell Lines
- METHOD DETAILS
  - Biological Experiments
  - Synthetic Procedure
- QUANTIFICATION AND STATISTICAL ANALYSIS
- DATA AND CODE AVAILABILITY

SUPPLEMENTAL INFORMATION

Supplemental Information can be found online at https://doi.org/10.1016/j.chembiol.2019.06.005.

ACKNOWLEDGMENTS

Research at the Max Planck Institute of Molecular Physiology was supported by the Max Planck Society and the European Research Council under the European Union's Seventh Framework Program (FP7/2007–2013, ERC Grant agreement no. 268309). J.C. and E.S.R. acknowledge the International Max-Planck Research School for a doctoral scholarship. G.K. received funding from the Alexander von Humboldt-Stiftung for a post-doctoral fellowship. The compound management and screening center (COMAS) in Dortmund is acknowledged for performing the high-throughput screening and the orthogonal and counter screens. The Lead Discovery Center is acknowledged for sharing the cell panel data. We acknowledge Beate Schölermann for the technical support.

AUTHOR CONTRIBUTIONS

S.Z. and H.W. designed the research. E.S.R., G.K., M.S., J.N., S.B., A.C., and A.B. performed the biological research. E.S.R., J.N., and M.C.M.S. performed the compound synthesis. E.S.R., G.K., M.S., J.N., M.C.M.S., A.B., and S.Z. analyzed the data. J.C. contributed to compound development. L.K. and C.S. performed the X-ray structure analysis. E.S.R., S.Z., and H.W. wrote the manuscript. All authors discussed the results and commented on the manuscript.

DECLARATION OF INTERESTS

H.W. is sponsor of a drug discovery program at the Lead Discovery Center of the Max-Planck-Gesellschaft aimed at the development of GLUT inhibitors.

Received: February 22, 2019
Revised: May 31, 2019
Accepted: June 17, 2019
Published: July 11, 2019

REFERENCES

Akins, N.S., Nielson, T.C., and Le, H.V. (2018). Inhibition of glycolysis and glutaminolysis: an emerging drug discovery approach to combat cancer. Curr. Top. Med. Chem. *18*, 494–504.

Allen, C.L., Atkinson, B.N., and Williams, J.M.J. (2012). Transamidation of primary amides with amines using hydroxylamine hydrochloride as an inorganic catalyst. Angew. Chem. Int. Ed. *51*, 1383–1386.

Altman, B.J., Stine, Z.E., and Dang, C.V. (2016). From Krebs to clinic: glutamine metabolism to cancer therapy. Nat. Rev. Cancer *16*, 619–634.

Ardawi, M.S. (1988). Glutamine and glucose metabolism in human peripheral lymphocytes. Metabolism *37*, 99–103.

Ayala, F.R.R., Rocha, R.M., Carvalho, K.C., Carvalho, A.L., da Cunha, I.W., Lourenço, S.V., and Soares, F.A. (2010). GLUT1 and GLUT3 as potential prognostic markers for oral squamous cell carcinoma. Molecules *15*, 2374–2387.

Bliss, C.I. (1939). The toxicity of poisons applied jointly. Ann. Appl. Biol. *26*, 585–615.

Carr, E.L., Kelman, A., Wu, G.S., Gopaul, R., Senkevitch, E., Aghvanyan, A., Turay, A.M., and Frauwirth, K.A. (2010). Glutamine uptake and metabolism are coordinately regulated by ERK/MAPK during T lymphocyte activation. J. Immunol. *185*, 1037–1044.

Chrostowska, A., Matrane, A., Maki, D., Khayar, S., Ushiki, H., Graciaa, A., Belachemi, L., and Guillemin, J.-C. (2012). Are unsaturated isocyanides so different from the corresponding nitriles? Chemphyschem *13*, 226–236.

Cliff, T.S., and Dalton, S. (2017). Metabolic switching and cell fate decisions: implications for pluripotency, reprogramming and development. Curr. Opin. Genet. Dev. *46*, 44–49.

Creedon, S.M., Crowley, H.K., and McCarthy, D.G. (1998). Dehydration of formamides using the Burgess Reagent: a new route to isocyanides. J. Chem. Soc. Perkin Trans. *1*, 1015–1018.

Daemen, A., Peterson, D., Sahu, N., McCord, R., Du, X., Liu, B., Kowanetz, K., Hong, R., Moffat, J., Gao, M., et al. (2015). Metabolite profiling stratifies pancreatic ductal adenocarcinomas into subtypes with distinct sensitivities to metabolic inhibitors. Proc. Natl. Acad. Sci. U S A *112*, E4410–E4417.

Davidson, S.M., Papagiannakopoulos, T., Olenchock, B.A., Heyman, J.E., Keibler, M.A., Luengo, A., Bauer, M.R., Jha, A.K., O'Brien, J.P., Pierce, K.A., et al. (2016). Environment impacts the metabolic dependencies of Ras-driven non-small cell lung cancer. Cell Metab. *23*, 517–528.

Daye, D., and Wellen, K.E. (2012). Metabolic reprogramming in cancer: unraveling the role of glutamine in tumorigenesis. Semin. Cell Dev. Biol. *23*, 362–369.

Di Veroli, G.Y., Fornari, C., Wang, D., Mollard, S., Bramhall, J.L., Richards, F.M., and Jodrell, D.I. (2016). Combenefit: an interactive platform for the analysis and visualization of drug combinations. Bioinformatics *32*, 2866–2868.

Dolomanov, O.V., Bourhis, L.J., Gildea, R.J., Howard, J.A.K., and Puschmann, H. (2009). OLEX2: a complete structure solution, refinement and analysis program. J. Appl. Crystallogr. *42*, 339–341.

Eagle, H. (1955). Nutrition needs of mammalian cells in tissue culture. Science *122*, 501–514.

Escoll, P., and Buchrieser, C. (2018). Metabolic reprogramming of host cells upon bacterial infection: why shift to a Warburg-like metabolism? FEBS J. *285*, 2146–2160.

Fonteyne, P., Casneuf, V., Pauwels, P., van Damme, N., Peeters, M., Dierckx, R., and van de Wiele, C. (2009). Expression of hexokinases and glucose transporters in treated and untreated oesophageal adenocarcinoma. Histol. Histopathol. *24*, 971–977.

Friedrich, J., Seidel, C., Ebner, R., and Kunz-Schughart, L.A. (2009). Spheroid-based drug screen: considerations and practical approach. Nat. Protoc. *4*, 309–324.

Fulmer, G.R., Miller, A.J.M., Sherden, N.H., Gottlieb, H.E., Nudelman, A., Stoltz, B.M., Bercaw, J.E., and Goldberg, K.I. (2010). NMR chemical shifts of trace impurities: common laboratory solvents, organics, and gases in deuterated solvents relevant to the organometallic chemist. Organometallics *29*, 2176–2179.

Gross, M.I., Demo, S.D., Dennison, J.B., Chen, L., Chernov-Rogan, T., Goyal, B., Janes, J.R., Laidig, G.J., Lewis, E.R., Li, J., et al. (2014). Antitumor activity of the glutaminase inhibitor CB-839 in triple-negative breast cancer. Mol. Cancer Ther. *13*, 890–901.

Gualdoni, G.A., Mayer, K.A., Kapsch, A.-M., Kreuzberg, K., Puck, A., Kienzl, P., Oberndorfer, F., Frühwirth, K., Winkler, S., Blaas, D., et al. (2018). Rhinovirus induces an anabolic reprogramming in host cell metabolism essential for viral replication. Proc. Natl. Acad. Sci. U S A *115*, E7158–E7165.

Güemes, M., Rahman, S.A., and Hussain, K. (2016). What is a normal blood glucose? Arch. Dis. Child. *101*, 569–574.

Hanahan, D., and Weinberg, R.A. (2011). Hallmarks of cancer: the next generation. Cell *144*, 646–674.

Huang, C.-C., Wang, S.-Y., Lin, L.-L., Wang, P.-W., Chen, T.-Y., Hsu, W.-M., Lin, T.-K., Liou, C.-W., and Chuang, J.-H. (2015). Glycolytic inhibitor 2-deoxyglucose simultaneously targets cancer and endothelial cells to suppress neuroblastoma growth in mice. Dis. Model. Mech. *8*, 1247–1254.

Ilyn, A.P., Trifilenkov, A.S., Tsirulnikov, S.A., Kurashvily, I.D., and Ivachtchenko, A.V. (2005). Synthesis of 4-oxo-4,5,6,7-tetrahydropyrazolo1,5-apyrazine-6-carboxamides using a modification of Ugi condensation. J. Comb. Chem. *7*, 806–808.

Jones, W., and Bianchi, K. (2015). Aerobic glycolysis: beyond proliferation. Front. Immunol. *6*, 227.

Jóźwiak, P., Krześlak, A., Pomorski, L., and Lipińska, A. (2012). Expression of hypoxia-related glucose transporters GLUT1 and GLUT3 in benign, malignant and non-neoplastic thyroid lesions. Mol. Med. Rep. *6*, 601–606.

Kajanus, J., Jacobson, I., Åstrand, A., Olsson, R.I., Gran, U., Björe, A., Fjellström, O., Davidsson, Ö., Emtenäs, H., Dahlén, A., et al. (2016). Isoindolinone compounds active as Kv1.5 blockers identified using a multicomponent reaction approach. Bioorg. Med. Chem. Lett. *26*, 2023–2029.

Karageorgis, G., Reckzeh, E.S., Ceballos, J., Schwalfenberg, M., Sievers, S., Ostermann, C., Pahl, A., Ziegler, S., and Waldmann, H. (2018). Chromopynones are pseudo natural product glucose uptake inhibitors targeting glucose transporters GLUT-1 and -3. Nat. Chem. *10*, 1103–1111.

Khayat, Z.A., McCall, A.L., and Klip, A. (1998). Unique mechanism of GLUT3 glucose transporter regulation by prolonged energy demand: increased protein half-life. Biochem. J. *333*, 713–718.

Koppenol, W.H., Bounds, P.L., and Dang, C.V. (2011). Otto Warburg's contributions to current concepts of cancer metabolism. Nat. Rev. Cancer *11*, 325–337.

Krzeslak, A., Wojcik-Krowiranda, K., Forma, E., Jozwiak, P., Romanowicz, H., Bienkiewicz, A., and Brys, M. (2012). Expression of GLUT1 and GLUT3 glucose transporters in endometrial and breast cancers. Pathol. Oncol. Res. *18*, 721–728.

Lea, M.A., Altayyar, M., and desBordes, C. (2015). Inhibition of growth of bladder cancer cells by 3-(3-pyridinyl)-1-(4-pyridinyl)-2-propen-1-one in combination with other compounds affecting glucose metabolism. Anticancer Res. *35*, 5889–5899.

Lee, Y.-M., Lee, G., Oh, T.-I., Kim, B.M., Shim, D.-W., Lee, K.-H., Kim, Y.J., Lim, B.O., and Lim, J.-H. (2016). Inhibition of glutamine utilization sensitizes lung cancer cells to apigenin-induced apoptosis resulting from metabolic and oxidative stress. Int. J. Oncol. *48*, 399–408.

Liu, X., Wang, L., Jiang, W., Lu, W., Yang, J., and Yang, W. (2018). B cell lymphoma with different metabolic characteristics show distinct sensitivities to metabolic inhibitors. J. Cancer *9*, 1582–1591.

Liu, Y., Cao, Y., Zhang, W., Bergmeier, S., Qian, Y., Akbar, H., Colvin, R., Ding, J., Tong, L., Wu, S., et al. (2012). A small-molecule inhibitor of glucose transporter 1 downregulates glycolysis, induces cell-cycle arrest, and inhibits cancer cell growth in vitro and in vivo. Mol. Cancer Ther. *11*, 1672–1682.

Livak, K.J., and Schmittgen, T.D. (2001). Analysis of relative gene expression data using real-time quantitative PCR and the 2(-Delta Delta C(T)) method. Methods *25*, 402–408.

Loewe, S. (1953). The problem of synergism and antagonism of combined drugs. Arzneimittelforschung *3*, 285–290.

Lukey, M.J., Katt, W.P., and Cerione, R.A. (2018). Targeting therapy resistance: when glutamine catabolism becomes essential. Cancer Cell *33*, 795–797.

Ma, Y.-S., Yang, I.-P., Tsai, H.-L., Huang, C.-W., Juo, S.-H.H., and Wang, J.-Y. (2014). High glucose modulates antiproliferative effect and cytotoxicity of 5-fluorouracil in human colon cancer cells. DNA Cell Biol. *33*, 64–72.

Macintyre, A.N., Gerriets, V.A., Nichols, A.G., Michalek, R.D., Rudolph, M.C., Deoliveira, D., Anderson, S.M., Abel, E.D., Chen, B.J., Hale, L.P., et al. (2014). The glucose transporter Glut1 is selectively essential for CD4 T cell activation and effector function. Cell Metab. *20*, 61–72.

Marín-Hernández, A., López-Ramírez, S.Y., Del Mazo-Monsalvo, I., Gallardo-Pérez, J.C., Rodríguez-Enríquez, S., Moreno-Sánchez, R., and Saavedra, E. (2014). Modeling cancer glycolysis under hypoglycemia, and the role played by the differential expression of glycolytic isoforms. FEBS J. *281*, 3325–3345.

Marroquin, L.D., Hynes, J., Dykens, J.A., Jamieson, J.D., and Will, Y. (2007). Circumventing the Crabtree effect: replacing media glucose with galactose increases susceptibility of HepG2 cells to mitochondrial toxicants. Toxicol. Sci. *97*, 539–547.

Martinez-Outschoorn, U.E., Peiris-Pagés, M., Pestell, R.G., Sotgia, F., and Lisanti, M.P. (2017). Cancer metabolism: a therapeutic perspective. Nat. Rev. Clin. Oncol. *14*, 11–31.

Massari, F., Ciccarese, C., Santoni, M., Iacovelli, R., Mazzucchelli, R., Piva, F., Scarpelli, M., Berardi, R., Tortora, G., Lopez-Beltran, A., et al. (2016). Metabolic phenotype of bladder cancer. Cancer Treat. Rev. *45*, 46–57.

Matsushita, K., Uchida, K., Saigusa, S., Ide, S., Hashimoto, K., Koike, Y., Otake, K., Inoue, M., Tanaka, K., and Kusunoki, M. (2012). Glycolysis inhibitors as a potential therapeutic option to treat aggressive neuroblastoma expressing GLUT1. J. Pediatr. Surg. *47*, 1323–1330.

Mellanen, P., Minn, H., Grénman, R., and Härkönen, P. (1994). Expression of glucose transporters in head-and-neck tumors. Int. J. Cancer *56*, 622–629.

Moffat, J.G., Vincent, F., Lee, J.A., Eder, J., and Prunotto, M. (2017). Opportunities and challenges in phenotypic drug discovery: an industry perspective. Nat. Rev. Drug Discov. *16*, 531–543.

Nagamatsu, S., Sawa, H., Inoue, N., Nakamichi, Y., Takeshima, H., and Hoshino, T. (1994). Gene expression of GLUT3 glucose transporter regulated by glucose in vivo in mouse brain and in vitro in neuronal cell cultures from rat embryos. Biochem. J. *300* (Pt 1), 125–131.

National Cancer Institute (2019). Developmental therapeutics program. http://dtp.cancer.gov.

Neochoritis, C.G., Stotani, S., Mishra, B., and Dömling, A. (2015). Efficient isocyanide-less isocyanide-based multicomponent reactions. Org. Lett. *17*, 2002–2005.

Palmer, C.S., Cherry, C.L., Sada-Ovalle, I., Singh, A., and Crowe, S.M. (2016). Glucose metabolism in T cells and monocytes: new perspectives in HIV pathogenesis. EBioMedicine *6*, 31–41.

Reckzeh, E.S., Brockmeyer, A., Metz, M., Waldmann, H., and Janning, P. (2019). Target engagement of small molecules: thermal profiling approaches on different levels. Methods Mol. Biol. *1888*, 73–98.

Schmidt, T., Samaras, P., Frejno, M., Gessulat, S., Barnert, M., Kienegger, H., Krcmar, H., Schlegl, J., Ehrlich, H.-C., Aiche, S., et al. (2018). ProteomicsDB. Nucleic Acids Res. *46*, D1271–D1281.

Scriver, C.R., and Rosenberg, L.E. (1973). Amino acid metabolism and its disorders. Major Probl. Clin. Pediatr. *10*, 1–478.

Sheldrick, G.M. (2008). A short history of SHELX. Acta Crystallogr. A *64* (Pt 1), 112–122.

Sheldrick, G.M. (2015). SHELXT - integrated space-group and crystal-structure determination. Acta Crystallogr. A *71* (Pt 1), 3–8.

Shi, Y., Liu, S., Ahmad, S., and Gao, Q. (2018). Targeting key transporters in tumor glycolysis as a novel anticancer strategy. Curr. Top. Med. Chem. *18*, 454–466.

Siebeneicher, H., Bauser, M., Buchmann, B., Heisler, I., Müller, T., Neuhaus, R., Rehwinkel, H., Telser, J., and Zorn, L. (2016a). Identification of novel GLUT inhibitors. Bioorg. Med. Chem. Lett. *26*, 1732–1737.

Siebeneicher, H., Cleve, A., Rehwinkel, H., Neuhaus, R., Heisler, I., Müller, T., Bauser, M., and Buchmann, B. (2016b). Identification and optimization of the first highly selective GLUT1 inhibitor BAY-876. ChemMedChem *11*, 2261–2271.

Simpson, I.A., Dwyer, D., Malide, D., Moley, K.H., Travis, A., and Vannucci, S.J. (2008). The facilitative glucose transporter GLUT3: 20 years of distinction. Am. J. Physiol. Endocrinol. Metab. *295*, E242–E253.

Still, E.R., and Yuneva, M.O. (2017). Hopefully devoted to Q: targeting glutamine addiction in cancer. Br. J. Cancer *116*, 1375–1381.

Stock, K., Estrada, M.F., Vidic, S., Gjerde, K., Rudisch, A., Santo, V.E., Barbier, M., Blom, S., Arundkar, S.C., Selvam, I., et al. (2016). Capturing tumor complexity in vitro: comparative analysis of 2D and 3D tumor models for drug discovery. Sci. Rep. *6*, 28951.

Sun, L., Yin, Y., Clark, L.H., Sun, W., Sullivan, S.A., Tran, A.-Q., Han, J., Zhang, L., Guo, H., Madugu, E., et al. (2017). Dual inhibition of glycolysis and glutaminolysis as a therapeutic strategy in the treatment of ovarian cancer. Oncotarget *8*, 63551–63561.

Tan, X., Hu, L., Luquette, L.J., Gao, G., Liu, Y., Qu, H., Xi, R., Lu, Z.J., Park, P.J., and Elledge, S.J. (2012). Systematic identification of synergistic drug pairs targeting HIV. Nat. Biotechnol. *30*, 1125–1130.

Vander Heiden, M.G., Cantley, L.C., and Thompson, C.B. (2009). Understanding the Warburg effect: the metabolic requirements of cell proliferation. Science *324*, 1029–1033.

Vichai, V., and Kirtikara, K. (2006). Sulforhodamine B colorimetric assay for cytotoxicity screening. Nat. Protoc. *1*, 1112–1116.

Yamamoto, N., Sato, T., Kawasaki, K., Murosaki, S., and Yamamoto, Y. (2006). A nonradioisotope, enzymatic assay for 2-deoxyglucose uptake in L6 skeletal muscle cells cultured in a 96-well microplate. Anal. Biochem. *351*, 139–145.

Yamamoto, T., Seino, Y., Fukumoto, H., Koh, G., Yano, H., Inagaki, N., Yamada, Y., Inoue, K., Manabe, T., and Imura, H. (1990). Over-expression of facilitative glucose transporter genes in human cancer. Biochem. Biophys. Res. Commun. *170*, 223–230.

Yin, Y., Choi, S.-C., Xu, Z., Perry, D.J., Seay, H., Croker, B.P., Sobel, E.S., Brusko, T.M., and Morel, L. (2015). Normalization of CD4+ T cell metabolism reverses lupus. Sci. Transl. Med. *7*, 274ra18.

Younes, M., Brown, R.W., Stephenson, M., Gondo, M., and Cagle, P.T. (1997). Overexpression of Glut1 and Glut3 in stage I nonsmall cell lung carcinoma is associated with poor survival. Cancer *80*, 1046–1051.

Zhang, Z., Zi, Z., Lee, E.E., Zhao, J., Contreras, D.C., South, A.P., Abel, E.D., Chong, B.F., Vandergriff, T., Hosler, G.A., et al. (2018). Differential glucose requirement in skin homeostasis and injury identifies a therapeutic target for psoriasis. Nat. Med. *24*, 617–627.

Zhao, F.-Q., and Keating, A.F. (2007). Functional properties and genomics of glucose transporters. Curr. Genomics *8*, 113–128.

STAR★METHODS

KEY RESOURCES TABLE

REAGENT or RESOURCE	SOURCE	IDENTIFIER
Antibodies		
Mouse monoclonal anti-GLUT-1 (1:5,000)	Abcam	Cat# ab40084; RRID: AB_2190927
Rabbit polyclonal anti-GLUT-2 (1:200)	Santa Cruz	Cat# sc-9117; RRID: AB_641068
Rabbit monoclonal anti-GLUT-3 (1:5,000)	Abcam	Cat# ab191071; RRID: AB_2736916
Rabbit monoclonal anti-GLUT-3 (1:5,000)	Santa Cruz	Cat# sc-74399; RRID: AB_1124975
Rabbit polyclonal anti-GLUT-4 (1:500)	Millipore	Cat# 07-1404; RRID: AB_1587080
Rabbit monoclonal anti-Na^+/K^+-ATPase (1:10,000)	Abcam,	Cat# ab76020; RRID: AB_1310695
Mouse monoclonal anti-Vinculin (1:10,000)	Santa Cruz	Cat# sc-59803; RRID: AB_794011
Donkey anti-mouse (1:5,000), infrared dye 800CW-labeled	LI-COR	Cat# 926-32212; RRID: AB_621847
Donkey anti-rabbit (1:5,000), infrared dye 680RD-labeled	LI-COR	Cat# 926-68073; RRID: AB_10954442
Donkey anti-rabbit (1:5,000), infrared dye 800CW-labeled	LI-COR	Cat# 926-32213; RRID: AB_621848
Donkey anti-mouse (1:5,000), infrared dye 680RD-labeled	LI-COR	Cat# 926-68072; RRID:AB_10953628
Goat polyclonal anti-rabbit (1:100,000), horseradish peroxidase-labeled	Thermo Fisher Scientific	Cat# 31430; RRID: AB_228307
Goat polyclonal anti-mouse, (1:10,000) horseradish peroxidase-labeled	Thermo Fisher Scientific	Cat# 31460; RRID: AB_228341
Chemicals, Peptides, and Recombinant Proteins		
Chemical: 3-Bromopyruvate	Alfa Aesar	Cat# L00720 CAS: 1113-59-3
Chemical: 2-Deoxy-α-*D*-glucose (2-DG)	Santa Cruz	Cat# sc-202010 CAS: 154-17-6
Protein: Diaphorase, *Clostridium kluyvery*	Sigma-Aldrich	Cat# D5540-500UN CAS: 9001-18-7
Protein: Glucose-6-phosphate dehydrogenase, *Leuconostoc mesenteroides*	Sigma-Aldrich	Cat# G8404 CAS: 9001-40-5
Protein: Insulin, bovine pancreas	Sigma-Aldrich	Cat# I6634 CAS: 11070-73-8
Chemical: $NADP^+$	AppliChem	Cat# A1394,0001 CAS: 1184-16-3
Chemical: NP-40 alternative	Merck-Calbiochem	Cat# 492016 CAS: 9016-45-9
Chemical: Propidium iodide (PI)	Sigma-Aldrich	Cat# P4864 CAS: 25535-16-4
Chemical: Resazurin	Acros Organics	Cat# AC418900050 CAS: 62758-13-8
Critical Commercial Assays		
Sso Advanced SYBR Green Mix	Bio-Rad	Cat# 1725270
SuperSignal West Pico Chemiluminescent	Thermo Fisher Scientific	Cat# 10177533

(*Continued on next page*)

Continued

REAGENT or RESOURCE	SOURCE	IDENTIFIER
SuperSignal West Femto Maximum Sensitivity Substrate	Thermo Fisher Scientific	Cat# 34095
QuantiTect Reverse transcription kit	Qiagen	Cat# 205313
Seahorse Glycolysis Stress test	Agilent	Cat# 103020-100
Deposited Data		
X-ray structure compound **(*R*)-2a**	This paper	CCDC: 1883523
Experimental Models: Cell Lines		
Human: DLD-1 cells (male)	Horizon Discovery	Cat# HD PAR-086; RRID: CVCL_0248
Human: DLD-1 *GLUT1*(-/-) cells (male)	Horizon Discovery	Cat# HD R00-024; RRID: CVCL_HD63
Human: UM-UC-3 cells (male)	ATCC	Cat# CRL-1749; RRID: CVCL_1783
Human: HCT116 cells (male)	DSMZ	Cat# ACC581; RRID: CVCL_0291
Human: BxPC-3 cells (female)	DSMZ	Cat# ACC760; RRID: CVCL_0186
Human: UO-31 cells (female)	National Cancer Institute	MTA #1-4488-14; RRID: CVCL_1911
Human: MIA PaCa-2 (male)	ATCC	Cat# CRM-CRL-1420; RRID: CVCL_0428
Human: SW480 cells (male)	ATCC	Cat# CCL-228; RRID: CVCL_0546
Hamster: CHO cells (female)	ATCC	Cat# CRL-9618; RRID: CVCL_0214
Oligonucleotides		
Primers for *GLUT1*, see Table S5	Eurofins	N/A
Primers for *GLUT2*, see Table S5	Eurofins	N/A
Primers for *GLUT3*, see Table S5	Eurofins	N/A
Primers for *GLUT4*, see Table S5	Eurofins	N/A
Primers for *ACTB*, see Table S5	Eurofins	N/A
Primers for *TUBB*, see Table S5	Eurofins	N/A
Primers for *ATP1A1*, see Table S5	Eurofins	N/A
Recombinant DNA		
Plasmid: GLUT-1 (pTCN)	transOMIC	Cat# BC121804
Plasmid: GLUT-2 (pTCN)	transOMIC	Cat# BC060041
Plasmid: GLUT-3 (pCMV-SPORT 6)	Dharmacon	Cat# OHS1770-202314070
Plasmid: GLUT-4 (pTCN)	transOMIC	Cat# BC034387
Plasmid: pTCN	transOMIC	Cat# BC060823
Plasmid: pCMV-SPORT 6	Dharmacon	N/A
Software and Algorithms		
CFX Manager	Bio-Rad	RRID: SCR_003375 http://www.bioconductor.org/packages/release/bioc/html/HTqPCR.html
Prism 5	GraphPad	RRID:SCR_002798 http://www.graphpad.com/
Prism 7	GraphPad	RRID:SCR_002798 http://www.graphpad.com/
Combenefit	(Di Veroli et al., 2016)	N/A
Image Studio Ver. 5.2	LI-COR	RRID:SCR_015795 https://www.licor.com/bio/products/software/image_studio/

(*Continued on next page*)

Continued

REAGENT or RESOURCE	SOURCE	IDENTIFIER
IncuCyte ZOOM 2015/2016A	(EssenBioscience) Satorius	https://www.essenbioscience.com/en/products/software/
IncuCyte S3 2017A	(EssenBioscience) Satorius	https://www.essenbioscience.com/en/products/software/
APEX 3 Suite (v.2017.3-0)	Bruker	https://www.bruker.com/products/microtomography/micro-ct-software/3dsuite.html

CONTACT FOR REAGENT AND RESOURCE SHARING

Further information and requests for resources and reagents should be directed to and will be fulfilled by the Lead Contact, Herbert Waldmann (herbert.waldmann@mpi-dortmund.mpg.de).

EXPERIMENTAL MODEL AND SUBJECT DETAILS

Cell Lines

HCT116 (human, male), UM-UC-3 (human, male), UO-31 (human, female), MIA PaCa-2 (human, male) were grown in 4.5 g/l glucose Dulbecco's modified Eagle's medium (DMEM, PAN Biotech) supplemented with 10% v/v fetal calf serum (FCS, Invitrogen-Gibco) with 1 mM sodium pyruvate (PAN Biotech) and 100 U/mL penicillin/ 0.1 mg/mL streptomycin (PAN Biotech). CHO cells (hamster, female) were cultured in in 4.5 g/l glucose Dulbecco's modified Eagle's medium (DMEM, PAN Biotech) supplemented with 10% v/v fetal calf serum (FCS, Invitrogen-Gibco), 100 U/mL penicillin/ 0.1 mg/mL streptomycin (PAN Biotech) and non-essential amino acids (PAN Biotech). DLD-1 (human, male) and DLD-1 *GLUT1* (-/-) (human, male) as well as BxPC-3 (human, female) cells were cultured in RPMI1640 medium supplemented with 10% fetal calf serum (FCS, Invitrogen-Gibco) and 1100 U/mL penicillin/ 0.1 mg/mL streptomycin (PAN Biotech). SW480 cells (human, male) were cultured in Leibovitz L-15 medium supplemented with 10% fetal calf serum (FCS, Invitrogen-Gibco) and 1100 U/mL penicillin/ 0.1 mg/mL streptomycin (PAN Biotech). All cell lines were grown at 37°C with 5% CO_2 in humidified atmosphere and regularly tested negative for mycoplasma contamination.

METHOD DETAILS

Biological Experiments

Resazurin-coupled 2-DG Uptake Assay

Cells were seeded in a 96-well plate (black wall, clear bottom, Corning) in complete medium with a density of 40,000 cells/well. Cells were grown for 24 h at 37°C with 5% CO_2 in humidified atmosphere. Adherent cells were washed three times with freshly prepared Krebs-Ringer bicarbonate (KRB) buffer (20 mM HEPES, 5 mM KH_2PO_4, 1 mM $MgSO_4$, 1 mM $CaCl_2$, 136 mM NaCl, 4.7 mM KCl, pH 7.4, 0.1% w/v BSA). 1 mM 2-DG was added to the cells together with the respective compound dilution and incubated for 30 min at room temperature. DMSO served as a control. The assay buffer was removed and the 2-DG uptake was stopped by washing the cells thrice with ice-cold KRB buffer. 60 μL 0.06 M HCl supplemented with 1% w/v CHAPS was added to the cells and the cells were incubated for 15 min at 65°C for cell lysis. Neutralization was performed with 20 μL 0.5 M Tris at room temperature. 60 μL enzyme mix (16 U/mL glucose-6-phosphate dehydrogenase (Sigma Aldrich), 0.2 U/mL diaphorase (Sigma-Aldrich), 0.1 mM $NADP^+$ (Applichem), 2.5 μg/mL resazurin (Acros Organics) in 0.125 M Tris-HCl (Carl Roth), pH 8.4 supplemented with 0.1% w/v BSA) was added and the plate was incubated for 2 h in the dark. Fluorescence of resorufin (ex/em 535 nm/590 nm) was measured using the Tecan Infinite M200 (Tecan Trading). The background (no addition of 2-DG) was subtracted from the raw values prior to normalization to the DMSO control. IC_{50} values were calculated using a nonlinear regression fit with variable slope (four parameters) using GraphPad Prims 5 or 7.

The semi-automated screening was performed as described above with slight modifications: 15,000 HCT116 cells/well were seeded into 384- well black-walled, clear bottomed plates (CellBIND, Corning) and incubated overnight. Compounds were tested at 30 μM concentration (for the screening) or in serial dilutions staring from 30 μM (IC_{50} determinations) from DMSO stocks with an acoustic nanoliter dispenser (ECHO 520). Fluorescence intensity (ex/em 535 nm/590 nm) was measured with a SpectraMax Paradigm Multi-Mode Microplate Reader (Molecular devices, bottom read-out) using the Rhodamine filter settings. For hit compounds, cell viability was assessed using the CellTiter Glo reagent (Promega) after 30 min of treatment in HCT116 cells. Washing steps and liquid additions were performed by means of automated cell washer or multidrop device, respectively.

Hexokinase Assay

HCT116 cells were grown to confluence, washed thrice with PBS and lysed with RIPA buffer (10 mM Tris-Cl (pH 8.0, 1 mM EDTA, 1% Triton X-100, 0.1% sodium deoxycholate, 0.1% SDS, 140 mM NaCl, 1 mM phenylmethylsulfonyl fluoride (PMSF)) that was supplemented with protease inhibitor cocktail as recommended by the manufacturer (Roche). Cells were lysed on ice for 5 min and collected. The lysate was centrifuged (500 x g, 4°C, 10 min) and the supernatant transferred to a fresh tube. After protein

concentration determination with Bradford reagent (Bio-Rad), the lysates were snap frozen and stored at -80°C until further usage. The assay was performed in a black 96 well plate in 100 μL total volume. 10% v/v cell lysate (conc. 0.04 mg/mL) were supplemented with 0.3 mM ATP, 10% v/v of 2-DG (concentration range 0-15.6 mM), 43% v/v enzyme mix (0.1 mM $NADP^+$, 16 U/mL G6PDH in assay buffer) and 10% v/v compound (300 μM Glutor or 300 μM 3-bromopyruvate) (Matsushita et al., 2012) and filled up with assay buffer (100 mM Tris, 5 mM $MgCl_2$, pH 8.5). Samples were incubated for 40 min at 37°C. Fluorescence intensity of $NADPH+H^+$ (ex/em 340 nm/445 nm) was measured with the Tecan Infinite M200 (Tecan Trading). The background was subtracted and all values were normalized to the maximal fluorescence intensity at 15.6 mM 2-DG.

Cell Panel Profiling

Cell panel profiling to assess the growth behavior of 94 cell lines in presence of Glutor was performed by Oncolead (Germany). Determination of cell growth was performed after 72 h of compound treatment using sulforhodamine B assay (Vichai and Kirtikara, 2006). Cells were fixed by addition of 10% TCA (adherent cells) or 50% TCA (semi-adherent or suspension cells) for 1 h at 4°C followed by two washing steps with 400 μl deionized water. After drying, cells were stained with 100 μL of 0.04% w/v sulforhodamine B and incubated for at least 30 min at room temperature. Unbound dye was removed by washing six times with 1% acetic acid and drying samples at room temperature. Bound sulforhodamine B was dissolved in 100 μL of 10 mM Tris. Absorbance was determined at 492, 520 and 560 nm using a Deelux-LED96 plate reader (Deelux Labortechnik GmbH, Germany).

Glycolysis Stress Test

Glycolysis Stress Test (Agilent) was performed using the Seahorse XFp analyzer (Agilent). Briefly, 24 h prior the experiment cells were seeded with a density of 75,000 cells/well in the respective full medium. The next day, medium was exchanged to glucose-free assay medium (Agilent) and cells were incubated at 37°C without CO_2 for 45 min. After compound addition (first injection, 30 min incubation) the glycolysis stress test protocol was performed according to the manufacturer's instructions. The data was analyzed using the Wave software (Agilent) and all oxygen consumption rate (OCR) and extracellular acidification rate (ECAR) values were normalized to the time point before compound addition (3^{rd} measurement). A second normalization was done to calculate the rate relative to the DMSO control. For metabolic profiles, the second of three measurements from one experimental phase (e.g. after glucose addition) was used to plot the glycolytic reserve, glycolytic capacity and the OXPHOS reduction.

Reverse Transcription-Quantitative PCR

DLD-1 or HCT116 cells were seeded at 63,000 cells/well in a 12-well plate and incubated for 24 h prior to treatment. Cells were incubated with 0.5 μM Glutor (RPMI medium for DLD-1 cells; DMEM medium for HCT116 cells) or different glucose concentrations (DMEM medium) for the indicated time points. Total RNA was isolated by means of RNeasy Mini Kit as described by the manufacturer (Qiagen). The Bioanalyzer (Agilent) was used with the corresponding RNA 6000 nano Kit (Agilent) to perform integrity measurements of the isolated RNA following the manufacturer's instructions. Reverse transcription was done using QuantiTect Reverse transcription kit (Qiagen) and according to the instructions of the manufacturer. RT-qPCR was performed with Sso Advanced SYBR Green Mix (Bio-Rad) using the iCycler iQ5 thermal cycler (Bio-Rad). Gene-specific primer sequences, their respective efficiencies and amplicon sizes are depicted in Table S5. Data was analyzed using CFX Manager. *GLUT1-4* values were normalized to the levels of *ACTB*, *TUBB* and *ATP1A1* using the $\Delta\Delta C_t$-method (Livak and Schmittgen, 2001). Efficiencies were measured in DLD-1 wt lysates (*GLUT1*, *GLUT3*, *ACTB*, *TUBB*, *ATP1A1*) or with isoform-specific plasmids (*GLUT2*, *GLUT4*).

Immunoblotting

DLD-1 cells were seeded in a 6-well plate with $3.06*10^5$ cells/well (24 h treatment) or $1.53*10^5$ cells/well (48 h treatment) 24 h prior to the experiment. Different glucose concentrations were tested in DMEM medium. Cells were treated with Glutor in RPMI1640 medium. DMSO served as a control. Cells were treated for 24 or 48 h prior to cell lysis. Briefly, cells were washed once with PBS, detached with cell dissociation solution (Sigma Aldrich) and washed again with PBS. After centrifugation for 5 min (4°C, 1,200 rpm) the pellet was lysed in PBS supplemented with 2% w/v dodecyl-β-D-maltoside (Carl Roth) on ice (15 min). After centrifugation at 14,000 rpm (4°C, 15 min) the supernatant was collected to determine the protein concentration by means of DC protein assay (Bio-Rad) or with Bradford reagent (Bio-Rad). SDS-PAGE was carried out using 6% SDS gels followed by transfer on polyvinyldiene difluoride membrane (PVDF, Merck) by means of semi-dry electrophoretic device (Bio-Rad). Membranes were blocked using Odyssey® blocking buffer (LI-COR) for 1 h at room temperature. The proteins GLUT-1 and GLUT-3 were detected using the primary antibodies anti-GLUT-1 (mouse) and anti-GLUT-3 (rabbit, Abcam) in Odyssey blocking buffer (LI-COR). Na^+/K^+-ATPase (rabbit) and vinculin (mouse) were detected for normalization (housekeeping proteins). The primary antibodies were incubated over night at 4°C and washed three times with PBS. For detection, infrared dye-labeled 800CW anti-mouse (donkey) and 680RD anti-rabbit (donkey) secondary antibody were used to detect GLUT-1 and Na^+/K^+-ATPase and 800CW donkey anti-rabbit and 680RD anti-mouse secondary antibody to detect GLUT-3 and vinculin. The membranes were incubated with the secondary antibody solutions for 1 h at room temperature followed by two washing steps with PBS-T (0.1% Tween-20) and one washing step with PBS. The fluorescence detection was carried out using the Odyssey CLx imaging system (LI-COR). Densitometric analysis was used for protein band quantification (Image Studio Ver. 5.2).

GLUT-1-4 Overexpression in CHO Cells

$1x10^6$ CHO cells were seeded 10 cm (diameter) cell culture plates and incubated overnight. Cells were transiently transfected with the respective GLUT-isoform containing plasmids using Lipofectamine 3000 according to the supplier's instructions. Briefly, DNA-lipid complexes (100 μg plasmid DNA, DNA:lipid ratio 1:2) were prepared in OptiMEM and added to the cells. GLUT-4-transfected cells

were treated with insulin (100 μg/mL). After 48 h the cells were reseeded (40,000 cell/well) in 96-well plates for 2-DG uptake monitoring or lysed to assess protein expression level by means of immunoblotting. For immunoblotting, samples were lysed in 1.5x SDS sample buffer without bromophenol blue. Protein concentrations were determined by means of DC protein assay (Bio-Rad). Proteins were separated using SDS-PAGE and transferred to PVDF membrane via semi-dry transfer. Blocking was performed using 5% w/v skimmed milk in 0.1% Tween-20 in Tris buffer (TBS-T) for 1 h at room temperature. The primary antibody GLUT-1, GLUT-2, GLUT-3 (Santa Cruz), GLUT-4 or/and Na^+-K^+-ATPase (housekeeping protein) (TBS-T) was incubated at 4°C overnight. The respective secondary horseradish peroxidase-labeled antibody (TBS-T) was incubated for 1 h at room temperature after washing with TBS-T. Signals visualization was performed using SuperSignal West Pico Chemiluminescent or Femto Maximum Sensitivity Substrate (Thermo Fischer) employing the Odyssey Fc imaging system (Li-COR). Band quantification was analyzed by means of densitometric analysis.

Real-Time Live-Cell Imaging and Analysis

Cells were seeded 24 h prior to treatment at 5,000 cells/well in a 96-well plate. In case the nutrient concentrations were varied, DMEM medium without glucose and glutamine was used. Glutor or DMSO was added to the cells and the growth behavior of the cells were monitored for 48 h or 120 h, depending on the duration of the experiment using the IncuCyte ZOOM or IncuCyte S3. Cell confluence was analyzed as a measure of cell growth using the respective software IncuCyte ZOOM 2016B or IncuCyte S3 2017A.

3D vs. 2D Cell Culture

Cells were seeded at 750 cells/well (380 μm spheroids) or 10,000 cells/well (800 μm spheroids) in monolayer or as spheroids in ultra-low attachment (ULA) plates (Corning) in full DMEM medium (200 μL/well). After 48 h 100 μL medium of the large spheroids (and monolayer control) was exchanged by fresh medium. After 72 h the cells were treated with the compound or different glucose concentrations in the presence of propidium iodide (PI) (0.02 mg/mL, Sigma Aldrich) to assess cell toxicity. For different glucose concentrations, 100 μL of medium was exchanged six times by the respective medium to achieve the desired concentration of glucose. For compound addition, 100 μL medium were exchanged for 100 μL fresh medium containing 2x the desired compound concentration. Cell growth was monitored by means of live-cell imaging using IncuCyte S3. Analysis of PI intensity was performed using the IncuCyte S3 2017A software. Spheroid toxicity was evaluated using all brightfield objects red mean intensities (RCU) whereas toxicity of monolayer cultured cells was analyzed by red confluence (%). EC_{50} values were calculated using a nonlinear regression fit with variable slope (four parameters) with GraphPad Prims 5 or 7.

Synergism/Antagonism Scores

Data generated during live-cell imaging (growth rates) in co-treatment experiments were normalized to DMSO-treated cells (%) and analyzed using different models.

Definition of synergy models as implemented in the open source software combenefit (Di Veroli et al., 2016).

a=drug A, b=drug B, a_u=dose drug A, b_u=dose drug B, R=reference effect, E=efficacy

Loewe Model. The reference effect for the combination of drug A and drug b (R_{AB}) is calculated by determining the two doses a_u and b_u such that the efficacy of both drugs is equal (Loewe, 1953).

Formula to define the reference effect:

$$R_{AB\_Loewe}(a,b) = E(a_u) = E\_B\ (b_u)$$

With the extension:

$$R_{AB\_Loewe}(a,b) = E(b_u) = E_B(b)$$

The extension is included for cases when drug A and drug B have a different maximum effect.

Bliss Model. The reference effect for the combination of drug A and drug b (R_{AB}) is calculated by multiplying the effects at the concentrations of drug A and drug B (Bliss, 1939).

Formula to define the reference effect:

$$R_{AB\_Bliss}(a,b) = E_A(a) \times E_B(b)$$

With the definition:

The effect of drug A (or drug B) is the fraction of the cell population that is not affected by treatment.

Highest Single Agent (HAS) Model. The reference effect for the combination of drug A and drug b (R_{AB}) is calculated by determining the greatest difference between the drug A and drug B, when given as single agent (Tan et al., 2012).

Formula to define the reference effect:

$$R_{AB\_HSA}(a,b) = MIN(E_A(a), E_B(b))$$

Cellular Thermal Shift Assay (CETSA)

For whole cell lysates, SW480 cells were grown to nearly confluence, washed with PBS and detached using cellular detachment solution (Sigma Aldrich) according to Reckzeh et al. (Reckzeh et al., 2019). Cells were resuspended using PBS, centrifuged at 1,200 rpm and washed with PBS. After a second centrifugation step, the pellet was resuspended in lysis buffer (PBS, 0.4% v/v NP40 alternative) on ice. To lyse the cells, four freeze-and-thaw cycles were applied to the cell suspension, followed by short sonication step (10 s). The

supernatant was collected after ultracentrifugation (4°C, 20 min, 100,000 x g) and the protein concentration was determined by using a Bradford reagent (Bio-Rad). Samples were snap frozen and stored at -80°C. For cellular thermal shift assay (CETSA), lysates were diluted to 2 mg/mL and divided into two reaction tubes. One fraction was treated with 10 μM Glutor, whereas the control fraction was supplemented with 1% (v/v) DMSO. The lysates were incubated for 10 min at room temperature, followed by fractionation (10 tubes) and subjection to a temperature gradient (36.9-67°C) for 3 min. After ultracentrifugation (4°C, 20 min, 100,000 x g), the soluble fractions were collected and analyzed using immunoblotting with antibodies against GLUT-1 and GLUT-3.

Mitochondrial Toxicity

Mitochondrial toxicity was analyzed by assessing compound sensitivity of HCT116 under 25 mM glucose and 10 mM galactose (Marroquin et al., 2007). Briefly, cell were seeded at 5,000 cells/well in 96-well plates and treated after 24 h with the inhibitor and in the presence of glucose or galactose. Oligomycin was used as a control for mitochondrial toxicity. Cell growth was monitored by means of live-cell imaging using IncuCyte ZOOM and analyzed as described above.

Synthetic Procedure

Materials

All chemicals were obtained from Acros Organics, Activate Scientific, Alfa Aesar or Sigma-Aldrich and used as provided, unless otherwise indicated. Dry solvents over molecular sieves were purchased from Sigma-Aldrich or Acros Organics.

Instrumentation

Proton and carbon nuclear magnetic resonance (^{1}H- and ^{13}C-NMR) spectra were recorded on Varian Mercury 400 (400 MHz), Bruker Avance DRX 500 (500 MHz), INOVA 500 (500 MHz), Bruker AV600 (600 MHz) and Bruker AV700 (700 MHz) at ambient temperature. Proton chemical shifts are indicated as parts per million (ppm, δ-scale) and are referenced to residual protium in the NMR solvent ($CHCl_3$, δ7.26 ppm; CH_2Cl_2, δ5.30 ppm; $(CH_3)_2SO$, δ2.50 ppm, CH_3OH, δ3.31 ppm) (Fulmer et al., 2010). Data are represented as follows: chemical shift, multiplicity (s = singlet, bs = broad singlet, d = doublet, dd= doublet of doublets, ddd= doublet of doublet of doublets, dt = doublet of triplets, t = triplet, td = triplet of doublets, q = quartet, s = septet, m = multiplet), coupling constant (*J*) in Hertz (Hz) and integration. Carbon chemical shifts are expressed in parts per million (ppm, δ-scale) and are referenced to the carbon resonances of the NMR solvent ($CDCl_3$, δ77.16 ppm; CD_2Cl_2, δ53.84 ppm; $(CH_3)_2SO$, δ39.52 ppm; CD_3OD, δ49.00 ppm). All NMR spectra were analyzed using MastReNova Version 12.0.0 and are depicted in Data S1. Low resolution mass spectra were collected via 7890a (Agilent) equipped with a 5975c mas spectrometer (Agilent) and a hp-5ms column (Agielnt) (MS-EI) or using uHPLC system 1290 infinity system (Agilent) equipped with a 6150 mass spectrometer (Agilent) and zorbax eclipse plus C18 rapid resolution HD 2.1x50mm 1.8 μm material column (Agilent). High resolution mass spectra (HR-MS) were recorded on a LTQ Orbitrap mass spectrometer 5 coupled to an Acceka HPLC-System (HPLC column: Hypersyl GOLD, 0 m x 1 mm, particle size 1.9 μm, ionization method: electron spray ionization). One exemplary spectrum of **3a** is depicted in Data S1. Systematic names for molecules according to IUPAC rules were generated using ChemDraw Professional version 16.0.

Synthetic Methods

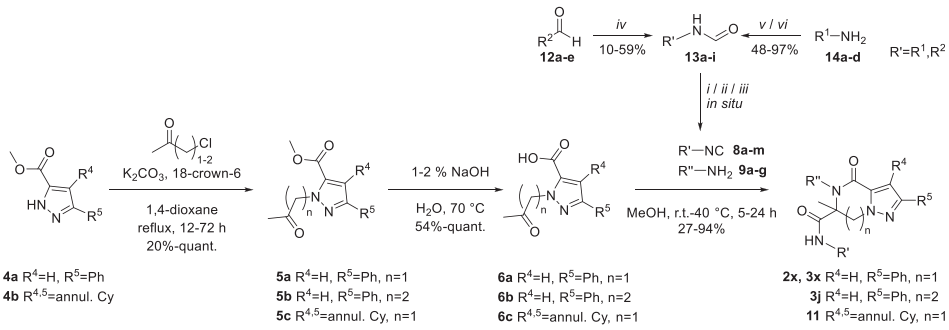

Scheme of synthetic procedure to generate piperazin-2-one-based compound library. *i*) Triphosgene, ACN, 0°C, 0.5-2 h; *ii*) Burgess reagent, ACN / MeOH (5:1), rt, 2 h; *iii*) Benzenesulfonyl chloride, trioctylamine, 80°C, 2 h; *iv*) $HCONH_2$, HCO_2H, 180°C, conventional heating 0.5-2 h or microwave 3 min; *v*) HCO_2Et, 60°C, 24 h; *vi*) $HCONH_2$, H_2NOH*HCl, toluene, 110°C, 24 h; R^1=heteroaromatic, R^2=alkyl, aromatic, heteroaromatic, R'=R^1,R^2, R''=aromatic. annul. Cy=annulated cyclohexane. **2x**=**2a**, **2b**, **2c**, **2e**, **2h**; **3x**=**3a**, **3b**, **3c**, **3e**, **3f**, **3g**, **3h**, **3i**, **3l**, **3m**, **3n**, **3o**, **3p**, **3s**. Late stage functionalization to generate **2i**, **3d**, **3k**, **3q** and **3r** are described in the compound characterization.

General Procedure 1A. Modified Leuckart-Wallach reaction (Neochoritis et al., 2015)

General Procedure for Conventional Heating. A microwave vial was charged with the corresponding aldehyde (3.6 mmol, 1 equiv.) dissolved in formamide (36 mmol, 10 equiv.) and formic acid (18 mmol, 5 equiv.). The reaction mixture was vigorously stirred at 180°C for 2-4 h. After cooling the mixture to room temperature, the reaction was extracted with DCM and the combined organic layers were dried over Na_2SO_4, filtered and concentrated under reduced pressure. The crude product was subsequently purified by flash silica gel column chromatography (elute as indicated) to yield the corresponding formamide.

General Procedure for Microwave Irradiation. A microwave vial was charged with the corresponding aldehyde (0.4 mmol, 1 equiv.) dissolved in formamide (18.4 mmol, 50 equiv.) and formic acid (1.8 mmol, 5 equiv.). The reaction mixture was irradiated in a microwave oven for 30 sec. at 180°C, quenched with 10 mL water and extracted with DCM. The combined organic layers were dried over Na_2SO_4, filtered and concentrated under reduced pressure. Residual formamide was removed *in vacuo*. The crude residue was purified by means of flash silica gel column chromatography (elute as indicated) to yield the corresponding formamide.

Formamide Formation from Amines

Formamides were synthesized from amines as described by Kajanus et al. (Kajanus et al., 2016) or Allen et al. (Allen et al., 2012).

All amines and isocyanides that were incorporated in the modified Ugi reaction are depicted in Table S4.

General Procedure 2: Modified Ugi Reaction. The bifunctional carboxylic acid/ketone (0.20 mmol, 1.0 equiv.) and the amine (0.20 mmol, 1.0 equiv. or 0.18 mmol, 0.9 equiv.) were dissolved in MeOH (1 mL), stirred for 30min at room temperature and the isocyanide (0.20 mmol, 1.0 equiv.) was added. The mixture was vigorously stirred at 40°C until full conversion of the starting material was indicated by TLC. The solvent was removed under reduced pressure and the product was extracted thrice with a mixture of water and dichloromethane (15 mL). The combined organic layers were dried over Na_2SO_4, filtered and concentrated under reduced pressure. The product was purified by flash silica gel column chromatography (eluate: petroleum ether / EtOAc or DCM / MeOH) (Ilyn et al., 2005).

General Procedure 3A: Modified Ugi Reaction with In Situ *Isocyanide Formation Using Phosgene*. The reaction was performed as described by Neochoritis et al. (2015). The corresponding formamide (0.06 mmol, 1.0 equiv.) was dissolved in DCM (1 mL) and cooled to 0°C. Triethylamine (0.15 mmol, 2.5 equiv.) was added, the mixture was stirred for 10 min and triphosgene (0.02 mmol, 0.3 equiv.) in DCM (1 mL) was added dropwise over a period of 30 min. After consumption of the formamide (monitored by TLC), the corresponding bifunctional carboxylic acid/ketone (0.07 mmol, 1.2 equiv.) and amine (0.06 mmol, 1.0 equiv.) were added and the reaction mixture was vigorously stirred for 5-72 h. The crude mixture was concentrated under reduced pressure and purified by means of silica gel chromatography using the indicated elute.

General Procedure 3B: Modified Ugi Reaction with In Situ *Isocyanide Formation Using Burgess Reagent*. The reaction was performed as described by Creedon et al. (Creedon et al., 1998). Briefly, an oven-dried Schlenck tube was charged with the formamide derivative (220 μmol, 1 eq) and dry acetonitrile under argon atmosphere. Solid Burgess reagent (348 μmol, 1.5-2 eq) was added and the solution was stirred for 0.5-2 h at room temperature. The reaction progress was checked by means of thin layer chromatography (TLC). The amine (198 μmol, 0.9 eq) and bifunctional compound (220 μmol, 1 eq) were combined in MeOH, stirred for approximately 10 min and added to the reaction mixture. The reaction mixture was vigorously stirred at room temperature for 1-5 days. Saturated $NaHCO_3$ was added to the reaction mixture and the product was extracted thrice with DCM. The combined organic layers were dried over Na_2SO_4, filtered and concentrated under reduced pressure. Purification was performed over silica or by recrystallization from MeOH as indicated.

Propargyl isocyanide was alternatively synthesized *in situ* from *N*-(propargyl)formamide as described by Chrostowska et al. (Chrostowska et al., 2012).

Preparative HPLC-MS

Separations were performed by means of mass-directed preparative HPLC (Agilent Series, 1100/LC/MSD VL) using reversed-phase C18 column with a constant flow of 20.0 mL/min. Solvent A: water +0.1% v/v TFA; solvent B: acetonitrile +0.1% v/v TFA.

Separation of the Enantiomeric Mixture

Chiral separation was performed by means of solid phase separation via an Ultimate 3000 HPLC (Dionex, Thermo Fisher) employing an IC column (CHIRALPAK IC, column no. IC00CG-MA004) column. An isocratic gradient was used to separate both enantiomers (elute: isohexane / DCM/MeOH(5%)).

Single Crystal X-ray Structure Analyses

Data collection was conducted on a *Bruker D8 Venture* four-circle diffractometer by *Bruker AXS GmbH* using a *PHOTON100* CMOS area detector by *Bruker AXS GmbH.* X-ray radiation was generated by microfocus sources *IμS* Cu or Mo by *Incoatec GmbH* with HELIOS mirror optics and a single-hole collimator by *Bruker AXS GmbH*.

For the data collection, the programs APEX 3 Suite (v.2017.3-0) with the integrated programs SAINT (integration) and SADABS (adsorption correction) by Bruker AXS GmbH were used. Using Olex2 (Dolomanov et al., 2009), the structures were solved with the ShelXT (Sheldrick, 2015) structure solution program using Intrinsic Phasing and refined with the XL (Sheldrick, 2008) refinement package using Least Squares minimization.

Compound Characterization

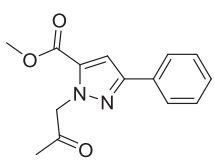

*Methyl 1-(2-oxopropyl)-3-phenyl-1*H*-pyrazole-5-carboxylate (**5a**)*. Methyl 3-phenyl-1*H*-pyrazole-5-carboxylate **4a** (30.0 mg, 0.15 mmol, 1.0 equiv.), 3-chloroacetone (11.9 μL, 0.15 mmol, 1.0 equiv.), K_2CO_3 (24.6 mg, 0.18 mmol, 1.2 equiv.) and 18-crown-6-ether (0.4 mg, 1.5 μmol, 0.01 equiv.) were suspended in 1,4-dioxane (1 mL) and vigorously stirred under reflux conditions for 6 h. Afterwards, water (50 mL) and DCM (50 mL) were added to the reaction mixture and the layers were separated. The aqueous phase was extracted two more times with DCM (2x 50 mL) and the combined organic layers were dried over $MgSO_4$, filtrated and evaporated under reduced pressure. The residue was purified by means of silica gel column chromatography (elute: cyclohexane / EtOAc) and obtained as white solid (23.0 mg, 0.15 mmol, quant.). R_f = 0.24 (cyclohexane / EtOAc = 3:1). ^{1}H NMR (400 MHz, $CDCl_3$) δ 7.79 (d, *J* = 7.3 Hz, 2H), 7.41 (t, *J* = 7.3 Hz, 2H), 7.33 (t, *J* = 7.3 Hz, 1H), 7.19 (s, 1H), 5.39 (s, 2H), 3.88 (s, 3H), 2.23 ppm (s, 3H). ^{13}C NMR (100 MHz, $CDCl_3$) δ 201.3, 162.9, 146.5, 143.9, 129.9, 129.4, 129.4, 129.1, 109.6, 59.8, 52.5, 27.4 ppm. HR-MS: calc. for $[M+H]^+$ $C_{14}H_{15}N_2O_3$ 259.1077 found 259.1075.

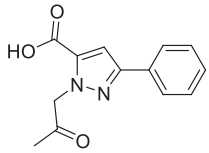

*1-(2-Oxopropyl)-3-phenyl-1*H*-pyrazole-5-carboxylic acid (**6a**)*. Methyl 1-(2-oxopropyl)-3-phenyl-1*H*-pyrazole-5-carboxylate **5a** (30.0 mg, 0.12 mmol, 1.0 equiv.) was suspended in water (1 mL) and NaOH was added slowly (5.6 mg, 0.14 mmol, 1.2 equiv.) and stirred thoroughly at 70°C for 3 h. Afterwards, HCl (0.5 mL, 1 M) was added to the crude reaction mixture. Water (40 mL) and EtOAc (40 mL) were added to the crude reaction and the phases were separated. The aqueous phase was extracted two more times with EtOAc (2x 40 mL) and the combined organic layers were dried over Na_2SO_4, filtered and concentrated under reduced pressure. The product was obtained as light yellow solid (28.3 mg, 0.12 mmol, quant.). R_f = 0.41 (dichloromethane / MeOH = 7:3). ^{1}H NMR (400 MHz, $CDCl_3$) δ 7.88 (d, *J* = 7.3 Hz, 2H), 7.42 (t, *J* = 7.3 Hz, 2H), 7.35 (t, *J* = 7.3 Hz, 1H), 7.31 (s, 1H), 5.41 (s, 2H), 2.23 ppm (s, 3H). ^{13}C NMR (100 MHz, $CDCl_3$) δ 201.2, 163.6, 151.4, 133.4, 132.0, 128.9, 128.6, 125.9, 110.0, 61.5, 27.0 ppm. HR-MS: calc. for $[M+H]^+$ $C_{13}H_{13}N_2O_3$ 245.0921 found 245.0929.

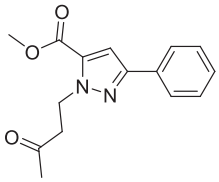

*Methyl 1-(3-oxobutyl)-3-phenyl-1*H*-pyrazole-5-carboxylate (**5b**)*. Methyl 3-phenyl-1-pyrazole-5-carboxylate **4a** (100 mg, 495 μmol, 1.0 equiv.) was dissolved in 1,4-dioxane (1.5 mL) and potassium carbonate (82 mg, 593 μmol, 1.2 equiv.), 18-Crown-6 ether (1.5 mg, 5 μmol, 0.01 equiv.) and 4-chlorobutan-2-one (47.3 μL, 495 μmol, 1.0 equiv.) were added. The solution was stirred thoroughly at 140°C for 4 h. The product was purified by means of silica gel column chromatography (elute: cyclohexane / EtOAc) and obtained as white solid (55 mg, 202 μmol, 40%). R_f = 0.30 (cyclohexane / EtOAc = 3:1). ^{1}H NMR (700 MHz, $CDCl_3$) δ 7.77 (dd, *J* = 8.0, 1.2 Hz, 2H), 7.40 (t, *J* = 8.0 Hz, 2H), 7.34 – 7.30 (m, 1H), 7.11 (s, 1H), 4.86 (t, *J* = 7.2 Hz, 2H), 3.92 (s, 3H), 3.09 (t, *J* = 7.2 Hz, 2H), 2.21 ppm (s, 3H). ^{13}C NMR (176 MHz, $CDCl_3$) δ 206.0, 160.3, 150.3, 133.4, 132.6, 128.9, 128.3, 125.7, 108.3, 52.2, 46.9, 43.5, 30.3 ppm. HR-MS: calc. for $[M+H]^+$ $C_{15}H_{17}N_2O_3$ 273.12337 found 273.12343.

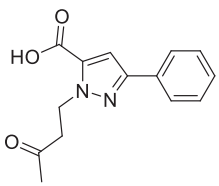

*1-(3-Oxobutyl)-3-phenyl-1*H*-pyrazole-5-carboxylic acid (**6b**)*. Methyl 1-(3-oxobutyl)-3-phenyl-1*H*-pyrazole-5-carboxylate **5b** (70 mg, 0.26 mmol, 1.0 equiv.) was subjected to NaOH (2% w/v in water, 617 μL, 0.31 mmol, 1.2 equiv.) and stirred at 70°C for 4 h. The crude was acidified to pH 2 using 1 M HCl and extracted with EtOAc. The combined organic layers were dried over Na_2SO_4, filtered and concentrated under reduced pressure. The product was purified by means of silica gel column chromatography (elute: cyclohexane / EtOAc +2% v/v acetic acid) and obtained as crystalline white solid (58 mg, 0.22 mmol, 87%). R_f = 0.37 (EtOAc +2% v/v acetic acid). ^{1}H NMR (700 MHz, $CDCl_3$) δ 7.80-7.76 (m, 2H), 7.41 (t, *J* = 7.7 Hz, 2H), 7.36 – 7.31 (m, 1H), 7.22

(s, 1H), 4.87 (t, *J* = 7.2 Hz, 2H), 3.12 (t, *J* = 7.2 Hz, 2H), 2.23 ppm (s, 3H). ^{13}C NMR (176 MHz, $CDCl_3$) δ 206.2, 162.8, 150.5, 132.7, 132.4, 128.9, 128.4, 125.7, 109.6, 46.9, 43.4, 30.3 ppm. HR-MS: calc. for $[M+H]^+$ $C_{14}H_{15}N_2O_3$ 259.10772 found 259.10779.

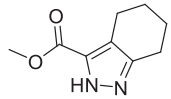

*Methyl 4,5,6,7-tetrahydro-2*H*-indazole-3-carboxylate (**4b**)*. 4,5,6,7-Tetrahydro-2*H*-indazole-3-carboxylate (324 mg, 2.13 mmol, 1.0 equiv.) was dissolved in 7.8 mL methanol and cooled to -10°C before thionyl chloride (278.3 μL, 3.84 mmol, 1.8 equiv.) was added dropwise to the solution. The reaction was vigorously stirred at room temperature for 5 days. The crude reaction mixture was concentrated under reduced pressure. The product was extracted thrice with EtOAc (20 mL) from water (20 mL) and the combined organic layers were dried over Na_2SO_4 and filtered. The filtrate was concentrated under reduced pressure and the residual was purified by means of silica gel column chromatography (elute: DCM / MeOH) and obtained as white solid (161.7 mg, 0.9 mmol, 42%). R_f = 0.23 (DCM +4% v/v MeOH). ^{1}H NMR (500 MHz, $CDCl_3$) δ 3.89 (s, 3H), 2.72 (td, *J* = 25.9, 6.1 Hz, 4H), 1.84-1.71 ppm (m, 4H). ^{13}C NMR (126 MHz, $CDCl_3$) δ 162.5, 119.9, 51.8, 22.9, 22.6, 22.2, 21.5 ppm. HR-MS: calc. for $[M+H]^+$ $C_9H_{13}N_2O_2$ 181.09715 found 181.09697.

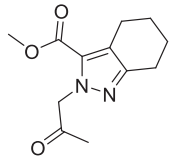

*Methyl 2-(2-oxopropyl)-4,5,6,7-tetrahydro-2*H*-indazole-3-carboxylate (**5c**)*. Methyl-4,5,6,7-tetrahydro-2*H*-indazol-3-carboxylate **4b** (90.4 mg, 0.5 mmol, 1.0 equiv.) and 1-chloroactone (161.44 μL, 2.01 mmol, 4.0 equiv.) were dissolved in 2.3 mL acetone and K_2CO_3 (153.22 mg, 1.1 mmol, 2.2 equiv.) was added. The reaction mixture was vigorously stirred at 60°C for 2 days. The crude reaction mixture was adjusted to pH 7 with 0.5 M HCl. The solvent was evaporated under reduced pressure. The crude reaction was extracted thrice with EtOAc (3x 50 mL) from water (50 mL) and the combined organic layers were dried over Na_2SO_4 and filtered. The filtrate was evaporated under reduced pressure and purified by means of silica gel column chromatography (elute: DCM / MeOH). The isomers were separated using preparative HPLC. The 2-alkylated product was obtained as white solid (24 mg, 0.1 mmol, 20%). R_f = 0.66 (DCM +5% v/v MeOH). ^{1}H NMR (500 MHz, $CDCl_3$) δ 4.88 (s, 2H), 3.90 (s, 3H), 2.77 (t, *J* = 6.0 Hz, 2H), 2.45 (t, *J* = 6.2 Hz, 2H), 2.14 (s, 3H), 1.84 – 1.74 ppm (m, 4H). ^{13}C NMR (126 MHz, $CDCl_3$) δ 201.0, 163.1, 141.0, 139.8, 120.7, 58.7, 52.0, 26.9, 22.3, 22.0, 21.3, 21.1 ppm. HR-MS: calc. for $[M+H]^+$ $C_{12}H_{17}N_2O_3$ 237.12547 found 237.12337.

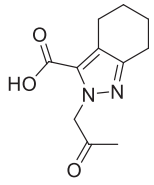

*2-(2-Oxopropyl)-4,5,6,7-tetrahydro-2*H*-indazole-3-carboxylate (**6c**)*. Methyl 2-(2-oxopropyl)-4,5,6,7-tetrahydro-2*H*-indazole-3-carboxylate **5c** (24 mg, 0.1 mmol, 1.0 equiv.) was solved in 0.8 mL water and NaOH (4.9 mg, 0.12 mmol, 1.2 equiv.) was added subsequently to the solution. The reaction mixture was stirred at 70°C for 5 h. The crude was acidified to pH 4-5 using 1 M HCl and extracted thrice with EtOAc (3x 50 mL) from water (50 mL). The combined organic layers were dried over Na_2SO_4, filtered and concentrated under reduced pressure. The product was obtained as white solid (12.2 mg, 0.05 mmol, 54%). R_f = 0.56 (DCM +35% v/v MeOH). ^{1}H NMR (500 MHz, CD_3CN) δ 5.23 (s, 2H), 4.44 (s, 1H), 2.71 (t, *J*= 6.1 Hz, 2H), 2.62 – 2.57 (m, 2H), 2.13 (s, 3H), 1.82 – 1.70 ppm (m, 4H). ^{13}C NMR (126 MHz, CD_3CN) δ 203.4, 161.9, 149.5, 129.7, 62.0, 27.3, 23.9, 23.8, 23.8, 23.1 ppm. HR-MS: calc. for $[M+H]^+$ $C_{11}H_{15}N_2O_3$ 223.10772 found 223.1080.

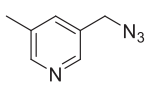

3-(Azidomethyl)-5-methylpyridine. 3-(Chloromethyl)-5-methylpyridine (300 mg, 1.7 mmol, 1.0 equiv.) and sodium azide (470 mg, 7.2 mmol, 4.2 equiv.) were dissolved in ACN (6.2 mL). *N,N*-Diisopropylethylamide (287 μL, 1.7 mmol, 1.0 equiv.), tetrabutylammonium iodide (6 mg, 20 μmol, 0.1 equiv.) and 18-crown-6 (4 mg, 20 μmol, 0.1 equiv.) were added. The reaction mixture was stirred at room temperature overnight. EtOAc was added to the crude product and the mixture was extracted with saturated $NaHCO_3$. The aqueous layer was extracted twice with EtOAc and the combined organic layers were concentrated under reduced pressure. The product was obtained as white crystalline solid (238 mg, 1.61 mmol, 95%) and used in the following step without further purification. R_f = 0.71 (EtOAc / MeOH / TEA = 9:1:0.1). ^{1}H NMR (500 MHz, $CDCl_3$) δ 8.43 (d, *J* = 2.0 Hz, 1H), 8.38 (d, *J* = 2.0 Hz, 1H), 7.47 (m, 1H), 4.35

(s, 2H), 2.37 ppm (s, 3H). ^{13}C NMR (126 MHz, $CDCl_3$) δ 150.5, 146.6, 136.4, 133.5, 130.7, 52.2, 18.5 ppm. HR-MS: calc. for $[M+H]^+$ $C_7H_9N_4$ 149.08217 found 149.08198.

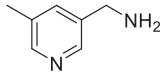

*(5-Methylpyridin-3-yl)methanamine (**14a**)*. 3-(Azidomethyl)-5-methylpyridine (244 mg, 1.7 mmol, 1.0 equiv.) was dissolved in 55 mL EtOAc / MeOH (2:1) and Pd/C (175 mg, 0.17 mmol, 0.1 equiv.) was added. The solution was stirred under inert hydrogen atmosphere for 1 h. The reaction mixture was filtered over Celite® and the filtrate was concentrated under reduced pressure. The residual was purified by means of silica gel column chromatography (elute: EtOAc / MeOH +1% v/v TEA) and the product was obtained as pale yellow oil (108.6 mg, 0.89 mmol, 54%). R_f = 0.23 (DCM / EtOH / sat.NH_4OH = 50:8:1). ^{1}H NMR (500 MHz, $CDCl_3$) δ 8.35 (d, *J* = 1.5 Hz, 1H), 8.33 (d, *J* = 1.5 Hz, 1H), 7.49 – 7.47 (m, 1H), 3.87 (s, 2H), 2.33 ppm (s, 3H). ^{13}C NMR (126 MHz, $CDCl_3$) δ 149.0, 146.2, 137.7, 135.6, 133.1, 43.9, 18.5 ppm. HR-MS: *m/z* calculated for $[M+H]^+$ $C_7H_{11}N_2$ 123.09167 found 123.09139.

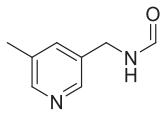

N-*((5-methylpyridin-3-yl)methyl)formamide (**13a**)*. (5-Methylpyridin-3-yl)methanamine **14a** (100 mg, 0.82 mmol, 1.0 equiv.) was dissolved in ethyl formate (200 μL, 2.5 mmol, 3.0 equiv.) and the solution was vigorously stirred at 60°C for 24 h. The solvent was removed under reduced pressure and the residual was purified by means of silica gel column chromatography (elute: EtOAc / MeOH +1% v/v TEA). The product was obtained as yellow oil (111 mg, 0.74 mmol, 90%). ^{1}H NMR (500 MHz, $CDCl_3$) δ 8.34 (d, *J* = 14.4 Hz, 2H), 8.29 (s, 1H), 7.46 (s, 1H), 4.47 (d, *J* = 6.1 Hz, 2H), 2.33 ppm (s, 3H). ^{13}C NMR (126 MHz, $CDCl_3$) δ 161.2, 149.7, 146.3, 136.4, 133.5, 133.0, 39.6, 18.5 ppm. HR-MS: *m/z* calculated for $[M+H]^+$ $C_8H_{11}N_2O$ 151.08659 found 151.08616.

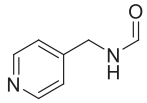

N-*(4-Picolyl)formamide (**13b**)*. 4-Picolylamine **14b** (305 μL, 3.0 mmol, 1.0 equiv.) was dissolved in ethyl formate (724 μL, 9.0 mmol, 3 equiv.) and the solution was vigorously stirred at 60°C for 24 h. The reaction mixture was evaporated under reduced pressure and the product was obtained as yellow oil (398 mg, 2.9 mmol, 97%). R_f = 0.21 (EtOAc / MeOH / TEA = 90:10:1). ^{1}H NMR (500 MHz, DMSO-d_6) mixture of rotamers is observed, major rotamer is given; δ 8.62 (bs, 1H), 8.50 (d, *J* = 6.0 Hz, 2H), 8.19 (s, 1H), 7.26 (d, *J* = 6.0 Hz, 2H), 4.33 ppm (d, *J* = 6.2 Hz, 2H). ^{13}C NMR (126 MHz, DMSO-d_6) δ 161.5, 149.6, 148.0, 122.2, 39.8 ppm (under solvent signal, determined by HSQC). LC-MS: *m/z* calculated for $[M+H]^+$ $C_7H_9N_2O$ 137 found 137.

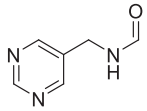

N-*(Pyrimidine-5-ylmethyl)formamide (**13c**)*. Prepared according to general procedure 1A with pyrimidine-5-carbaldehyde **12a** (300 mg, 2.8 mmol, 1.0 equiv.), formic acid (838 μL, 22 mmol, 7.9 equiv.) and formamide (1.6 mL, 33 mmol, 11.8 equiv.) under conventional heating at 180°C for 30 min. The product was purified by means of silica gel column chromatography (elute: EtOAc / MeOH +1% v/v TEA) to obtain the product as colorless oil (41 mg, 0.3 mmol, 10%). R_f = 0.17 (EtOAc / MeOH / TEA = 90:10:1). ^{1}H NMR (600 MHz, $CDCl_3$) mixture of rotamers is observed, major rotamer is given; δ 9.15 (s, 1H), 8.71 (s, 2H), 8.32 (s, 1H), 6.16 (bs, 1H), 4.51 ppm (d, *J* = 6.2 Hz, 2H). ^{13}C NMR (151 MHz, $CDCl_3$) δ 161.3, 158.3, 156.6, 131.5, 37.6 ppm. HR-MS: *m/z* calculated for $[M+H]^+$ $C_6H_8N_3O$ 138.0662 found 138.06579.

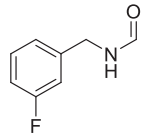

N-*(3-Fluorobenzyl)formamide (**13d**)*. Prepared according to general procedure 1A with 3-fluorobenzaldehyde **12b** (300 μL, 2.8 mmol, 1.0 equiv.), formic acid (530 μL, 14 mmol, 5.0 equiv.) and formamide (1.3 mL, 28 mmol, 10.0 equiv.) under conventional heating. The product was obtained by means of flash silica gel column chromatography (elute: cyclohexane / EtOAc) as pale yellow

oil (244 mg, 1.6 mmol, 56%). R_f = 0.27 (cyclohexane / EtOAc = 1:1). ^{1}H NMR (400 MHz, DMSO-d_6) mixture of rotamers is observed, major rotamer is given; δ 8.54 (bs, 1H), 8.15 (d, *J* = 0.8 Hz, 1H), 7.41-7.33 (m, 1H), 7.14 – 7.03 (m, 3H), 4.32 ppm (d, *J* = 6.2 Hz, 2H). ^{13}C NMR (101 MHz, DMSO-d_6) mixture of rotamers; δ 165.0, 163.4, 161.2, 142.1, 142.0, 130.3, 130.3, 123.3, 123.2, 114.0, 113.8, 113.7, 113.5, 40.2 ppm. LC-MS: *m/z* calculated for $[M+H]^+$ C_8H_9FNO 154.0 found 154.0.

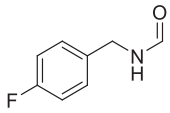

N-*(4-Fluorobenzyl)formamide (**13e**)*. Prepared according to general procedure 1A with 4-fluorobenzaldehyde **12c** (300 μL, 2.8 mmol, 1.0 equiv.), formic acid (530 μL, 14 mmol, 5.0 equiv.) and formamide (1.3 mL, 28 mmol, 10.0 equiv.) under conventional heating. The product was obtained by means of flash silica gel column chromatography (elute: cyclohexane / EtOAc) as white crystalline solid (254 mg, 1.7 mmol, 59%). R_f = 0.23 (cyclohexane / EtOAc = 1:1). ^{1}H NMR (400 MHz, DMSO-d_6) mixture of rotamers is observed, major rotamer is given; δ 8.50 (bs, 1H), 8.12 (s, 1H), 7.34-7.25 (m, 2H), 7.21-7.10 (m, 2H), 4.28 ppm (d, *J* = 6.2 Hz, 2H). ^{13}C NMR (101 MHz, DMSO-d_3) δ 161.1, 129.3, 129.3, 115.2, 115.0, 40.0 ppm. LC-MS: *m/z* calculated for $[M+H]^+$ C_8H_9FNO 154.0 found 154.0.

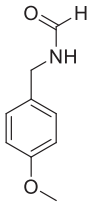

N-*(4-Methoxybenzyl)formamide (**13f**)*. Prepared according to general procedure 1A using 4-methoxybenzaldehyde **12d** (44.6 μL, 0.37 mmol, 1.0 equiv.), formic acid (72.9 μL, 1.84 mmol, 5.0 equiv.) and formamide (731.9 μL, 18.36 mmol, 50.0 equiv.) using microwave irradiation. The product was purified by means of flash silica gel column chromatography (elute: cyclohexane / EtOAc) and obtained as off-white solid (29.9 mg, 0.18 mmol, 49%). R_f = 0.24 (cyclohexane / EtOAc 1:3). ^{1}H NMR (400 MHz, $CDCl_3$) mixture of rotamers, only major rotamer given; δ 8.24 (s, 1H), 7.22 (d, *J* = 8.7 Hz, 2H), 6.87 (d, *J* = 8.7 Hz, 2H), 5.75 (bs, 1H), 4.42 (d, *J* = 5.8 Hz, 2H), 3.80 ppm (s, 3H). ^{13}C NMR (100 MHz, $CDCl_3$) mixture of rotamers, only major rotamer given; δ 160.9, 159.4, 129.4, 128.5, 114.3, 55.5, 41.9 ppm. MS-EI: *m/z* (%): 165 (100) $[M]^+$, 136 (56), 121 (85), 109 (20), 91 (18), 77 (26).

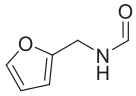

N-*(Furan-2-ylmethyl)formamide (**13g**)*. Prepared according to general procedure 1A with furfural **12e** (300 μL, 3.6 mmol, 1.0 equiv.), formic acid (683 μL, 18 mmol, 5.0 equiv.) and formamide (1.7 mL, 36 mmol, 10.0 equiv.) under conventional heating. The product was obtained by means of flash silica gel column chromatography (elute: cyclohexane / EtOAc) as brown oil (164 mg, 1.3 mmol, 36%). R_f = 0.11 (cyclohexane / EtOAc = 1:1). ^{1}H NMR (600 MHz, DMSO-d_6) mixture of rotamers is observed, major rotamer is given; δ 8.47 (bs, 1H), 8.06 (s, 1H), 7.62-7.55 (m, 1H), 6.39 (dd, *J* = 3.0, 1.9 Hz, 1H), 6.25 (d, *J* = 3.2 Hz, 1H), 4.28 ppm (d, *J* = 5.8 Hz, 2H). ^{13}C NMR (151 MHz, DMSO-d_6) δ 160.9, 151.8, 142.2, 110.5, 107.0, 34.0 ppm. MS-EI: *m/z* (%): 125 (100) $[M]^+$, 108 (5), 96 (50), 81 (48), 68 (20), 53 (20).

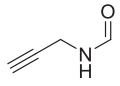

*N-(Propargyl)formamide (**13h**)*. Propargylamine **14c** (500 μL, 9.1 mmol, 1.0 equiv.) and formamide (360 μL, 9.1 mmol, 1.0 equiv.) were dissolved in toluene (8 mL) and hydroxylamine hydrochloride (63 mg, 0.9 mmol, 0.1 equiv.) was added. The reaction mixture was stirred to reflux for 24 h. The reaction mixture was allowed to cool down to room temperature and concentrated under reduced pressure. The crude reaction was extracted with DCM and the organic layer was washed twice with water. The combined organic layers were dried over Na_2SO_4, filtered and concentrated under reduced pressure. The product was obtained by means of silica gel column chromatography (elute: cyclohexane / EtOAc) as white crystalline solid (367 mg, 4.4 mmol, 48%). R_f = 0.28 (cyclohexane / EtOAc = 1:1). ^{1}H NMR (500 MHz, $CDCl_3$) mixture of rotamers is observed, major rotamer is given; δ 8.19 (s, 1H),

5.86 (bs, 1H), 4.10 (ddd, *J* = 5.4, 2.6, 0.8 Hz, 2H), 2.26 ppm (t, *J* = 2.6 Hz, 1H). ^{13}C NMR (126 MHz, $CDCl_3$) δ 160.7, 78.9, 72.1, 28.0 ppm.

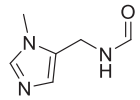

N-*((1-Methyl-1*H*-imidazol-5-yl)methyl)formamide* ***(13i)***. (1-Methyl-1*H*-imidazol-5-yl)methanamine **14d** (233 mg, 2.1 mmol, 1.0 equiv.) was dissolved in ethyl formate (505 μL, 6.3 mmol, 3.0 equiv.) and the solution was transferred into a sealed glass vial. The reaction was vigorously stirred at 60°C for 24 h. After completion of the reaction, the reaction mixture was evaporated under reduced pressure and purified by means of silica gel column chromatography (EtOAc / MeOH). The product was obtained as colorless oil (252 mg, 1.81 mmol, 86%). R_f = 0.16 (EtOAc / MeOH / TEA = 90:10:1). ^{1}H NMR (700 MHz, DMSO-d_6) mixture of rotamers is observed, major rotamer is given; δ 8.36 (bs, 1H), 8.04 (s, 1H), 7.53 (s, 1H), 6.78 (s, 1H), 4.28 (d, *J* = 5.7 Hz, 2H), 3.55 ppm (s, 3H). ^{13}C NMR (176 MHz, DMSO-d_6) δ 160.8, 138.4, 128.6, 127.6, 30.9, 30.5 ppm. LC-MS: *m/z* calculated for $[M+H]^+$ $C_6H_{10}N_3O$ 140; found, 140.

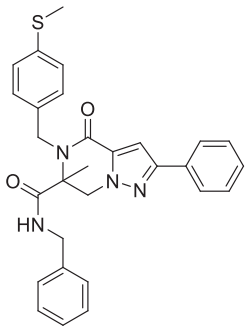

N-*Benzyl-6-methyl-5-(4-(methylthio)benzyl)-4-oxo-2-phenyl-4,5,6,7-tetrahydropyrazolo[1,5-a]pyrazine-6-carboxamide* ***(2a)***. Prepared according to general procedure 2 using 1-(2-oxopropyl)-3-phenyl-1*H*-pyrazole-5-carboxylic acid **6a** (200.0 mg, 0.82 mmol, 1.0 equiv.), 4-(methylthio)benzylamine **9e** (144.1 μL, 0.82 mmol, 1.0 equiv.) and benzylisocyanide **8k** (99.7 μL, 0.82 mmol, 1.0 equiv.). The product was obtained as white solid (382.4 mg, 0.77 mmol, 94%). Enantiomers were separated by means of chiral preparative HPLC. Optical rotation after enantiomer separation: *R* -0.250 °; *S* +0.258 °. Crystals for X-ray structure determination were grown in Et_2O / DCM (5:1). R_f = 0.45 (cyclohexane / EtOAc = 1:1). ^{1}H NMR (500 MHz, $CDCl_3$) δ 7.77 (d, *J* = 7.4 Hz, 2H), 7.41 (t, *J* = 7.4 Hz, 2H), 7.35 (t, *J* = 7.4 Hz, 1H), 7.27 (d, *J* = 7.9 Hz, 1H), 7.16 (d, *J* = 8.3 Hz, 2H), 7.12 – 7.08 (m, 3H), 7.06 (s, 1H), 6.78 (d, *J* = 6.4 Hz, 2H), 6.31 (s, 1H), 5.15 (d, *J* = 15.5 Hz, 1H), 5.06 (d, *J* = 13.0 Hz, 1H), 4.61 (d, *J* = 15.5 Hz, 1H), 4.37 (dd, *J* = 14.9, 6.7 Hz, 1H), 4.19 (d, *J* = 13.0 Hz, 1H), 4.01 (dd, *J* = 14.9, 5.0 Hz, 1H), 2.45 (s, 3H), 1.70 ppm (s, 3H). ^{13}C NMR (126 MHz, $CDCl_3$) δ 170.7, 159.1, 152.4, 138.5, 137.1, 134.6, 134.1, 132.3, 128.9, 128.7, 128.5, 128.2, 127.6, 127.1, 127.0, 125.8, 105.4, 66.0, 55.8, 45.7, 44.1, 22.0, 15.8 ppm. HR-MS: calc. for $[M+H]^+$ $C_{29}H_{29}N_4O_2S$ 497.2006 found 497.2002.

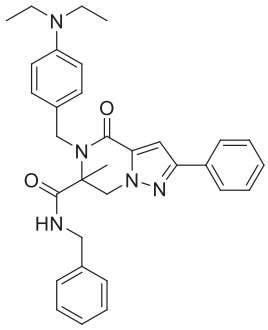

N-*Benzyl-5-(4-(diethylamino)benzyl)-6-methyl-4-oxo-2-phenyl-4,5,6,7-tetrahydropyrazolo[1,5-a]pyrazine-6-carboxamide* ***(2b)***. Prepared according to general procedure 2 using 1-(2-oxopropyl)-3-phenyl-1*H*-pyrazole-5-carboxylic acid **6a** (20.0 mg, 0.08 mmol, 1.0 equiv.), (4-aminomethyl)-*N*,*N*-diethylaniline **9c** (13.3 μL, 0.07 mmol, 0.9 equiv.) and benzyl isocyanide **8k** (10.0 μL,

0.08 mmol, 1.0 equiv.). The product was obtained as light yellow solid (11.5 mg, 0.02 mmol, 27%). R_f = 0.42 (cyclohexane / EtOAc = 1:1). ^{1}H NMR (500 MHz, $CDCl_3$) δ 7.80 (d, *J* = 7.4 Hz, 2H), 7.41 (t, *J* = 7.4 Hz, 2H), 7.34 (t, *J* = 7.4 Hz, 1H), 7.28 (s, 1H), 7.13 – 7.02 (m, 4H), 6.70 (d, *J* = 7.0 Hz, 2H), 6.55 – 6.56 (m, 2H), 6.20 – 6.13 (m, 1H), 5.10 (d, *J* = 12.8 Hz, 1H), 4.95 (d, *J* = 15.0 Hz, 1H), 4.70 (d, *J* = 15.0 Hz, 1H), 4.32 (dd, *J* = 15.0, 7.0 Hz, 1H), 4.17 (d, *J* = 12.8 Hz, 1H), 3.80 (dd, *J* = 15.0 Hz, 1H), 3.31 (q, *J* = 7.0 Hz, 4H), 1.80 (s, 3H), 1.13 ppm (t, *J* = 7.0 Hz, 6H). ^{13}C NMR (126 MHz, $CDCl_3$) δ 171.2, 159.1, 152.1, 147.5, 137.2, 134.5, 132.5, 129.8, 128.9, 128.6, 128.4, 127.4, 127.0, 125.8, 123.8, 112.1, 105.2, 65.9, 55.9, 45.4, 44.4, 44.0, 21.8, 12.6 ppm. HR-MS: calc. for $[M+H]^+$ $C_{32}H_{36}N_5O_2$ 522.2864 found 522.2873, calc. for $[M+Na]^+$ $C_{32}H_{35}N_5O_2Na$ 544.2694 found 544.2694.

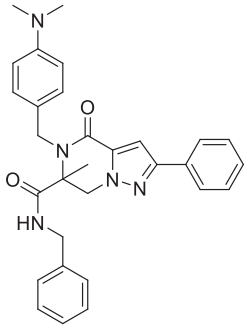

N-*Benzyl-5-(4-(dimethylamino)benzyl)-6-methyl-4-oxo-2-phenyl-4,5,6,7-tetrahydropyrazolo[1,5-a]pyrazine-6-carboxamide* (***2c***). Prepared according to the general procedure 2 using 1-(2-oxopropyl)-3-phenyl-1*H*-pyrazole-5-carboxylic acid **6a** (36.7 mg, 0.15 mmol, 1.0 equiv.), (4-aminomethyl)-*N*,*N*-dimethylaniline **9b** (22.2 μL, 0.15 mmol, 1.0 equiv.) and benzyl isocyanide **8k** (18.3 μL, 0.15 mmol, 1.0 equiv.). The product was obtained as light-yellow solid (44.4 mg, 0.09 mmol, 60%). R_f = 0.38 (cyclohexane / EtOAc = 1:1). ^{1}H NMR (500 MHz, $CDCl_3$) δ 7.81 – 7.79 (m, 2H), 7.42 (t, *J* = 7.5 Hz, 2H), 7.35 (t, *J* = 7.5 Hz, 1H), 7.29 (d, *J* = 8.6 Hz, 2H), 7.14 – 7.03 (m, 5H), 6.72 (d, *J* = 7.1 Hz, 2H), 6.61 (bs, 1H), 6.14 (t, *J* = 5.4 Hz, 1H), 5.10 (d, *J* = 12.8 Hz, 1H), 4.91 (d, *J* = 14.7 Hz, 1H), 4.77 (d, *J* = 14.7 Hz, 1H), 4.28 (dd, *J* = 14.9, 7.0 Hz, 1H), 4.17 (d, *J* = 12.8 Hz, 1H), 3.88 (dd, *J* = 14.9, 4.6 Hz, 1H), 2.92 (s, 6H), 1.78 ppm (s, 3H). ^{13}C NMR (126 MHz, $CDCl_3$) δ 171.1, 159.1, 152.2, 137.2, 134.4, 132.4, 129.4, 128.9, 128.6, 128.4, 127.4, 127.1, 125.8, 112.9, 105.2, 77.4, 65.9, 60.6, 55.9, 45.4, 44.1, 40.6, 21.8 ppm. HR-MS: calc. for $[M+H]^+$ $C_{30}H_{32}N_5O_2$ 494.2551 found 494.2561, calc. for $[M+Na]^+$ $C_{30}H_{31}N_5O_2Na$ 516.2370 found 516.2382.

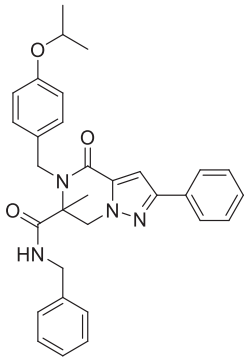

N-*Benzyl-5-(4-isopropoxybenzyl)-6-methyl-4-oxo-2-phenyl-4,5,6,7-tetrahydropyrazolo[1,5-a]pyrazine-6-carboxamide* (***2e***). Prepared according to general procedure 2 using 1-(2-oxopropyl)-3-phenyl-1*H*-pyrazole-5-carboxylic acid **6a** (20.0 mg, 0.08 mmol, 1.0 equiv.), (4-isopropoxyphenyl)-methanamine **9d** (13.7 μL, 0.08 mmol, 1.0 equiv.) and benzyl isocyanide **8k** (10.0 μL, 0.08 mmol, 1.0 equiv.). The product was obtained as brown solid (24.9 mg, 0.05 mmol, 60%). R_f = 0.55 (cyclohexane / EtOAc = 1:1). ^{1}H NMR (500 MHz, $CDCl_3$) δ 7.99 (d, *J* = 7.2 Hz, 2H), 7.71 – 7.45 (m, 5H), 7.31 (d, *J* = 7.2 Hz, 3H), 6.98 – 7.03 (m, 4H), 6.65 – 6.77 (m, 1H), 5.55 – 5.23 (m, 2H), 4.88 (d, *J* = 15.0 Hz, 1H), 4.73 (hept, *J* = 6.0 Hz, 1H), 4.59 (d, *J* = 15.0 Hz, 1H), 4.39 – 4.44 (m, 1H), 4.22 (d, *J* = 15.0 Hz, 1H), 1.94 (s, 3H), 1.55 ppm (d, *J* = 6.0 Hz, 6H). ^{13}C NMR (126 MHz, $CDCl_3$) δ 170.9, 159.1, 157.6, 152.2, 137.2,

134.3, 132.3, 129.6, 129.2, 128.9, 128.6, 128.4, 127.5, 127.0, 125.8, 116.3, 105.3, 69.9, 65.9, 55.8, 45.5, 44.0, 22.1, 21.9 ppm. HR-MS: calc. for $[M+H]^+$ $C_{31}H_{33}N_4O_3$ 509.2547 found 509.2561, calc. for $[M+Na]^+$ $C_{31}H_{32}N_4O_3Na$ 531.2367 found 531.2382.

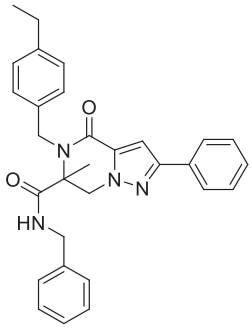

N-*Benzyl-5-(4-ethylbenzyl)-6-methyl-4-oxo-2-phenyl-4,5,6,7-tetrahydropyrazolo[1,5-a]pyrazine-6-carboxamide* (***2h***). Prepared according to the general procedure 2 using 1-(2-oxopropyl)-3-phenyl-1*H*-pyrazole-5-carboxylic acid **6a** (50.0 mg, 0.20 mmol, 1.0 equiv.), (4-ethylphenyl)methanamine **9f** (29.2 μL, 0.20 mmol, 1.0 equiv.) and benzyl isocyanide **8k** (24.9 μL, 0.20 mmol, 1.0 equiv.). The product was obtained as light-yellow solid (72.8 mg, 0.15 mmol, 74%). R_f = 0.56 (cyclohexane / EtOAc = 1:1). ^{1}H NMR (400 MHz, $CDCl_3$) δ 7.96 (d, *J* = 7.3 Hz, 2H), 7.58 (t, *J* = 7.3 Hz, 2H), 7.52 (d, *J* = 7.3 Hz, 1H), 7.49 – 7.41 (m, 2H), 7.33 – 7.23 (m, 5H), 6.93 (d, *J* = 7.1 Hz, 2H), 6.38 (t, *J* = 5.6 Hz, 1H), 5.24 (dd, *J* = 15.0, 5.4 Hz, 2H), 4.89 (d, *J* = 15.0 Hz, 1H), 4.53 (dd, *J* = 15.0, 5.1 Hz, 1H), 4.37 (d, *J* = 15.0 Hz, 1H), 4.10 (dd, *J* = 15.0, 5.1 Hz, 1H), 2.78 (q, *J* = 7.7 Hz, 2H), 1.89 (s, 3H), 1.38 ppm (t, *J* = 7.7 Hz, 3H). ^{13}C NMR (101 MHz, $CDCl_3$) δ 170.9, 159.1, 152.4, 144.2, 137.2, 135.2, 134.3, 132.4, 128.9, 128.8, 128.7, 128.4, 127.8, 127.6, 127.1, 125.9, 105.4, 66.0, 55.9, 45.9, 44.1, 28.6, 21.9, 15.6 ppm. HR-MS: calc. for $[M+H]^+$ $C_{30}H_{31}N_4O_2^+$ 479.2442 found 479.2454, calc. for $[M+Na]^+$ $C_{30}H_{30}N_4O_2Na$ 501.2261 found 501.2273.

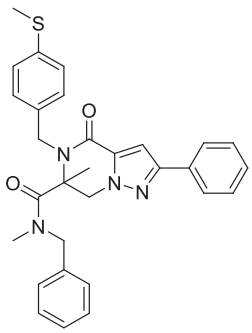

N-*Benzyl-N,6-dimethyl-5-(4-(methylthio)benzyl)-4-oxo-2-phenyl-4,5,6,7-tetrahydropyrazolo[1,5-a]pyrazine-6-carboxamide* (***2i***). *N*-Benzyl-6-methyl-5-(4-(methylthio)benzyl)-4-oxo-2-phenyl-4,5,6,7-tetrahydropyrazolo[1,5-a]pyrazine-6-carboxamide **2a** (11 mg, 22 μmol, 1.0 equiv.) was dissolved in DMF (0.5 mL) and cooled to 0°C. Sodium hydride (1.8 mg, 44 μmol, 2.0 equiv.) was thereto added and the solution was stirred at 0°C for 10 min. Subsequently, methyl iodide (1.7 μL, 27 μmol, 1.2 equiv.) was added and the solution was allowed to warm up to room temperature overnight. The excess of sodium hydride was quenched by addition of 1 mL water at 0°C. The product was extracted thrice with EtOAc and the combined organic layers were concentrated under reduced pressure. The product was purified by means of silica gel column chromatography (elute: cyclohexane / EtOAc) and obtained as white solid (4 mg, 8 μmol, 35%). R_f = 0.67 (cyclohexane / EtOAc = 1:1). ^{1}H NMR (600 MHz, $CDCl_3$) δ 7.81 – 7.77 (m, 2H), 7.42 (d, *J* = 7.2 Hz, 2H), 7.36 – 7.33 (m, 1H), 7.31 – 7.27 (m, 5H), 7.23 (s, 1H), 7.21 – 7.18 (m, 2H), 7.10 (d, *J* = 7.2 Hz, 2H), 4.77 – 4.67 (m, 2H), 4.61 (d, *J* = 15.4 Hz, 2H), 4.36 (d, *J* = 13.5 Hz, 2H), 2.79 (s, 3H), 2.48 (s, 3H), 1.65 ppm (s, 3H). ^{13}C NMR (151 MHz,

$CDCl_3$) δ 168.2, 158.6, 152.7, 138.3, 135.9, 134.7, 134.3, 132.3, 129.5, 129.0, 129.0, 128.6, 128.0, 127.8, 126.6, 125.8, 105.6, 66.5, 53.8, 53.7, 47.3, 36.6, 23.8, 16.0 ppm. HR-MS: calc. for $[M+H]^+$ $C_{30}H_{31}N_4O_2S$ 511.21622 found 511.21567.

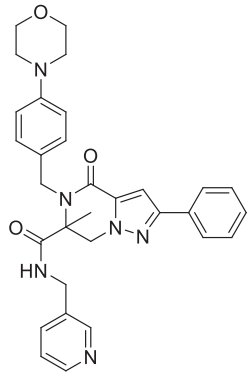

6-Methyl-5-(4-morpholinobenzyl)-4-oxo-2-phenyl-N-*(pyridin-3-ylmethyl)-4,5,6,7-tetrahydropyrazolo[1,5-a]pyrazine-6-carboxamide (**3a**)*. Prepared according to general procedure 2 using 1-(2-oxopropyl)-3-phenyl-1*H*-pyrazole-5-carboxylic acid **6a** (100.0 mg, 0.41 mmol, 1.0 equiv.), 4-(morpholinophenyl)methanamine **9a** (78.7 mg, 0.41 mmol, 1.0 equiv.) and 3-(isocyanomethyl)pyridine **8j** (48.4 mg, 0.41 mmol, 1.0 equiv.). The product was obtained as white solid (97.2 mg, 0.18 mmol, 44%). Enantiomers were separated by means of chiral preparative HPLC. Optical rotation after enantiomer separation: *R* -0.431 °; *S* +0.390 °. R_f = 0.51 (dichloromethane / MeOH = 4:1). ^{1}H NMR (400 MHz, $CDCl_3$) δ 8.33 (dd, *J* = 4.7, 1.4 Hz, 1H), 8.19 (d, *J* = 1.4 Hz, 1H), 7.81 – 7.68 (m, 2H), 7.46 – 7.30 (m, 3H), 7.27 (s, 1H), 6.98 (s, 1H), 6.97 (dt, *J* = 7.8, 1.9 Hz, 1H), 6.90 (dd, *J* = 7.8, 4.7 Hz, 1H), 6.79 (d, *J* = 8.7 Hz, 2H), 6.64 (t, *J* = 5.5 Hz, 1H), 5.06 (d, *J* = 13.0 Hz, 1H), 4.97 (d, *J* = 15.3 Hz, 1H), 4.73 (d, *J* = 15.3 Hz, 1H), 4.25 (dd, *J* = 15.1, 6.5 Hz, 1H), 4.16 (d, *J* = 13.0 Hz, 1H), 4.00 (dd, *J* = 15.1, 5.5 Hz, 1H), 3.84 (t, *J* = 4.8 Hz, 4H), 3.10 (t, *J* = 4.8 Hz, 4H), 1.72 ppm (s, 3H). ^{13}C NMR (101 MHz, $CDCl_3$) δ 171.3, 159.1, 152.3, 151.0, 148.9, 148.8, 134.8, 134.3, 133.1, 132.2, 129.0, 128.9, 128.7, 128.5, 125.8, 123.6, 115.9, 105.2, 66.9, 65.9, 55.8, 48.9, 45.5, 41.5, 21.8 ppm. HR-MS: calc. for $[M+H]^+$ $C_{31}H_{33}N_6O_3$ 537.2609 found 537.2601.

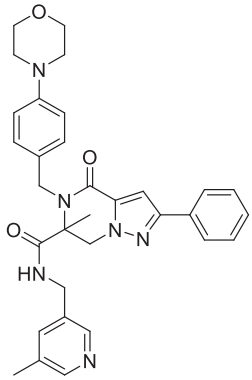

6-Methyl-N-*((5-methylpyridin-3-yl)methyl)-5-(4-morpholinobenzyl)-4-oxo-2-phenyl-4,5,6,7-tetrahydropyrazolo[1,5-a]pyrazine-6-carboxamide (**3b**)*. Prepared according to general procedure 3B using Burgess reagent (95 mg, 400 μmol, 2.0 equiv.), *N*-((5-methylpyridin-3-yl)methyl)formamide **13a** (30 mg, 200 μmol, 1.0 equiv.), 1-(2-oxopropyl)-3-phenyl-1*H*-pyrazole-5-carboxylic acid **6a** (49 mg, 200 μmol, 1.0 equiv.) and 4-(morpholinophenyl)methanamine **9a** (35 mg, 180 μmol, 1.0 equiv.) in MeOH (1.2 mL) and ACN (5.5 mL). The product was purified by means of silica gel column chromatography (DCM / EtOH / sat. NH_4OH) and obtained as white crystalline solid (13 mg, 24 μmol, 13%). ^{1}H NMR (700 MHz, $CDCl_3$) δ 8.18 (d, *J* = 2.1 Hz, 1H), 7.99 (d, *J* = 2.1 Hz, 1H), 7.77 (d, *J* = 7.1 Hz, 2H), 7.42 – 7.36 (m, 2H), 7.34 – 7.29 (m, 3H), 7.07 (s, 1H), 6.83 – 6.81 (m, 2H), 6.81 – 6.79 (m, 1H), 6.34 (t, *J* = 6.3 Hz, 1H), 5.08 (d, *J* = 12.8 Hz, 1H), 4.91 (d, *J* = 15.3 Hz, 1H), 4.81 (d, *J* = 15.3 Hz, 1H), 4.26 (dd, *J* = 15.1, 6.3 Hz, 1H), 4.16 (d, *J* = 12.8 Hz, 1H), 3.90 (dd, *J* = 15.1, 6.3 Hz, 1H), 3.85 (t, *J* = 4.9 Hz, 4H), 3.11 (td, *J* = 4.3, 1.5 Hz, 4H), 2.02 (s, 3H), 1.75 ppm (s, 3H). ^{13}C NMR (176 MHz, $CDCl_3$)

δ 171.3, 159.0, 152.3, 151.1, 149.6, 145.8, 135.3, 134.3, 133.3, 132.5, 132.2, 129.2, 128.9, 128.7, 128.5, 125.8, 116.0, 105.1, 66.9, 65.9, 55.8, 49.0, 45.5, 41.4, 21.9, 18.2 ppm. HR-MS: calc. for $[M+H]^+$ $C_{32}H_{35}N_6O_3$ 551.27652 found 551.27602.

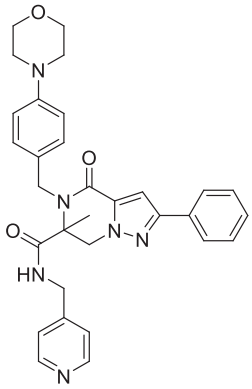

6-Methyl-5-(4-morpholinobenzyl)-4-oxo-2-phenyl-N-*(pyridin-4-ylmethyl)-4,5,6,7-tetrahydropyrazolo[1,5-a]pyrazine-6-carboxamide* (***3c***). Prepared according to general procedure 3B using Burgess reagent (83 mg, 348 μmol, 1.6 equiv.), *N*-(4-picolyl)formamide **13b** (30 mg, 220 μmol, 1.0 equiv.), 1-(2-oxopropyl)-3-phenyl-1*H*-pyrazole-5-carboxylic acid **6a** (54 mg, 220 μmol, 1.0 equiv.) and 4-(morpholinophenyl) methanamine **9a** (38 mg, 198 μmol, 0.9 equiv.) in MeOH (1.2 mL) and ACN (5.5 mL). The product was purified twice by means of silica gel column chromatography (1st elute: DCM / MeOH; 2nd elute: DCM / EtOH / sat. NH_4OH) and obtained as white solid (12 mg, 22 μmol, 11%). R_f = 0.29 (DCM / EtOH / sat. NH_4OH = 75:4:0.5). ^1H NMR (700 MHz, CD_2Cl_2) δ 8.27-8.22 (m, 2H), 7.85 – 7.80 (m, 2H), 7.46 – 7.41 (m, 2H), 7.38 – 7.35 (m, 1H), 7.34 (d, *J* = 8.7 Hz, 2H), 7.15 (s, 1H), 6.84 – 6.80 (m, 2H), 6.60 – 6.57 (m, 2H), 6.31 (t, *J* = 6.2 Hz, 1H), 5.03 (d, *J* = 12.8 Hz, 1H), 4.88 (s, 2H), 4.26 (dd, *J* = 16.0, 6.2 Hz, 1H), 4.22 (d, *J* = 12.8 Hz, 1H), 3.94 (dd, *J* = 16.0, 6.2 Hz, 1H), 3.83 – 3.78 (m, 4H), 3.07 (m, 4H), 1.76 ppm (s, 3H). ^{13}C NMR (176 MHz, CD_2Cl_2) δ 171.9, 159.2, 152.4, 151.5, 150.1, 146.7, 134.9, 132.7, 129.4, 129.2, 129.0, 128.7, 125.9, 121.8, 116.1, 105.2, 67.1, 66.2, 56.2, 49.2, 45.6, 43.0, 21.8 ppm. HR-MS: calc. for $[M+H]^+$ $C_{31}H_{33}N_6O_3$ 537.26087 found 537.26006.

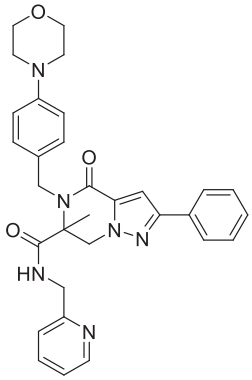

6-Methyl-5-(4-morpholinobenzyl)-4-oxo-2-phenyl-N-*(pyridin-2-ylmethyl)-4,5,6,7-tetrahydropyrazolo[1,5-a]pyrazine-6-carboxamide* (***3d***). 6-Methyl-5-(4-morpholinobenzyl)-4-oxo-2-phenyl-4,5,6,7-tetrahydropyrazolo[1,5-a]pyrazine-6-carboxamide **3k** (30 mg, 67 μmol, 1.0 equiv.) was dissolved in DMF (0.50 mL) and cooled to 0°C. Solid sodiumhydride (60% dispersion in mineral oil, 3 mg, 75 μmol, 1.1 equiv.) was added and the resulting suspension was stirred at 0°C for half an hour. 2-Picolyl chloride (basic workup of the commercially obtained HCl salt with saturated $NaHCO_3$ yielded the free chloride derivative) (7.2 μL, 75 μmol, 1.1 equiv.) was added to via a syringe and the vial was allowed to warm up to room temperature overnight. Afterwards, the mixture was cooled to 0°C and water (1 mL) was added. The mixture was extracted thrice with EtOAc, the combined organic layers were washed with brine, dried over Na_2SO_4, filtered and concentrated under reduced pressure. The product was purified by means of silica gel column chromatography (elute: EtOAc/ MeOH / TEA) and obtained as white solid (7 mg, 13 μmol, 19%). R_f = 0.53 (EtOAc / MeOH / TEA = 90:10:1). ^1H NMR (700 MHz, $CDCl_3$) δ 8.43 (d, *J* = 4.9 Hz, 1H), 7.81 – 7.76 (m, 2H), 7.45 (td, *J* = 7.7, 1.8 Hz, 1H), 7.40 (t, *J* = 7.7 Hz, 2H), 7.35 – 7.30 (m, 1H), 7.28 (d, *J* = 8.7 Hz, 2H), 7.22 (t, *J* = 4.9 Hz, 1H), 7.15 (s, 1H), 7.10 – 7.06 (m, 1H), 6.83 (t, *J* = 8.1 Hz, 3H), 5.38 (d, *J* = 15.6 Hz, 1H), 5.04 (d, *J* = 13.0 Hz, 1H), 4.53 (d, *J* = 15.6 Hz, 1H), 4.45 (dd, *J* = 16.6, 4.9 Hz, 1H), 4.28 (dd, *J* = 16.6, 4.9 Hz, 1H), 4.20 (d, *J* = 13.0 Hz,

1H), 3.86 – 3.82 (m, 4H), 3.13 – 3.07 (m, 4H), 1.71 ppm (s, 3H). ^{13}C NMR (176 MHz, $CDCl_3$) δ 171.0, 159.1, 155.3, 152.2, 150.8, 149.1, 136.8, 134.5, 132.5, 129.4, 128.9, 128.7, 128.4, 125.8, 122.5, 121.4, 116.0, 105.3, 67.0, 65.8, 55.8, 49.3, 45.7, 44.8, 22.2 ppm. HR-MS: calc. for $[M+H]^+$ $C_{31}H_{33}N_6O_3$ 537.26087 found 537.26033.

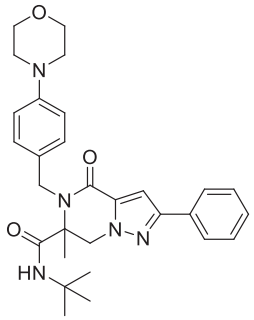

N-*(Tert-butyl)-6-methyl-5-(4-morpholinobenzyl)-4-oxo-2-phenyl-4,5,6,7-tetrahydropyrazolo[1,5-a]pyrazine-6-carboxamide* ***(3e)***. Prepared according to general procedure 2 using 1-(2-oxopropyl)-3-phenyl-1*H*-pyrazole-5-carboxylic acid **6a** (108 mg, 0.44 mmol, 1.0 equiv.), 4-(morpholinophenyl) methanamine **9a** (85 mg, 0.44 mmol) and *tert*-butylisocyanide **8l** (50 μL, 0.44 mmol, 1.0 equiv.). The product was purified by means of silica gel column chromatography (elute: pentane / EtOAc) and obtained as yellow solid (126 mg, 0.25 mmol, 57%). R_f = 0.21 (cyclohexane / EtOAc = 1:1). ^{1}H NMR (700 MHz, $CDCl_3$) δ 7.82 – 7.79 (m, 2H), 7.42 – 7.39 (m, 4H), 7.35 – 7.31 (m, 1H), 7.17 (s, 1H), 6.91 – 6.88 (m, 2H), 5.41 (s, 1H), 4.97 (d, *J* = 12.9 Hz, 1H), 4.94 (d, *J* = 15.2 Hz, 1H), 4.69 (d, *J* = 15.2 Hz, 1H), 4.14 (d, *J* = 12.8 Hz, 1H), 3.87 – 3.84 (m, 4H), 3.17 – 3.10 (m, 4H), 1.74 (s, 3H), 0.94 ppm (s, 9H). ^{13}C NMR (176 MHz, $CDCl_3$) δ 169.8, 159.2, 152.1, 151.3, 134.3, 132.6, 129.8, 129.0, 128.9, 128.4, 125.9, 116.3, 104.9, 67.0, 66.2, 56.1, 51.7, 49.3, 45.4, 28.2, 21.6 ppm. HR-MS: calc. for $[M+H]^+$ $C_{29}H_{36}N_5O_3$ 502.28127 found 502.28028.

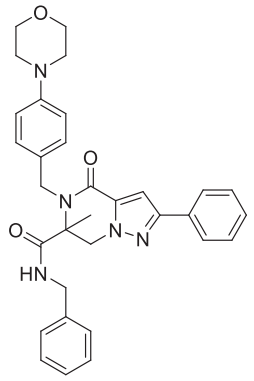

N-*Benzyl-6-methyl-5-(4-morpholinobenzyl)-4-oxo-2-phenyl-4,5,6,7-tetrahydropyrazolo[1,5-a]pyrazine-6-carboxamide* ***(3f)***. Prepared according to general procedure 2 using 1-(2-oxopropyl)-3-phenyl-1*H*-pyrazole-5-carboxylic acid **6a** (30.0 mg, 0.12 mmol, 1.0 equiv.), (4-morpholino-phenyl)methanamine **9a** (21.2 μL, 0.12 mmol, 1.0 equiv.) and benzyl isocyanide **8k** (15.0 μL, 0.12 mmol, 1.0 equiv.). The product was obtained as brown solid (44.3 mg, 0.08 mmol, 67%). R_f = 0.25 (cyclohexane / EtOAc = 3:7). ^{1}H NMR (500 MHz, $CDCl_3$) δ 7.79 (d, *J* = 7.3 Hz, 2H), 7.41 (t, *J* = 7.3 Hz, 2H), 7.35 (t, *J* = 7.3 Hz, 1H), 7.30 (d, *J* = 8.7 Hz, 2H), 7.13 – 7.07 (m, 4H), 6.80 (d, *J* = 8.7 Hz, 2H), 6.75 (d, *J* = 6.4 Hz, 2H), 6.21 (t, *J* = 5.4 Hz, 1H), 5.08 (d, *J* = 12.9 Hz, 1H), 4.98 (d, *J* = 15.0 Hz, 1H), 4.74 (d, *J* = 15.0 Hz, 1H), 4.35 (dd, *J* = 15.0, 6.8 Hz, 1H), 4.18 (d, *J* = 12.9 Hz, 1H), 3.94 (dd, *J* = 15.0, 5.4 Hz, 1H), 3.85 (t, *J* = 4.8 Hz, 4H), 3.11 (t, *J* = 4.8 Hz, 4H), 1.74 ppm (s, 3H). ^{13}C NMR (126 MHz, $CDCl_3$) δ 171.0, 159.1, 152.3, 150.9, 137.2, 134.3,

132.4, 129.1, 128.9, 128.7, 128.4, 127.5, 127.0, 125.8, 116.0, 105.3, 66.9, 65.9, 55.9, 49.1, 45.5, 44.1, 29.8, 21.9 ppm. HR-MS: calc. for $[M+H]^+$ $C_{32}H_{34}N_5O_3$ 536.2656 found 536.2668, calc. for $[M+Na]^+$ $C_{32}H_{33}N_5O_3Na$ 558.2476 found 558.2487.

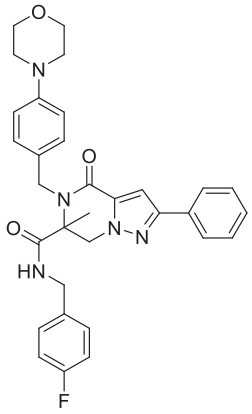

N-*(4-Fluorobenzyl)-6-methyl-5-(4-morpholinobenzyl)-4-oxo-2-phenyl-4,5,6,7-tetrahydropyrazolo[1,5-a]pyrazine-6-carboxamide* (***3g***). Prepared according to general procedure 3B using Burgess reagent (70 mg, 293 μmol, 2.0 equiv.), *N*-(4-fluorobenzyl)formamide **13e** (30 mg, 196 μmol, 1.0 equiv.), 1-(2-oxopropyl)-3-phenyl-1*H*-pyrazole-5-carboxylic acid **6a** (48 mg, 196 μmol, 1.0 equiv.) and 4-(morpholinophenyl)methanamine **9a** (34 mg, 176 μmol, 0.9 equiv) in MeOH (1.2 ml) and ACN (5.5 ml). The crude was filtered and the remaining product was washed thrice with cold ACN. The product was obtained as a white solid (15 mg, 27 μmol, 15%). R_f = 0.47 (cyclohexane / EtOAc = 1:4). ^{1}H NMR (500 MHz, $CDCl_3$) δ 7.77 (d, *J* = 7.3 Hz, 2H), 7.41 (t, *J* = 7.3 Hz, 2H), 7.35 (t, *J* = 7.3 Hz, 1H), 7.30 (d, *J* = 8.6 Hz, 2H), 7.06 (s, 1H), 6.80 (d, *J* = 8.6 Hz, 2H), 6.75 (t, *J* = 8.3 Hz, 2H), 6.73-6.68 (m, *J* = 8.3 Hz, 2H), 6.25 (s, 1H), 5.07 (d, *J* = 12.9 Hz, 1H), 4.94 (d, *J* = 15.2 Hz, 1H), 4.76 (d, *J* = 15.2 Hz, 1H), 4.27 (dd, *J* = 14.9, 6.7 Hz, 1H), 4.18 (d, *J* = 12.9 Hz, 1H), 3.91 (dd, *J* = 14.9, 5.1 Hz, 1H), 3.88-3.81 (m, 4H), 3.17-3.06 (m, 4H), 1.74 ppm (s, 3H). ^{13}C NMR (126 MHz, $CDCl_3$) δ 171.0, 163.1, 161.1, 159.1, 152.3, 151.0, 134.3, 133.0, 132.2, 129.1, 128.9, 128.8, 128.8, 128.5, 125.8, 115.9, 115.6, 115.4, 105.3, 66.9, 65.9, 55.9, 49.0, 45.5, 43.4, 21.8 ppm. HR-MS: calc. for $[M+H]^+$ $C_{32}H_{33}FN_5O_3$ 554.25619 found 554.25544.

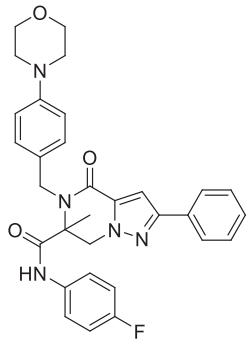

N-*(4-fluorophenyl)-6-methyl-5-(4-morpholinobenzyl)-4-oxo-2-phenyl-4,5,6,7-tetrahydropyrazolo[1,5-a]pyrazine-6-carboxamide* (***3h***). Prepared according to general procedure 2 using 1-(2-oxopropyl)-3-phenyl-1*H*-pyrazole-5-carboxylic acid **6a** (50.0 mg, 0.20 mmol, 1.0 equiv.), (4-morpholino-phenyl)methanamine **9a** (35.4 μL, 0.20 mmol, 1.0 equiv.) and *N*-(4-fluorophenyl)formamide **8m** (25 mg, 0.20 mmol, 1.0 equiv.). The product was obtained as light brown solid (33.7 mg, 0.06 mmol, 31%). R_f = 0.18 (cyclohexane / EtOAc = 1:9). ^{1}H NMR (500 MHz, $CDCl_3$) δ 7.77 (d, *J* = 7.5 Hz, 2H), 7.51 (d, *J* = 8.5 Hz, 2H), 7.38 (t, *J* = 7.5 Hz, 3H), 7.31 (t, *J* = 7.5 Hz, 1H), 7.14 (s, 1H), 6.91 (d, *J* = 8.5 Hz, 2H), 6.88 – 6.75 (m, 4H), 5.22 (d, *J* = 15.1 Hz, 1H), 5.17 (d, *J* = 12.9 Hz, 1H), 4.64 (d, *J* = 15.1 Hz, 1H), 4.22 (d, *J* = 12.9 Hz, 1H), 3.86 (t, *J* = 4.8 Hz, 4H), 3.14 (t, *J* = 4.8 Hz, 4H), 1.86 ppm (s, 3H). ^{13}C NMR (126 MHz, $CDCl_3$) δ 169.2, 159.1,

152.4, 151.4, 134.2, 132.2, 130.3, 128.8, 128.5, 128.5, 125.8, 122.4, 122.3, 116.3, 115.5, 115.3, 105.4, 66.9, 66.3, 55.7, 49.0, 45.6, 22.0 ppm. HR-MS: calc. for $[M+H]^+$ $C_{31}H_{31}FN_5O_3$ 540.2405 found 540.2413.

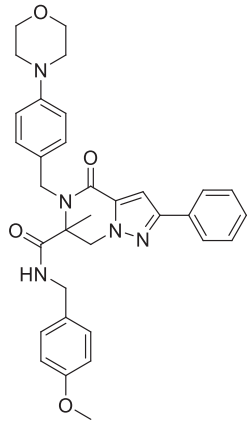

N-*(4-Methoxybenzyl)-6-methyl-5-(4-morpholinobenzyl)-4-oxo-2-phenyl-4,5,6,7-tetrahydropyrazolo[1,5-a]pyrazine-6-carboxamide* ***(3i)***. Prepared according to general procedure 3A using *N*-(4-methoxybenzyl)formamide **13f** (10.0 mg, 0.07 mmol, 1.0 equiv.), 1-(2-oxopropyl)-3-phenyl-1*H*-pyrazole-5-carboxylic acid **6a** (16.6 mg, 0.07 mmol, 1.0 equiv.) and (4-morpholinophenyl)methanamine **9a** (11.8 mg, 0.06 mmol, 0.9 equiv.). The product was obtained as light yellow solid (13.2 mg, 0.02 mmol, 34%). R_f = 0.39 (cyclohexane / EtOAc = 1:9). ^{1}H NMR (400 MHz, $CDCl_3$) δ 7.83 – 7.79 (m, 2H), 7.45 – 7.38 (m, 2H), 7.37 – 7.32 (m, 1H), 7.32 – 7.27 (m, 2H), 6.84 – 6.78 (m, 2H), 6.70 – 6.65 (m, 2H), 6.62 – 6.57 (m, 2H), 6.10 – 6.00 (m, 1H), 5.06 (d, *J* = 12.9 Hz, 1H), 4.98 (d, *J* = 15.3 Hz, 1H), 4.71 (d, *J* = 15.3 Hz, 1H), 4.31 (dd, *J* = 14.8 Hz, 1H), 4.18 (d, *J* = 12.9 Hz, 1H), 3.87 – 3.84 (m, 4H), 3.83 – 3.82 (m, 1H), 3.59 (s, 3H), 3.17 – 3.08 (m, 4H), 1.74 ppm (s, 3H). ^{13}C NMR (126 MHz, $CDCl_3$) δ 170.7, 159.0, 158.8, 152.1, 150.9, 134.2, 132.3, 129.1, 129.0, 128.8, 128.3, 128.3, 125.7, 115.9, 113.9, 105.2, 66.8, 65.8, 55.8, 55.1, 49.0, 45.3, 43.4, 26.9, 21.7 ppm. HR-MS: calc. for $[M+H]^+$ $C_{33}H_{36}N_5O_4$ 566.2762 found 566.2759, calc. for $[M+Na]^+$ $C_{33}H_{35}N_5O_4Na$ 588.2581 found 588.2579.

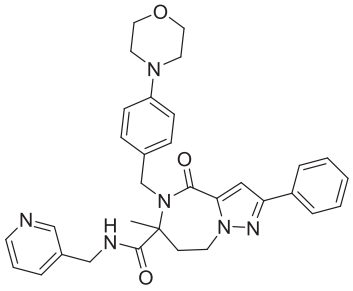

6-Methyl-5-(4-morpholinobenzyl)-4-oxo-2-phenyl-N-*(pyridin-3-ylmethyl)-5,6,7,8-tetrahydro-4*H*-pyrazolo[1,5-a][1,4]diazepine-6-carboxamide* ***(3j)***. Prepared according to general procedure 2 using 1-(3-oxobutyl)-3-phenyl-1*H*-pyrazole-5-carboxylic acid **6b** (50 mg, 190 μmol, 1.0 equiv.), 4-(morpholinophenyl)methanamine **9a** (34 mg, 170 μmol, 0.9 equiv.) and 3-(isocyanomethyl)pyridine **8j** (23 mg, 190 μmol, 1.0 equiv.). The product was purified by means of silica gel column chromatography (elute: DCM / EtOH / sat. NH_4OH) and obtained as off-white solid (7 mg, 13 μmol, 7%). R_f = 0.39 (DCM / EtOH / sat. NH_4OH = 175:4:0.5). ^{1}H NMR (700 MHz, $CDCl_3$) δ 8.39 (dd, *J* = 4.8, 2.0 Hz, 1H), 8.29 (d, *J* = 2.0 Hz, 1H), 7.77 – 7.74 (m, 2H), 7.44 – 7.39 (m, 2H), 7.34 – 7.29 (m, 3H), 7.23 (dt, *J* = 7.8, 2.0 Hz, 1H), 6.97 (ddd, *J* = 7.8, 4.8, 0.9 Hz, 1H), 6.87 (s, 1H), 6.83 – 6.80 (m, 2H), 6.07 (t, *J* = 6.0 Hz, 1H), 4.92 (d, *J* = 128.0 Hz, 2H), 4.60 (ddd, *J* = 14.2, 7.2, 4.5 Hz, 1H), 4.26 (ddd, *J* = 14.2, 9.2, 6.2 Hz, 1H), 4.10 (dd, *J* = 14.8, 5.9 Hz, 1H), 4.00 (dd, *J* = 14.8, 5.9 Hz, 1H), 3.86 (t, *J* = 4.8 Hz, 4H), 3.21 (ddd, *J* = 14.4, 9.2, 7.3 Hz, 1H), 3.16 – 3.09 (m, 4H), 2.07 (ddd, *J* = 14.4, 6.2, 4.6 Hz, 1H), 1.69 ppm (s, 3H). ^{13}C NMR (176 MHz, $CDCl_3$) δ 172.5, 163.0, 151.1, 156.0, 149.3, 149.2, 138.2, 135.9,

133.1, 132.6, 129.8, 128.9, 128.8, 128.2, 125.8, 123.7, 115.9, 107.9, 67.0, 65.8, 49.1, 47.3, 47.1, 41.7, 38.7, 27.4 ppm. HR-MS: calc. for $[M+H]^+$ $C_{32}H_{35}N_6O_3$ 551.27652 found 551.27590.

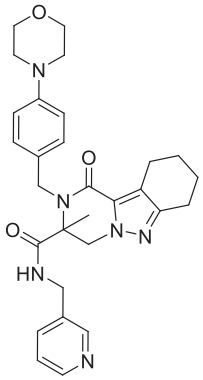

*3-Methyl-2-(4-morpholinobenzyl)-1-oxo-*N*-(pyridin-3-ylmethyl)-1,2,3,4,7,8,9,10-octahydropyrazino[1,2-b]indazole-3-carboxamide (**11**).* Prepared according to general procedure 2 using 2-(2-oxopropyl)-4,5,6,7-tetrahydro-2*H*-indazol-3-carboxylicacid **6c** (11.6 mg, 0.05 mmol, 1.0 equiv.), 4-morpholino-benzylamine **9a** (18.1 mg, 0.9 mmol, 1.8 equiv.) and 3-isocyanomethylpyridine **8j** (5.71 μL, 0.05 mmol, 1.0 equiv.). The product was purified by means of silica gel column chromatography (elute: DCM / MeOH) and obtained as white solid (9.9 mg, 0.02 mmol, 37%). R_f = 0.27 (DCM / MeOH = 95:5). ^{1}H NMR (500 MHz, $CDCl_3$) δ 8.46 (d, *J* = 4.6 Hz, 1H), 8.16 (s, 1H), 7.28 (d, *J* = 8.7 Hz, 2H), 7.09 (d, *J* = 7.8 Hz, 1H), 7.03 (d, *J* = 7.8 Hz, 1H), 6.79 (d, *J* = 8.7 Hz, 2H), 6.25 (t, *J* = 5.5 Hz, 1H), 4.93 – 4.88 (m, 2H), 4.71 (d, *J* = 15.3 Hz, 1H), 4.30 (dd, *J* = 15.3, 6.9 Hz, 1H), 4.04 (d, *J* = 12.7 Hz, 1H), 3.97 (dd, *J* = 15.3 Hz, 5.5 Hz, 1H), 3.85 (t, *J* = 4.8 Hz, 4H), 3.10 (t, *J* = 4.8 Hz, 4H), 2.91 – 2.80 (m, 1H), 2.72 – 2.65 (m, 2H), 2.65 – 2.59 (m, 1H), 1.85 – 1.78 (m, 2H), 1.78 – 1.71 (m, 2H), 1.69 ppm (s, 3H). ^{13}C NMR (126 MHz, $CDCl_3$) δ 171.7, 160.0, 150.9, 150.3, 149.0, 148.8, 134.8, 133.2, 129.0, 128.2, 123.5, 121.0, 115.9, 66.9, 65.9, 55.7, 49.0, 45.0, 41.4, 23.4, 23.0, 22.9, 21.7, 21.3 ppm. HR-MS: calc. for $[M+H]^+$ $C_{29}H_{35}N_6O_3$ 515.27652 found 515.27724.

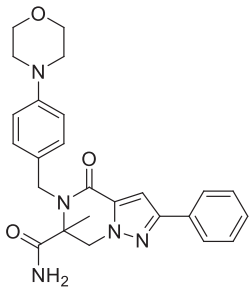

*6-Methyl-5-(4-morpholinobenzyl)-4-oxo-2-phenyl-4,5,6,7-tetrahydropyrazolo[1,5-a]pyrazine-6-carboxamide (**3k**).* *N*-(*tert*-butyl)-6-methyl-5-(4-morpholinobenzyl)-4-oxo-2-phenyl-4,5,6,7-tetrahydropyrazolo[1,5-a]pyrazine-6-carboxamide **3e** (52 mg, 104 μmol, 1.0 equiv.) was dissolved in *p*-xylene (0.5 mL) and methanesulfonic acid (1.0 mL, 15.4 mmol, 148 equiv.) was slowly added. The biphasic mixture was stirred vigorously for 5 min at room temperature and an additional hour at 40°C. The reaction mixture was allowed to cool down to room temperature and carefully transferred to a container with 25 mL saturated $NaHCO_3$. The resulting mixture was extracted thrice with EtOAc and the combined organic layers were dried over Na_2SO_4, filtered and concentrated under reduced pressure. The product was obtained as white solid (46 mg, 100 μmol, 99%). R_f = 0.60 (EtOAc / MeOH / TEA = 90:10:1). ^{1}H NMR (700 MHz, $CDCl_3$) δ 7.77 (dd, *J* = 7.6, 1.4 Hz, 2H), 7.38 (t, *J* = 7.6 Hz, 2H), 7.34 – 7.30 (m, 1H), 7.29 (d, *J* = 8.5 Hz, 2H), 7.14 (s, 1H), 6.87 – 6.84 (m, 2H), 5.93 (s, 1H), 5.63 (s, 1H), 5.16 (d, *J* = 15.5 Hz, 1H), 4.99 (d, *J* = 13.0 Hz, 1H), 4.57 (d, *J* = 15.5 Hz, 1H), 4.15 (d, *J* = 13.0 Hz, 1H), 3.88 – 3.83 (m, 4H), 3.16 – 3.11 (m, 4H), 1.68 ppm (s, 3H). ^{13}C NMR (176 MHz, $CDCl_3$) δ 173.6, 159.1,

152.4, 150.9, 134.4, 132.3, 129.0, 128.9, 128.9, 128.4, 125.8, 116.0, 105.4, 66.9, 65.5, 55.6, 49.2, 45.5, 22.0 ppm. HR-MS: calc. for $[M+H]^+$ $C_{25}H_{28}N_5O_3$ 446.31867 found 446.21830.

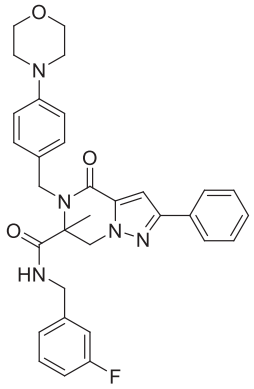

N-*(3-Fluorobenzyl)-6-methyl-5-(4-morpholinobenzyl)-4-oxo-2-phenyl-4,5,6,7-tetrahydropyrazolo[1,5-a]pyrazine-6-carboxamide* ***(3l)***. Prepared according to general procedure 3B using Burgess reagent (70 mg, 293 μmol, 2.0 equiv.), *N*-(3-fluorobenzyl)formamide **13d** (30 mg, 196 μmol, 1.0 equiv.), 1-(2-oxopropyl)-3-phenyl-1*H*-pyrazole-5-carboxylic acid **6a** (48 mg, 196 μmol, 1.0 equiv.) and 4-(morpholinophenyl)methanamine **9a** (34 mg, 176 μmol, 1.0 equiv.) in MeOH (1.2 mL) and ACN (5.5 mL). The product was purified by means of recrystallization from MeOH and obtained as brown solid (20 mg, 35 μmol, 20%). R_f = 0.50 (cyclohexane / EtOAc = 1:4). ^{1}H NMR (700 MHz, $CDCl_3$) δ 7.77 (dd, *J* = 7.6, 1.3 Hz, 2H), 7.39 (t, *J* = 7.6 Hz, 2H), 7.35 – 7.32 (m, 1H), 7.30 (d, *J* = 8.5 Hz, 2H), 7.08 (s, 1H), 7.02 (td, *J* = 7.9, 5.8 Hz, 1H), 6.81 – 6.77 (m, 3H), 6.53 – 6.51 (m, 1H), 6.48 (dt, *J* = 9.5, 2.0 Hz, 1H), 6.39 (t, *J* = 6.1 Hz, 1H), 5.08 (d, *J* = 12.8 Hz, 1H), 4.94 (d, *J* = 15.4 Hz, 1H), 4.79 (d, *J* = 15.4 Hz, 1H), 4.27 (dd, *J* = 15.2, 6.1 Hz, 1H), 4.17 (d, *J* = 12.8 Hz, 1H), 3.95 (dd, *J* = 15.2, 6.1 Hz, 1H), 3.84 (m, 4H), 3.13 – 3.08 (m, 4H), 1.75 ppm (s, 3H). ^{13}C NMR (176 MHz, $CDCl_3$) δ 171.1, 163.5, 162.1, 159.1, 152.4, 151.0, 139.9, 139.8, 134.3, 132.3, 130.2, 130.1, 129.1, 128.8, 128.8, 128.4, 125.9, 122.6, 122.6, 115.9, 114.5, 114.4, 114.1, 114.0, 105.3, 66.9, 65.9, 55.9, 49.0, 45.5, 43.5, 43.5, 21.9 ppm. HR-MS: calc. for $[M+H]^+$ $C_{32}H_{33}N_5O_3F$ 554.25619 found 554.25561.

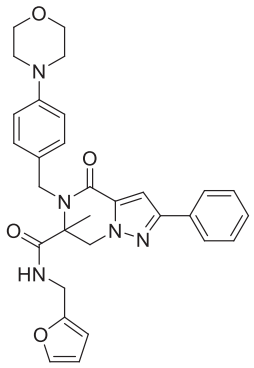

N-*(Furan-2-ylmethyl)-6-methyl-5-(4-morpholinobenzyl)-4-oxo-2-phenyl-4,5,6,7-tetrahydropyrazolo[1,5-a]pyrazine-6-carboxamide* ***(3m)***. Prepared according to general procedure 3B using Burgess reagent (43 mg, 180 μmol, 1.5 equiv.), *N*-(furan-2-ylmethyl)formamide **13g** (15 mg, 120 μmol, 1.0 equiv.), 1-(2-oxopropyl)-3-phenyl-1*H*-pyrazole-5-carboxylic acid **6a** (29 mg, 121 μmol, 1.0 equiv.) and 4-(morpholinophenyl)methanamine **9a** (21 mg, 109 μmol, 0.9 equiv.) in MeOH (0.6 mL) and ACN (2.75 mL). After work-up of the crude reaction mixture, the product was purified using preparative HPLC-MS followed by silica gel column chromatography (elute: DCM / EtOH / sat. NH_4OH) as white solid (10 mg, 19 μmol, 17%). R_f = 0.51 (cyclohexane / EtOAc = 1:4). ^{1}H NMR (500 MHz, CD_2Cl_2) δ 7.82 – 7.78 (m, 2H), 7.41 (t, *J* = 7.6 Hz, 2H), 7.36 – 7.32 (m, 1H), 7.30 (d, *J* = 8.5 Hz, 2H), 7.21 (d, *J* = 1.9 Hz, 1H), 7.11 (s, 1H), 6.92 – 6.88 (m, 2H), 6.17 (dd, *J* = 3.3, 1.9 Hz, 2H), 5.87 (d, *J* = 3.3 Hz, 1H), 5.02 (d, *J* = 15.5 Hz, 1H), 4.98 (d, *J* = 13.0 Hz, 1H), 4.65 (d, *J* = 15.5 Hz, 1H), 4.23 – 4.16 (m, 2H), 4.11 (dd, *J* = 15.6, 5.6 Hz, 1H), 3.85 – 3.81 (m, 4H), 3.16 – 3.12 (m, 4H), 1.68 ppm (s, 3H). ^{13}C NMR (126 MHz,

CD_2Cl_2) δ 171.1, 159.2, 152.2, 150.9, 150.5, 142.5, 134.8, 132.7, 130.1, 129.9, 129.1, 128.6, 125.9, 116.6, 110.6, 107.3, 105.1, 66.9, 66.0, 55.9, 49.8, 45.7, 37.4, 21.9 ppm. HR-MS: calc. for $[M+H]^+$ $C_{30}H_{32}N_5O_4$ 526.24488 found 526.24402.

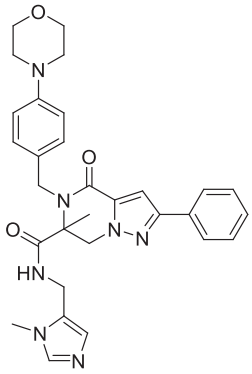

6-Methyl-N-*((1-methyl-1*H*-imidazol-5-yl)methyl)-5-(4-morpholinobenzyl)-4-oxo-2-phenyl-4,5,6,7-tetrahydropyrazolo[1,5-a]pyrazine-6-carboxamide (**3n**)*. Prepared according to general procedure 3B using Burgess reagent (128 mg, 539 μmol, 2.5 equiv.), *N*-((1-methyl-1*H*-imidazol-5-yl)methyl)formamide **13i** (30 mg, 216 μmol, 1.0 equiv.), 1-(2-oxopropyl)-3-phenyl-1*H*-pyrazole-5-carboxylic acid **6a** (53 mg, 216 μmol, 1.0 equiv.) and 4-(morpholinophenyl)methanamine **9a** (37 mg, 194 μmol, 0.9 equiv.) in MeOH (1.2 mL) and ACN (5.5 mL). The product was purified twice by means of silica gel column chromatography (1st elute: EtOAc / MeOH / TEA = 90:10:1; 2nd elute: DCM / EtOH / sat. NH_4OH = 125:4:0.5) and obtained as white solid (13 mg, 24 μmol, 12%). R_f = 0.40 (DCM / EtOH / sat. NH_4OH = 125:4:0.5). ^1H NMR (700 MHz, CD_2Cl_2) δ 7.80 (d, *J* = 7.5 Hz, 2H), 7.42 (t, *J* = 7.5 Hz, 2H), 7.35 (t, *J* = 7.5 Hz, 1H), 7.30 (d, *J* = 8.5 Hz, 2H), 7.23 (s, 1H), 7.10 (s, 1H), 6.81 (d, *J* = 8.5 Hz, 2H), 6.64 (s, 1H), 5.98 (s, 1H), 5.03 (d, *J* = 12.5 Hz, 1H), 4.89 (d, *J* = 15.4 Hz, 1H), 4.75 (d, *J* = 15.4 Hz, 1H), 4.23 (dd, *J* = 15.6, 6.2 Hz, 1H), 4.18 (d, *J* = 12.5 Hz, 1H), 3.93 (dd, *J* = 15.5, 6.2 Hz, 1H), 3.83 (t, *J* = 5.0 Hz, 4H), 3.14 (m, 4H), 3.09 (s, 3H), 1.74 ppm (s, 3H). ^{13}C NMR (176 MHz, CD_2Cl_2) δ 171.2, 159.1, 152.2, 151.4, 139.1, 135.0, 132.7, 129.4, 129.2, 128.9, 128.7, 128.7, 127.7, 125.9, 116.0, 105.0, 67.2, 66.1, 56.1, 49.2, 45.6, 33.8, 31.3, 21.7 ppm. HR-MS: calc. for $[M+H]^+$ $C_{30}H_{34}N_7O_3$ 540.27176 found 540.27094.

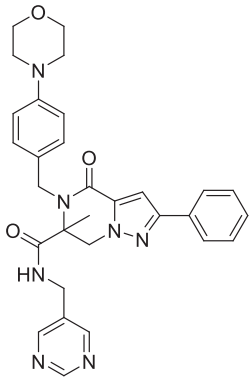

6-Methyl-5-(4-morpholinobenzyl)-4-oxo-2-phenyl-N-*(pyrimidin-5-ylmethyl)-4,5,6,7-tetrahydropyrazolo[1,5-a]pyrazine-6-carboxamide (**3o**)*. Prepared according to general procedure 3B using Burgess reagent (143 mg, 602 μmol, 2.6 equiv.), *N*-(pyrimidin-5-ylmethyl)formamide **13c** (32 mg, 233 μmol, 1.0 equiv.), 1-(2-oxopropyl)-3-phenyl-1*H*-pyrazole-5-carboxylic acid **6a** (53 mg, 218 μmol, 0.9 equiv.) and 4-(morpholinophenyl)methanamine **9a** (38 mg, 196 μmol, 0.8 equiv.) in MeOH (1.2 mL) and ACN (5.5 mL). The product was purified twice by means of silica gel column chromatography (1st elute: DCM / MeOH; 2nd elute: DCM / EtOH / sat. NH_4OH) and obtained as white solid (12 mg, 22 μmol, 12%). R_f = 0.21 (DCM / EtOH / sat.NH_4OH = 150:8:1). ^1H NMR (700 MHz, CD_2Cl_2) δ 8.96 (s, 1H), 8.21 (s, 2H), 7.82 – 7.79 (m, 2H), 7.42 (dd, *J* = 7.0, 8.4 Hz, 2H), 7.37 – 7.32 (m, 3H), 7.11 (s, 1H), 6.81 – 6.79 (m, 2H), 6.26 (t, *J* = 6.2 Hz, 1H), 5.03 (d, *J* = 12.8 Hz, 1H), 4.99 (d, *J* = 15.4 Hz, 1H), 4.71 (d, *J* = 15.4 Hz, 1H), 4.18 (d, *J* = 12.8 Hz, 1H), 4.08 (dd, *J* = 15.4, 6.2 Hz, 1H), 3.99 (dd, *J* = 15.4, 6.2 Hz, 1H), 3.82 (m, 4H), 3.10 (m, 4H), 1.75 ppm (s, 3H). ^{13}C NMR (176 MHz,

CD_2Cl_2) δ 172.0, 159.2, 158.3, 156.3, 152.3, 151.5, 134.8, 132.7, 131.4, 129.6, 129.1, 128.8, 128.6, 126.0, 116.0, 105.2, 67.1, 66.1, 56.0, 49.0, 45.6, 39.6, 21.8 ppm. HR-MS: calc. for $[M+H]^+$ $C_{30}H_{32}N_7O_3$ 538.25611 found 538.25529.

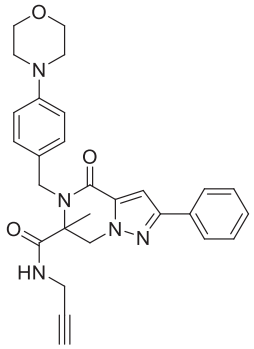

6-Methyl-5-(4-morpholinobenzyl)-4-oxo-2-phenyl-N-*(prop-2-yn-1-yl)-4,5,6,7-tetrahydropyrazolo[1,5-a]pyrazine-6-carboxamide* (***3p***). A round bottom flask was charged with formamide **13h** (106 mg, 1.3 mmol, 1 equiv.), benzenesulfonyl chloride (327 μL, 2.6 mmol, 2.0 qeuiv.) and trioctylamine (1.12 mL, 2.6 mmol, 2.0 equiv.). The flask was connected to a glass distillation tube and heated to 80°C. A two-neck receiver flask was cooled to -80°C to collect formed isocyanide under reduced pressure over 2 h. Subsequently, 4-(morpholinophenyl)methanamine **9a** (80 mg, 415 μmol, 0.3 equiv) and 1-(2-oxopropyl)-3-phenyl-1*H*-pyrazole-5-carboxylic acid **6a** (113 mg, 461 μmol, 0.4 equiv.) were added in MeOH (2.4 mL) to the freshly distilled isocyanide. The resulting mixture was stirred vigorously at room temperature for two days. Thereafter, the reaction mixture was diluted with EtOAc and washed with saturated $NaHCO_3$. The aqueous layer was extracted twice with EtOAc and the combined organic layers were dried over Na_2SO_4 and filtered. The filtrate was concentrated under reduced pressure and the product was purified by means of silica gel column chromatography (DCM / EtOH / sat. NH_4OH) and obtained as white crystalline solid (80 mg, 170 μmol, 40%). R_f = 0.5 (DCM / EtOH / sat.NH_4OH = 125:4:0.5). ^1H NMR (500 MHz, $CDCl_3$) δ 7.78 – 7.73 (m, 2H), 7.39 – 7.34 (m, 2H), 7.34 – 7.28 (m, 3H), 7.14 (s, 1H), 6.90 – 6.86 (m, 2H), 6.28 (q, *J* = 4.8 Hz, 1H), 5.11 (d, *J* = 15.4 Hz, 1H), 5.03 (d, *J* = 13.0 Hz, 1H), 4.66 (d, *J* = 15.4 Hz, 1H), 4.15 (d, *J* = 13.0 Hz, 1H), 3.87 – 3.80 (m, 5H), 3.72 (ddd, *J* = 17.5, 5.0, 2.6 Hz, 1H), 3.17 – 3.11 (m, 4H), 2.08 (t, *J* = 2.6 Hz, 1H), 1.69 ppm (s, 3H). ^{13}C NMR (126 MHz, $CDCl_3$) δ 170.8, 159.0, 152.3, 151.0, 134.2, 132.2, 128.9, 128.9, 128.8, 128.4, 125.8, 116.2, 105.4, 78.6, 72.1, 66.9, 65.7, 55.6, 49.2, 45.6, 30.1, 22.1 ppm. HR-MS: calc. for $[M+H]^+$ $C_{28}H_{30}N_5O_3$ 484.23432 found 484.23387.

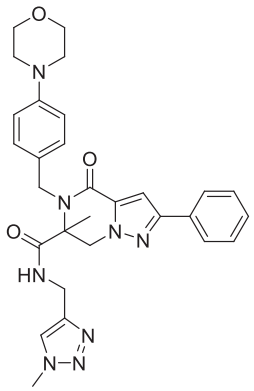

6-Methyl-N-*((1-methyl-1H-1,2,3-triazol-4-yl)methyl)-5-(4-morpholinobenzyl)-4-oxo-2-phenyl-4,5,6,7-tetrahydropyrazolo[1,5-a]pyrazine-6-carboxamide* (***3q***). Cupper(I)iodide (2.4 mg, 12.4 μmol, 0.2 equiv.) and sodium azide (8.8 mg, 136 μmol, 2.4 equiv.) were dissolved in H_2O / EtOH (400 μL, 1:1). To the reaction mixture methyl iodide (4.3 μL, 68 μmol, 1.2 equiv.) and sodium ascorbate (11 mg, 60 μmol, 0.9 equiv.) were added and the resulting mixture and stirred for 1 h at room temperature. Subsequently, 6-methyl-5-(4-morpholinobenzyl)-4-oxo-2-phenyl-*N*-(prop-2-yn-1-yl)-4,5,6,7-tetrahydropyrazolo[1,5-a]pyrazine-6-carboxamide **3p** (27 mg, 56 μmol, 1.0 equiv.) was added and the mixture was stirred at 50°C for 2 days. The product was purified by means of silica gel column chromatography (DCM / EtOH / sat. NH_4OH) followed by MS-assisted preparative HPLC. After basic extraction between saturated $NaHCO_3$ and DCM the product was obtained as white solid (12 mg, 22 μmol, 40%). R_f = 0.11 (DCM / EtOH / sat.NH_4OH = 175:4:0.5). ^1H NMR (700 MHz, $CDCl_3$) δ 7.79 (dd, *J* = 8.2, 1.3 Hz, 2H), 7.44 – 7.39 (m, 2H), 7.37 – 7.31 (m, 1H), 7.29 (d, *J* = 8.7 Hz, 2H), 7.08 (s, 1H), 6.89 – 6.84 (m, 2H), 6.78 (s, 1H), 6.64 (t, *J* = 6.2 Hz, 1H), 5.12 (d, *J* = 15.5 Hz, 1H), 5.02 (d, *J* = 12.8 Hz, 1H), 4.63 (d, *J* = 15.5 Hz, 1H), 4.43 (dd, *J* = 15.3, 6.6 Hz, 1H), 4.17 (d, *J* = 12.8 Hz, 1H), 4.05 (dd, *J* = 15.3, 5.4 Hz, 1H), 3.87 – 3.83 (m, 4H),

3.58 (s, 3H), 3.16 – 3.11 (m, 4H), 1.71 ppm (s, 3H). ^{13}C NMR (176 MHz, $CDCl_3$) δ 171.4, 159.0, 151.9, 151.0, 144.6, 134.6, 132.2, 129.0, 129.0, 128.9, 128.6, 125.7, 122.6, 116.1, 105.0, 67.0, 65.9, 56.1, 49.2, 45.5, 36.3, 36.0, 21.6 ppm. HR-MS: calc. for $[M+H]^+$ $C_{29}H_{33}N_8O_3$ 541.26701 found 541.26642.

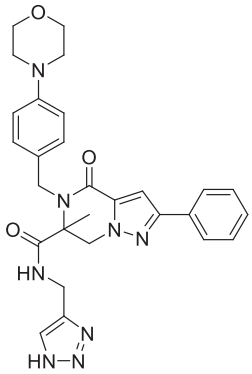

N-*((1H-1,2,3-triazol-4-yl)methyl)-6-methyl-5-(4-morpholinobenzyl)-4-oxo-2-phenyl-4,5,6,7-tetrahydropyrazolo[1,5-a]pyrazine-6-carboxamide* (***3r***). To a suspension of 6-methyl-5-(4-morpholinobenzyl)-4-oxo-2-phenyl-*N*-(prop-2-yn-1-yl)-4,5,6,7-tetrahydropyrazolo[1,5-a]pyrazine-6-carboxamide **3p** (30 mg, 62 μmol, 1.0 equiv.), cupper(I)iodide (1.3 mg 6.9 μmol, 0.1 equiv.), and sodium ascorbate (4.9 mg 25 μmol, 0.4 equiv.) in a DMF-water mixture (4:1, 1.0 mL) was added trimethylsilylazide (9 mg, 76 μmol, 1.2 equiv.). The resulting mixture was stirred at heating on 100°C overnight. The mixture was allowed to cool down to room temperature and was subsequently extracted between saturated NH_4Cl and DCM. The combined organic layers were dried over Na_2SO_4, filtered and concentrated under reduced pressure. The product was purified by means of silica gel column chromatography (elute: DCM / EtOH / sat. NH_4OH) and obtained as white crystalline solid (18 mg, 34 μmol, 55%). R_f = 0.27 (Pentane / DCM / EtOH / sat.NH_4OH = 60:50:8:1). ^{1}H NMR (700 MHz, $CDCl_3$) δ 12.79 (bs, 1H), 7.74 (dd, *J* = 7.5, 1.3 Hz, 2H), 7.37 (t, *J* = 7.5 Hz, 2H), 7.32 – 7.29 (m, 1H), 7.27 (s, 1H), 7.24 (d, *J* = 8.6 Hz, 2H), 7.08 (s, 1H), 6.87 (s, 1H), 6.82-6.78 (m, 2H), 5.13 (d, *J* = 15.7 Hz, 1H), 5.05 (d, *J* = 12.9 Hz, 1H), 4.57 (d, *J* = 15.7 Hz, 1H), 4.33 – 4.26 (m, 2H), 4.17 (d, *J* = 12.9 Hz, 1H), 3.85 – 3.81 (m, 4H), 3.12 – 3.08 (m, 4H), 1.68 ppm (s, 3H). ^{13}C NMR (176 MHz, $CDCl_3$) δ 171.4, 159.3, 152.4, 150.9, 144.8*, 134.4, 132.2, 128.9, 128.9, 128.8, 128.5, 125.9, 116.0, 105.4, 66.9, 65.8, 55.7, 49.1, 45.7, 35.4**, 21.9 ppm. HR-MS: calc. for $[M+H]^+$ $C_{28}H_{31}N_8O_3$ 527.25136 found 527.25070.

only observed in HMBC* or HSQC**

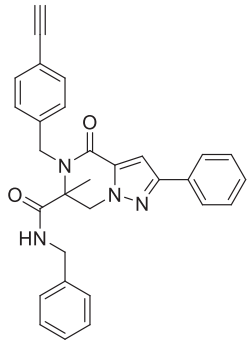

N-*Benzyl-5-(4-ethynylbenzyl)-6-methyl-4-oxo-2-phenyl-4,5,6,7-tetrahydropyrazolo[1,5-a]pyrazine-6-carboxamide* (***3s***). Prepared according to general procedure 2 using 1-(2-oxopropyl)-3-phenyl-1*H*-pyrazole-5-carboxylic acid **6a** (20.0 mg, 0.08 mmol, 1.0 equiv.), (4-ethynylphenyl)methanamine **9g** (10.7 μL, 0.08 mmol, 1.0 equiv.) and benzyl isocyanide **8k** (10.0 μL, 0.08 mmol, 1.0 equiv.). The product was obtained as white solid (13.4 mg, 0.03 mmol, 34%). R_f = 0.56 (cyclohexane / EtOAc = 3:7). ^{1}H NMR (500 MHz, $CDCl_3$, major rotamer given) δ 7.99 (d, *J* = 7.2 Hz, 2H), 7.69 – 7.62 (m, 4H), 7.60 (d, *J* = 7.2 Hz, 1H), 7.53 – 7.48 (m, 2H), 7.36 – 7.31 (m, 3H), 7.07 – 6.99 (m, 2H), 6.80 (t, *J* = 5.1 Hz, 1H), 5.56 (d, *J* = 15.9 Hz, 1H), 5.29 (d, *J* = 13.1 Hz, 1H), 4.74 (d, *J* = 15.9 Hz, 1H), 4.63 (dd, *J* = 14.9 Hz, 1H), 4.43 (d, *J* = 13.1 Hz, 1H), 4.33 (dd, *J* = 14.9, 5.1 Hz, 1H), 3.35 (s, 1H), 1.91 ppm (s, 3H). ^{13}C NMR (126 MHz, $CDCl_3$) δ 170.6, 159.2, 152.4, 138.7, 137.2, 134.1, 132.9, 132.2, 128.9, 128.7, 128.5, 127.6, 127.3, 127.1, 125.8, 121.8, 105.5, 83.1, 78.0, 66.0, 55.8, 46.0, 44.1, 22.0 ppm. HR-MS: calc. for $[M+H]^+$ $C_{30}H_{27}N_4O_2$ 475.2129 found 475.2124, calc. for $[M+Na]^+$ $C_{30}H_{26}N_4O_2Na$ 497.1948 found 497.1943.

QUANTIFICATION AND STATISTICAL ANALYSIS

All biological replicates were expressed as mean ±s.d. or median with interquartile range. For statistical analysis of the data from RT-qPCR experiments and immunoblot analysis an unpaired two-tailed t-test with Welch's correction (without assuming equal s.d.) was conducted (if indicated) using GraphPad Prism 5 or 7. *:$p<0.05$; **:$p<0.01$; ***:$p<0.001$. Linear regression was performed to evaluate association between two conditions. N: technical replicates; n: biological replicates. All statistical details of the conducted experiments can be found in the respective figure and table legends.

DATA AND CODE AVAILABILITY

The crystal structure of compound **(*R*)-2a** has been deposited in the CCDC database under ID code 1883523.